Technical Report Documentation Page

1. Report No.	2. Government Accession No.	3. Recipient's Catalog No.
FHWA/TX-03/0-2101-4		

4. Title and Subtitle	5. Report Date
IMPACT OF FIELD EXPOSURE CONDITIONS ON HIGH STRENGTH CONCRETE PRODUCED FOR PRESTRESSED BRIDGE GIRDERS	November 2003
	6. Performing Organization Code

7. Author(s)	8. Performing Organization Report No.
Mary Beth D. Hueste, Fayez Moutassem, David Trejo and Daren B. H. Cline	Report 0-2101-4

9. Performing Organization Name and Address	10. Work Unit No. (TRAIS)
Texas Transportation Institute The Texas A&M University System College Station, Texas 77843-3135	11. Contract or Grant No. Project No. 0-2101

12. Sponsoring Agency Name and Address	13. Type of Report and Period Covered
Texas Department of Transportation Research and Technology Implementation Office P. O. Box 5080 Austin, Texas 78763-5080	Research: January 2000-May 2003
	14. Sponsoring Agency Code

15. Supplementary Notes

Research performed in cooperation with the Texas Department of Transportation and the U.S. Department of Transportation, Federal Highway Administration.

Research Project Title: Allowable Stresses and Resistance Factors for High Strength Concrete

16. Abstract

This is the fourth in a series of four reports that document the findings of a Texas Department of Transportation sponsored project to evaluate the allowable stresses and resistance factors for high strength concrete (HSC) prestressed bridge girders. The third phase of this research study, which is documented in this report, focused on determining the impact of different exposure conditions on the compressive and flexural strength of HSC mixtures used for prestressed girders in Texas. The allowable tensile stress at service for HSC prestressed bridge girders was evaluated based on the results from the experimental program. This phase of the project involved several key tasks: (1) an experimental study to assess the effect of several field exposure conditions on the compressive and flexural strength of HSC and development of a modified tensile stress limit based on material testing from this project, (2) a parametric study to evaluate the impact of the modified tensile stress limit derived from the material testing in this study when applied to the design of HSC U54 prestressed girders, and (3) a reliability study to determine the probability that the tensile stress would exceed the modulus of rupture to determine the safety against flexural cracking for designs based on both the current and modified tensile stress limits when applied to HSC U54 prestressed girders.

It was observed that the concrete compressive strength was not highly influenced by the variations in field exposure conditions. However, the modulus of rupture was highly influenced by variations in field exposure conditions. Exposure factors were applied to data for plant-produced samples collected in Phase 1 of this study. A modified tensile stress limit for service conditions based on a lower bound to 95 percent of the data was suggested as $7\sqrt{f_c'}$ (psi units) as compared to the current American Association of State Highway and Transportation Officials (AASHTO) allowable tensile stress limit of $6\sqrt{f'_c}$ (psi units). When the modified tensile stress limit was used in the parametric study for U54 prestressed girders, there was only a small increase in the potential span (from 0.9 to 2.3 feet). This increase only occurs for cases where the tensile stress limit at service was the controlling limit state (when all 99 strand positions are used). Reliability indices were determined to evaluate the probability that the tensile stress would exceed the modulus of rupture. For both 0.5-inch and 0.6-inch diameter strands, most of the reliability indices for designs using the current stress limit range from 1.5 to 2.0, whereas typical reliability indices for designs using the modified tensile stress limit range from 1.0 to 1.5.

17. Key Words	18. Distribution Statement
Prestressed Concrete, High Strength Concrete, Allowable Stresses, Curing, Maturity, Reliability	No restrictions. This document is available to the public through NTIS: National Technical Information Service 5285 Port Royal Road Springfield, Virginia 22161

19. Security Classif.(of this report)	20. Security Classif.(of this page)	21. No. of Pages	22. Price
Unclassified	Unclassified	194	

Form DOT F 1700.7 (8-72) **Reproduction of completed page authorized**

IMPACT OF FIELD EXPOSURE CONDITIONS ON HIGH STRENGTH CONCRETE PRODUCED FOR PRESTRESSED BRIDGE GIRDERS

by

Mary Beth D. Hueste, P.E.
Assistant Research Engineer
Texas Transportation Institute

Fayez Moutassem
Graduate Research Assistant
Texas Transportation Institute

David Trejo, P.E.
Assistant Research Engineer
Texas Transportation Institute

and

Daren B. H. Cline
Professor of Statistics
Texas A&M University

Research Report Number 0-2101-4
Research Project 0-2101
Research Project Title: Allowable Stresses and Resistance Factors for High Strength Concrete

Sponsored by the
Texas Department of Transportation
In Cooperation with the
U.S. Department of Transportation
Federal Highway Administration

November 2003

TEXAS TRANSPORTATION INSTITUTE
The Texas A&M University System
College Station, Texas 77843-3135

DISCLAIMER

The contents of this report reflect the views of the authors, who are responsible for the facts and accuracy of the data presented herein. The contents do not necessarily reflect the official view or policies of the Texas Department of Transportation (TxDOT) or the Federal Highway Administration (FHWA). This report does not constitute a standard, specification, or regulation, nor is it intended for construction, bidding, or permit purposes. Trade names were used solely for information and not for product endorsement. The engineer in charge was Mary Beth D. Hueste, P.E. (TX 89660).

ACKNOWLEDGMENTS

This project was performed in cooperation with TxDOT and the FHWA, and was conducted at Texas A&M University (TAMU) through the Texas Transportation Institute (TTI) as part of project 0-2101, "Allowable Stresses and Resistance Factors for High Strength Concrete." The authors are grateful to the individuals who were involved with this project and provided invaluable assistance, including Kenny Ozuna (TxDOT, Research Project Director), J.C. Liu (TxDOT, Research Program Coordinator), John Vogel (TxDOT), Peter Keating (TAMU), and Dennis Mertz (University of Delaware).

The authors wish to thank Andrew Fawcett, Jeff Perry and Matt Potter of the Texas Engineering Experiment Station Machining, Testing and Repair Facility at TAMU; Scott Cronauer of the Department of Civil Engineering at TAMU; and the many students who provided help throughout the experimental study. The authors also wish to thank the three precasters who participated in this study for their help and cooperation, as well as the suppliers who provided materials for the experimental study.

TABLE OF CONTENTS

Page

LIST OF FIGURES

Page

Page

Page

LIST OF TABLES

Page

1 INTRODUCTION

1.1 BACKGROUND AND PROBLEM STATEMENT

High strength concrete (HSC) is regularly used for prestressed bridge girders. The provisions for the design of prestressed concrete members according to the AASHTO Standard and LRFD Specifications are based on mechanical properties determined for normal strength concrete (NSC). HSC characteristics can differ from NSC characteristics. As such, there is a need to evaluate the characteristics of HSC and, if possible, modify existing design specifications such that potential advantages or limitations of using HSC are incorporated into the design process.

This research is part of a three phase project sponsored by the Texas Department of Transportation (TxDOT). The complete project was summarized by Hueste et al. (2003a). The first phase report focused on establishing mechanical properties for HSC mixtures typically used by Texas precasters for bridge girders (Hueste et al. 2003b). Phase 1 included testing of plant-produced concrete samples for various mechanical properties and establishing appropriate statistical parameters to describe these mechanical properties. The second phase report included a survey of current practice relevant to the use of HSC prestressed girders by state highway agencies (Hueste and Cuadros 2003). In addition, a parametric study was conducted to determine the limit states that are predominant in limiting the potential span of typical HSC prestressed girders used in Texas. This included an assessment of the benefits of using higher concrete strengths, 0.5 and 0.6 inch diameter strands, and an evaluation of differences in designs based on the AASHTO Standard and LRFD Specifications. The third phase (this report) focuses on evaluating the allowable stress limits for the design of HSC prestressed girders. This was accomplished through several tasks.

1.2 OBJECTIVES AND SCOPE

The main objective of this research is to evaluate the allowable stresses for HSC prestressed bridge girders. The effects of field exposure (curing) conditions on the compressive

strength and the flexural tensile strength of HSC were determined. The HSC mixtures tested in this study were representative of mixtures used in Phase 1 of this research program. The plant-produced samples from the earlier study were laboratory cured after the first day of exposure (approximately 24 hours). Strength adjustment factors were needed to account for the effect of the different field exposure (curing) conditions. These factors were determined for representative HSC mixtures and applied to the compressive and flexural strength data from the Phase 1 study to evaluate the potential of increasing the limiting allowable stresses. A parametric study was conducted to evaluate the impact of a modified tensile stress limit on the design of typical HSC prestressed girders. The safety of the modified tensile stress limit was evaluated by applying structural reliability theory.

The research objectives were achieved by carrying out the following tasks.

1.2.1 Task 1: Review of Literature and Current Practices

A review of literature and current practices was performed to document background information needed for this research. Background is provided for the relevant design procedures and current allowable stress limits for prestressed concrete girders. Background and literature on the application of structural reliability used in investigating the safety of structures and code calibration is also reviewed. The current practices at precast plants that produce prestressed girders are documented, including batching, mixing, transporting, placing, consolidating, and curing. Factors affecting concrete strength are briefly described, including the influence of cement, aggregates, admixtures, water-cement ratio, and exposure (curing) effects. A thorough search on concrete curing was conducted. A brief review of literature related to the maturity method, used to predict concrete strength, is also provided.

1.2.2 Task 2: Experimental Program

The HSC mixtures evaluated in this study are representative of mixtures used by the three precasters that provided plant-produced samples in Phase 1 of this research program. The plant-produced HSC samples from Phase 1 study were laboratory-cured after one day of field exposure

(curing). Because actual girders are not cured under these conditions, necessary adjustments factors are needed to account for field exposure (curing) conditions. The focus of this experimental program is to evaluate the influence of different exposure (curing) conditions on the compressive and flexural tensile strength (modulus of rupture) of HSC. These mechanical properties must be quantified to determine the potential to increase allowable stress limits, including consideration of field exposure (curing) conditions. As such, this experimental program will provide compressive strength and modulus of rupture data for standard HSC concrete specimens exposed to varying exposure (curing) conditions to determine corresponding strength adjustment factors for these conditions.

1.2.3 Task 3: Data Analysis

The data analysis for this study includes a full analysis and evaluation of the results obtained for the compressive strength and the modulus of rupture of the HSC mixtures. This involves investigation of concrete strength development with time among different exposure (curing) conditions, determination of exposure (curing) factors, statistical analysis of the effects of the variables and their interactions on the measured strengths, investigation of the goodness of fit of prediction formulas, and investigation of the accuracy of the maturity method in predicting the concrete compressive strength and modulus of rupture.

1.2.4 Task 4: Evaluation of Tensile Stress Limits

The allowable tensile stress was evaluated for the design of HSC prestressed girders. This involved determination of the appropriate curing factors to be used in modifying the compressive strength and modulus of rupture for the plant-produced samples from Phase 1 of this research. Tensile stress limits were then determined based on the adjusted mechanical properties. These tensile stress limits provide different levels of confidence such that the modulus of rupture is not exceeded.

1.2.5 Task 5: Parametric Study and Reliability Analysis

A parametric study was conducted to evaluate the impact of an increased tensile stress limit for the design of HSC prestressed girders with a Texas U54 cross-section. This study was performed for both the AASHTO Standard and LRFD Specifications (AASHTO 1999, 2000). The specified concrete compressive strengths and girder spacings were varied. The diameters considered were 0.5 inch and 0.6 inch. For each concrete strength and girder spacing, the maximum span lengths that can be attained for the code design criteria using the modified stress limit were determined. This was done by varying the number of strands in order to maximize the span lengths while ensuring that all flexural design criteria for service and ultimate conditions were satisfied. Reliability theory was then used to investigate the adequacy of the current and modified tensile stress limits for different span lengths, girder spacings, and concrete strengths by determining the probability of exceeding the modulus of rupture for a given design. Comparisons were made between the reliability index obtained using the current and revised allowable tensile stress limits for service conditions.

1.2.6 Task 6: Summary and Conclusion

Conclusions were developed based on the results obtained in this study. Recommendations for design and future research are also provided.

1.3 OUTLINE

Chapter 2 provides background on the design and production of prestressed concrete girders, the theory of structural reliability, factors affecting concrete strength, and the maturity method used in predicting concrete strength. Chapter 3 provides information on the experimental program, including materials, sample fabrication and curing, and material testing. Chapter 4 provides experimental results obtained for the compressive strength and the modulus of rupture of concrete samples subjected to different exposure (curing) conditions. Chapter 5 provides modified tensile stress limits based on the curing factors obtained from this study. Chapter 6 documents a parametric study to determine the impact of the modified tensile stress

limits on design. The results of the structural reliability study, conducted to investigate the safety of the alternate tensile stress limit relative to current practice, are included. Chapter 7 provides a summary of the research program and the conclusions and recommendations. Test data, information on the mixture proportions of the concrete tested, and other relevant information are provided in the Appendices.

2 BACKGROUND

2.1 GENERAL OVERVIEW

The following sections provide background on the design and production of prestressed concrete girders, on the theory of structural reliability, on factors affecting concrete strength, and on the methods used in predicting concrete strength.

2.2 DESIGN OF PRESTRESSED CONCRETE GIRDERS

2.2.1 Design Procedure

Flexural design of reinforced concrete members requires checking only the limit state of strength at failure (ultimate limit state), whereas flexural design of prestressed concrete members requires checking the service limit state in addition to the ultimate limit state. This section provides basic background information on the flexural design of prestressed concrete girders.

2.2.1.1 Service Limit State

Checking the service limit state is necessary to ensure that cracking of the prestressed concrete girder does not occur (Nawy 2000). Cracks in prestressed girders are not desirable because these will provide a more direct path for aggressive compounds and ions to be transported to the prestressed strands. Cracks reduce the transport time for these compounds and/or ions to reach the prestressing steel, thereby reducing the time to corrosion and service-life. For the service limit state, it is required that the tensile and compressive stresses under service loads do not exceed the corresponding allowable tensile and compressive stress limits.

Prestressed bridge girders are often designed as simply supported beams and are treated as such in this report. The following equations are used to compute the stress at the top and bottom fibers of the precast section at transfer:

$$f_t = -\frac{P_i}{A} + \frac{P_i e c_t}{I} - \frac{M_D c_t}{I} \quad (2.1)$$

$$f_b = -\frac{P_i}{A} - \frac{P i c_b}{I} + \frac{M_D c_b}{I} \quad (2.2)$$

where f_t and f_b are the stresses at the top and bottom fibers, respectively (psi), P_i is the initial prestressing force at transfer (lbs.), A is the cross-sectional area of the precast member (inch^2), e is the eccentricity of the prestressing strands from the precast section center of gravity (inch), c_t and c_b are the distances of the top and bottom concrete fibers to the center of gravity of the precast concrete cross-section (inch), I is the moment of inertia of the concrete cross-section (inch^4), and M_D is the moment due to self weight of the girder (lb-inch). The computed stresses must be within the allowable tensile and compressive stress limits given in the code.

When designing for composite bridge girders, the allowable tensile and compressive stresses must be checked at different stages. For the first stage, which is at transfer, the external moment applied is due to the weight of the beam. For the second stage, which is immediately after casting the concrete slab, the external moment is due to the weight of the beam, the weight of the slab (or deck), and other structural elements such as diaphragms. For the third and final stage, which is at service, the external moment is due to all the loads discussed in addition to the live loads.

The effective prestressing force P is the product of the cross-sectional area of the strands and the effective prestress. The effective prestress depends on the initial prestress and the prestressing losses. The initial prestress is reduced with time, and losses can be divided into immediate losses and time-dependent losses. For pre-tensioned members, the immediate losses include losses due to elastic shortening of the concrete and some steel relaxation. The time-dependent losses include losses due to creep and shrinkage of the concrete and relaxation of the steel. Once the losses are calculated, the effective prestressing stress can be calculated using Equation 2.3 (Nawy 2000).

$$f_{ps} = f_{pi} - \Delta f_{pES} - \Delta f_{pR} - \Delta f_{pCR} - \Delta f_{pSH} \quad (2.3)$$

where f_{pi} is the initial prestress (psi), Δf_{pES} is the loss due to elastic shortening (psi), Δf_{pR} is the loss due to steel relaxation (psi), Δf_{pCR} is the loss due to creep (psi), and Δf_{pSH} is the loss due to shrinkage (psi).

The allowable tensile and compressive stresses of a prestressed concrete beam must not be exceeded in order for the design to be adequate as discussed previously. The allowable tensile stresses at service, were developed based on the modulus of rupture of concrete (PCI Industry Handbook Committee 1992). The allowable tensile stress limit can vary from zero to $6\sqrt{f_c'}$ and is dependent on the severity of exposure (curing) to the environment and on local practices (PCI Industry Handbook Committee 1992). This allowable stress limit is set in order to avoid cracking and exposing the prestressing strands to aggressive environmental conditions that could result in active corrosion. Even though some researchers proposed that cracking of prestressed concrete members can be allowed, design criteria were established for fatigue and deflection control considering that cracking does not occur. Table 2.1 is a summary of the allowable stress limits from various codes.

Table 2.1. Summary of Allowable Stress Limits.

Reference	f_c (psi)		f_t (psi)	
	Initial	**Service**	**Initial**	**Service**
AASHTO Standard Specs. (1999)	$0.60 f'_{ci}$	$0.40 f'_c$	$7.5\sqrt{f'_{ci}}$ $3\sqrt{f'_{ci}}$ (1)	$6\sqrt{f'_c}$ $3\sqrt{f'_c}$ (2)
AASHTO LRFD Specs. (2000)	$0.60 f'_{ci}$	$0.45 f'_c$ (3) $0.40 f'_c$ (4) $0.60 f'_c \varphi_w$ (5)	$7\sqrt{f'_{ci}}$ $3\sqrt{f'_{ci}}$ (1)	$6\sqrt{f'_c}$ $3\sqrt{f'_c}$ (2)
ACI 318 (2002)	$0.60 f'_{ci}$	$0.45 f'_c$ (3) $0.60 f'_c$ (6)	$3\sqrt{f'_{ci}}$ $6\sqrt{f'_{ci}}$ (7)	$7.5\sqrt{f'_c}$ (8) $7.5\sqrt{f'_c}$ to $12\sqrt{f'_c}$ (9) $12\sqrt{f'_c}$ (10)

Notations:

f'_{ci} = the compressive strength of concrete at time of initial prestress (psi).
f'_c = the specified compressive strength of concrete (psi).
f_c = the allowable compressive stress limit (psi).
f_t = the allowable tensile stress limit (psi).

Notes:

(1) In tension areas with no bonded reinforcement.
(2) For corrosive exposure conditions.
(3) For effective prestress plus sustained load.
(4) For live load plus half of effective prestress and sustained loads.
(5) For sum of prestress, sustained loads, and transient loads during shipping and handling. φ_w is the slenderness ratio reduction factor.
(6) For effective prestress plus total load.
(7) At ends of simply supported members.
(8) For Class U (uncracked) members.
(9) For Class T (transition between cracked and uncracked) members.
(10) For Class C (cracked) members.

2.2.1.2 Ultimate Limit State

For the ultimate limit state, it is required that the nominal moment capacity of the beam be greater than the moment due to the applied loads. The ultimate limit state for flexure usually does not govern the design for prestressed bridge girders except for very short spans (Hueste and Cuadros 2003). However, it is a requirement that this limit state always be checked to ensure

that the capacity of the structure is adequate. Equation 2.4 is the basic equation used to ensure structural safety against flexural failure.

$$\phi M_n \geq M_u \tag{2.4}$$

where M_n is the nominal moment capacity (lb-inch), M_u is the factored moment due to applied loads (lb-inch), and ϕ is the resistance factor. The resistance factor for the flexure limit state for prestressed concrete in both the AASHTO Standard and LRFD Specification is 1.00 (AASHTO 1999, 2000).

It is also a requirement that the ultimate limit state be checked for shear so that any necessary shear reinforcement is provided to prevent shear failure. Equation 2.5 is the basic equation used to ensure structural safety against shear failure.

$$\phi V_n \geq V_u \tag{2.5}$$

where V_n is the nominal shear capacity (lbs.), V_u is the factored shear due to applied loads (lb), and ϕ is the resistance factor. The resistance factor for the shear limit state for prestressed concrete in both the AASHTO Standard and LRFD Specification is 0.90 (AASHTO 1999, 2000).

The equation used for calculating the nominal moment capacity for the simple case of a rectangular section is shown in Equation 2.6.

$$M_n = 0.85 f_c' a b \left(d - \frac{a}{2} \right) \tag{2.6}$$

where M_n is the nominal moment capacity (lb-inch), f_c' is the concrete compressive strength (psi), b is the beam width (inch), d is the beam effective depth (inch), and a is the equivalent rectangular stress block depth (inch). The equation used for calculating the nominal moment capacity for flanged sections depends on the depth of the equivalent stress block. Depending on this depth, the nominal moment capacity can be calculated based on either assuming a

rectangular or flanged section behavior. Details on the ultimate limit state for flexure and shear can be found in many prestressed concrete books, such as Nawy (2000).

2.2.2 Reliability

2.2.2.1 Background

Uncertainties always exist in the analysis and design of engineered systems. Reliability theory considers such uncertainties and assesses the probability of survival of a structure. The term "reliability" is the probability of successful performance (Haldar and Mahadevan 2000). Equation 2.7 is the basic design formula that must be met for an ultimate limit state in order for the design to be reliable (Nowak 1999).

$$\sum \gamma_i X_i < \phi R_n \tag{2.7}$$

where X_i is the design load component i, γ_i is the load factor i, R_n is the design resistance, and ϕ is the resistance factor. The safety of the structure is often expressed in terms of a reliability index β defined as:

$$\beta = -\Phi^{-1}(P_F) \tag{2.8}$$

where Φ^{-1} is the inverse standard normal distribution function, and P_F is the probability of failure of the structure (Nowak 1995).

Failure occurs when the load S applied on the structure exceeds the resistance R of the structure, i.e. when the reliability margin $m = R\text{-}S$ is negative. The reliability index for a normal distribution is determined using the following equation:

$$\beta = \frac{\mu_m}{\sigma_m} = \frac{\left(\mu_R - \mu_S\right)}{\sqrt{\left(\sigma_R{}^2 + \sigma_S{}^2\right)}} \tag{2.9}$$

where μ_m and σ_m are the mean and standard deviation of the reliability margin, respectively.

There are many techniques used to determine the reliability index β of a structure. The Monte Carlo simulation is one technique commonly used (Haldar and Mahadevan 2000). An iterative procedure based on normal approximations to non-normal distributions was used in calibrating the LRFD code (Nowak 1995). In order to determine the reliability index of a structure, it is essential to have information on the statistical properties of load and resistance. The statistical parameters needed are the mean and standard deviation of each variable in addition to the type of probability distribution that best describes the variable. The Monte Carlo simulation technique is summarized as follows (Haldar and Mahadevan 2000):

1) The problem must be defined in terms of all random variables. This means that the limit state function under investigation for structural safety must be known and its variables must all be known.

The probabilistic characteristics of the random variables must be quantified. This involves knowing the mean, standard deviation, and the type of probability distribution for each variable.

Random numbers between 0 and 1 are then generated. These random numbers are then transformed to random numbers with appropriate characteristics (x_i). This is known as the inverse cumulative distribution function (CDF) method. In this method, the CDF is equated to the generated random number u_i and then x_i is calculated using Equation 2.10 by transforming it to the appropriate distribution as follows:

$$x_i = F^{-1}{}_X(u_i) \qquad (2.10)$$

Therefore, the input for this step is the distribution and statistics for each variable, and the output is the random variable x_i.

2) Probabilistic information can then be extracted using the simulation. The Monte Carlo method consists of choosing samples of the variables according to their probability distributions and then inserting them into the limit state function. Failure occurs when the limit state function $g( ) = R\text{-}L$ is less than zero. Many simulation cycles are performed, and the limit state function is determined for each cycle. The probability of failure p_f can then be calculated using the following equation:

$$p_f = \frac{N_f}{N} \tag{2.11}$$

where N is the total number of simulation cycles, and N_f is the total number of simulation cycles when the limit state function is less than zero. The reliability index β can then be calculated using Equation 2.8.

In order to determine the sample space for each deterministic variable considered, the statistical parameters and the type of distribution are needed. For normal distribution, each value of the sample space (x_i) is obtained using the following equation (Haldar and Mahadevan 2000).

$$x_i = \mu_x + \sigma_x \Phi^{-1}(u_i) \tag{2.12}$$

where μ_x is the mean value of the variable, σ_x is the standard deviation of the variable and $\Phi^{-1}(u_i)$ is the inverse standard normal distribution function applied to random number u_i. For lognormal distributions, each value of the sample space (x_i) is obtained using the following equation (Haldar and Mahadevan 2000).

$$x_i = e^{(\mu_{ln x} + \sigma_{ln x} \Phi^{-1}(u_i))} \tag{2.13}$$

where $\mu_{ln x}$ is the mean value of the natural logarithm of the variable, and $\sigma_{ln x}$ is the standard deviation of the natural logarithm of the variable.

For a normal distribution, the mean is sometimes expressed as the following:

$$\mu_x = Bias \times Nominal \tag{2.14}$$

where $Bias$ is the bias factor defined as the ratio of the mean value of a variable to the nominal value, and $Nominal$ is the specified design value. Figure 2.1 shows the bias factors for live load moment for the AASHTO LRFD specification.

For a normal distribution, the relationship between the standard deviation σ_x and the coefficient of variation (COV) is as follows:

$$\sigma_x = COV \times \mu_x \tag{2.15}$$

For a lognormal distribution, the mean is sometimes expressed as the following:

$$\mu_{lnx} = ln(\mu_x) - \frac{1}{2}\sigma^2_{lnx} \tag{2.16}$$

For a lognormal distribution, the relationship between the standard deviation of the natural logarithm of the variable σ_{lnx} and the coefficient of variation COV_x is as follows:

$$\sigma^2_{lnx} = ln(COV^2_x + 1) \tag{2.17}$$

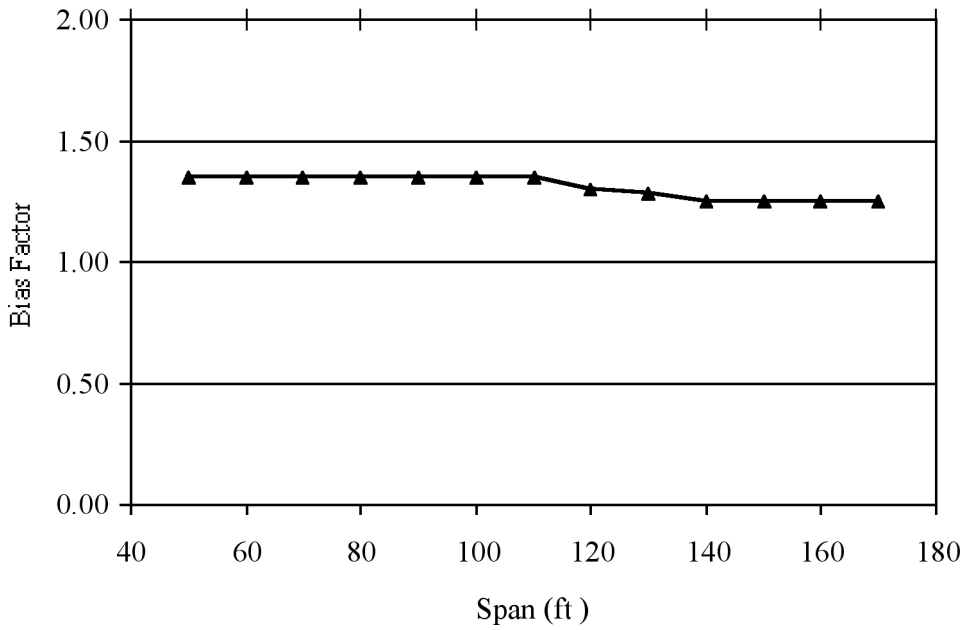

Figure 2.1. Bias Factors for Live Load Moment - AASHTO LRFD Specification (Adapted from Nowak 1995).

2.2.2.2 Literature Review

Naaman and Siriaksorn (1982) applied the Monte-Carlo simulation technique and investigated six serviceability limit states: maximum crack width, concrete fatigue, reinforcing steel fatigue, prestressing steel fatigue, live load deflection, and long term deflection. A large number of parameters were varied in order to determine their effects on the reliability index. These parameters included beam cross-sections, span lengths, magnitude of live load, and others. The methodology included the derivation of the resistance prediction equations in terms of basic variables and maximum allowable limitations, collection of statistical data for the basic variables in these equations, and selection of maximum allowable limitations from current codes. The Monte-Carlo simulation method was then applied in order to determine the reliability indices for each limit state considered.

Tabsh (1992) conducted a reliability-based parametric study on prestressed concrete bridge I and box girders. The parameters that were varied included the initial prestress, section size, and the allowable concrete stresses to determine their effects on the minimum number of strands and the reliability index. Monte Carlo simulation was used to find the statistical parameters of the resistance. However, the reliability index was determined by using the Rackwitz-Fiessler method. Loads were normally distributed, whereas resistances were lognormally distributed. The statistical parameters of the combination of dead loads and live loads were determined using Turkstra's rule. Both the statistical parameters of the dead load and the live load model developed by Nowak were used. Impact was taken to be equal to 15 percent of the live load.

Nowak (1999) conducted a reliability-based study to calibrate the LRFD code by the derivation of new load and resistance factors. These factors were derived such that the reliability of bridges is at a known and uniform level. Load and resistance variables were treated as random variables described by their statistical parameters. The Rackwitz-Fiessler iterative method was used in the reliability analysis. Reliability indices were determined for moments and shears of composite and non-composite steel girders, reinforced concrete T-beams, and prestressed concrete girders. The target reliability index used for calibration of the LRFD code was 3.5.

2.3 PRODUCTION OF PRESTRESSED GIRDERS

This section reviews the general process used by precast plants in the production process of prestressed girders. This process includes batching, mixing, transporting, placing, consolidating, and curing of concrete mixtures for precast girders. This section also includes a review of the production of prestressed concrete girders and the current practice at precast plants in the state of Texas.

2.3.1 Batching and Mixing

The precast plants visited as part of this study had on-site concrete mixers. These mixers had a typical capacity of 4 cubic yards. Most plants had at least 2 mixers. All batching was based on weight. Mixing time for most mixtures varied between 2 and 3 minutes, with most mixing times closer to two minutes.

2.3.2 Transporting

Precast concrete is typically transported in buckets carried on a forklift. The buckets are generally side casting to make the placement of the concrete in the girders forms easier for the workers. Typical bucket capacities were 4 to 6 cubic yards. In most cases, the concrete was placed into the girder forms between 3 and 5 minutes after mixing was complete. Figure 2.2 shows concrete being transferred from a bucket to the prestressed girder form.

Figure 2.2. Transportation and Placement of Concrete for Girders.

2.3.3 Placing and Consolidation

Adequate consolidation is commonly accomplished with thorough internal vibration. All plants visited as part of this research program used internal vibrators to consolidate the concrete in the prestressed girder forms.

2.3.4 Curing

Concrete curing should be done such that sufficient moisture is provided to ensure concrete hydration does not cease at an early age. In all cases observed during visits to the precast plants, curing was achieved by covering the exposed girder tops with wet burlap and/or sheathing. The formwork for the girders and sheathing are typically removed one day or less after casting. In most cases, the girders are then placed in storage with no special protection from the environment.

2.4 FACTORS AFFECTING CONCRETE STRENGTH

The strength of concrete is affected by five major factors, including cement, aggregate (type and quantity), admixtures, water-cement ratio, and exposure after casting. These factors are discussed below.

2.4.1 Cement

Cement combined with water make up the paste that hardens and binds aggregates together to form a concrete matrix. The basic materials used for manufacturing Portland cement are made of limestone and clay. Cement is manufactured using either a dry process or a wet process (Murdock and Brook 1979). The dry process involves crushing the materials, drying the materials, and finally grinding the materials in ball mills to a powder that is burnt. The wet process, which is more common, involves crushing the materials and then grinding them to form a slurry. The slurry is then pumped to a rotating kiln, which heats it until it clinkers. When the clinker cools down, it is ground to the desired fineness. The main constituents of cement are

C_3A (tricalcium aluminate), C_3S (dicalcium silicate), C_2S (tricalcium silicate), and C_4AF (tetracalcium ferroaluminates). The aluminates influence the stiffening (setting) of the concrete, while the silicates influence the strength gain. In addition, the C_3S and the C_3A constituents generate high heats of hydration at early ages, and the aluminates can also be susceptible to attack from sulfates. Thus, these constituents are commonly manipulated to produce cements for specific applications. The five main types of Portland cement are Types I through V (Popovics 1979). Table 2.2 shows the five cement types with their respective characteristics and typical applications.

The constituents react with water to produce a hardened cement paste. Hardened cement paste consists of cement gel, capillary pores, and gel pores. The cement gel is described as a consistent mass of material with water adsorbed on its surface (Meeks and Carino 1999). Capillary pores are the spaces between the masses of cement gel formed during hydration. Hydration reactions proceed through the consumption of water from these pores. Gel pores are spaces between the solid products of hydration within the cement gel. These pores are filled with water that is strongly bonded to the solids. The higher the number of these capillary and gel pores, the lower is the concrete strength. At early ages of concrete hydration, only the outer layers of cement particles hydrate. Particles of unhydrated cement will always exist but will continue absorbing moisture, producing calcium silicate hydrates and thus will continue gaining strength. This process can continue for several years, even though the rate of hydration, and thus strength gain, will decrease with time.

2.4.2 Aggregate

Concrete aggregate is often assumed to be an inert, granular, and inorganic filler material. Sand, gravel, crushed stone, and crushed slag are some examples. Although this is often not the case, for this presentation, durability issues associated with aggregates will not be addressed. Aggregates have different characteristics. These include the crushing strength, the resistance to impact, size and shape of particles, the porosity, the water absorption, and the resistance to shrinkage (Murdock and Brook 1979). The size and shape of the particles affect the bond with the cement paste. The porosity and water absorption affect the resistance to chemical and frost

attack. A No. 4 sieve usually separates the distinction between fine and coarse aggregates (Popovics 1979). The choice of suitable types of coarse and fine aggregates to be used in making concrete is very important. Making HSC typically requires a smaller maximum aggregate size when compared to normal strength concrete (NSC). In general, it is desired to use crushed aggregates because their irregular surface tends to develop a stronger mechanical bond with the hardened cement paste compared to river gravel.

Table 2.2. Summary of Cement Types, Characteristics, and Typical Applications.

Cement Type	Characteristics	Typical Application
I	No limits on principal chemical compounds.	Commonly used when no special properties are required.
II	$C_3A < 8\%$ $C_3A+C_3S < 58\%$ (optional)	Used for applications where moderate sulfate resistance or moderate heat of hydration is required.
III	$C_3A < 15\%$ and/or fine grind	Used for applications where high early strength is needed.
IV	$C_3S < 35\%$ $C_3A < 7\%$ $C_2S > 40\%$	Used for applications when low, early age heats of hydration are required. Mineral admixtures are commonly used with Type I cement to also accomplish this.
V	$C_3A < 5\%$	Used when sulfate resistance is required.

2.4.3 Admixtures

Concrete admixtures are special chemicals added to the concrete batch during mixing. Two commonly used admixtures are water-reducing and set-retarding admixtures. Water-reducing admixtures (superplasticizers) are used to reduce the amount of water required for the mixture by dispersing the cement particles and thus improve the concrete workability and the hydration process. Better particle dispersion typically results in concrete attaining a higher strength. Set-retarding admixtures are used to delay the setting time of concrete so that concrete stays workable during the entire placing period. Set-retarding admixtures are also used to keep

concrete plastic for a certain period of time so that later lifts can be positioned without the development of discontinuities in the structural unit (Popovics 1979).

2.4.4 Water-Cement Ratio

The most important factor affecting concrete strength is the relationship between the weight of the water and cement incorporated into the concrete mixture. In general, lower water-cement ratios produce higher concrete strengths. However, proper proportioning must be done to ensure workability and durability. The American Concrete Institute (ACI) Committee 211 (1993) presents certain guidelines for proportioning HSC. Having the water-cement ratio less than a critical value will result in dehydration, resulting in unhydrated cement particles that add little to the strength of the concrete. Also, water-cement ratios above a certain critical value will result in a porous microstructure with capillary pores partially filled with water. Larger pore volumes result in lower strengths.

For moderate to low water-cement ratios, as hydration proceeds and approaches completeness, the capillary pores become isolated or segmented because of the abundance of cement gel present. Abundance of the cement gel will cut off the continuous capillary pores, segmenting them. Segmentation of capillary pores is favorable in forming impermeable concrete with good durability and higher strength. Ensuring that the pores become filled and segmented can be achieved by exposing the concrete to a moist environment immediately after setting and continuing this exposure until sufficient strength (or permeability, diffusivity, etc.) has been achieved. The duration of the exposure period (or curing period) depends on the water-cement ratio, the hydration rate, and the temperature of the paste.

2.4.5 Curing and Exposure

Curing of concrete is a process by which cement matures over time as a result of continuous hydration. This can be achieved by maintaining adequate water availability, adequate and uniform temperature, and adequate time for sufficient hydration. Proper curing of concrete is extremely important in order to achieve its full potential and thus attain the desired physical

characteristics and mechanical properties. Cement hydrates by using the pore water in its capillary pores. When there is a shortage of water in these pores, hydration will slow and can terminate before full hydration. Typically, HSC has a low water content, resulting in lower availability of pore water is lower than that in conventional concrete (Haugaard and Riis 1997). Early exposure of HSC is critical because, unlike NSC, bleed water is either non-existent or only available in low quantities. The lack of sufficient bleed water can lead to cracking and lower mechanical properties.

2.4.5.2 Effect of Exposure Conditions on Strength

Carrasquillo and Carrasquillo (1988) conducting research to evaluate the effect of different early exposure (curing) conditions on the compressive and flexural strength of HSC. HSC mixtures were considered with a 28-day strength ranging from 6000 psi to 14,500 psi. Type I cement was used, and fly ash was included in some of the mixtures. They considered three exposure (curing) conditions. The first condition involved removing the specimens from their molds at 24 hours and then curing them at standard laboratory conditions. The second exposure (curing) condition involved removing the specimens from their molds at 24 hours and then applying a curing compound before storing them under ambient field conditions. The third curing condition involved removing the specimens from their molds at 24 hours and then immediately storing them under ambient field conditions (no curing compound). Ambient temperatures ranged from 80 ^{o}F to 100 ^{o}F, and the relative humidity ranged from 30 to 60 percent. Specimens cured at standard laboratory conditions were found to have higher mechanical properties than those cured under the field conditions and concluded that the curing condition influences the flexural strength much more than the compressive strength, especially for HSC. In another study, Carrasquillo et al. (1981) found that the humidity level affected HSC much more than NSC, especially for the flexural strength. They found that the dry curing to moist curing flexural strength ratio for HSC was 0.74 on average.

Cetin and Carrasquillo (1995) conducted another research study to determine the effects of varying the 1-day curing temperatures on the long-term compressive and flexural strengths of HSC. They used Type III cement, and the water-cement ratios ranged from 0.24 to 0.29. They

applied four different curing temperature regimes for a 1-day period. The maximum 1-day temperatures considered were 109 ^{o}F, 151 ^{o}F, and 190 ^{o}F. The specimens were then sealed and kept at room temperatures (73 ^{o}F) until the testing age. The main findings from the study was that an increase in the early curing temperature regime always increases the 1-day strength of concrete, but most of the times decreases the long-term strength for both compression and flexure.

Research was conducted by Maage et al. (1990) to compare air curing versus water curing procedures. The samples used were 4-inch cubes with water-cement ratios of 0.38. The laboratory specimens were removed from their molds after 24 hours and were then cured in water at a temperature of 68 ^{o}F. The other specimens were cured in air under the same conditions. Results showed that air cured specimens had a lower rate of strength gain when compared to moist-cured specimens. The researchers believed that this was because there was not sufficient moisture available to continue the hydration process. However, this was only the case at a certain temperature. When the temperature was increased for the air-cured specimens, the specimens gained strength at a higher rate due to the higher degree of hydration. Kovler et al. (1998) considered this issue in a research study. The main objective of the investigation was to study the influence of the mixture proportions and different curing conditions on the compressive strength of high performance concrete at different ages. Cubes were placed under water at 68 ^{o}F and other cubes were sealed at stored at 86 ^{o}F. The water-cement ratios evaluated were 0.25, 0.29, and 0.33. Results showed that the cubes sealed at 86 ^{o}F gave a much higher compressive strength at early ages compared with those submerged in water at 68 ^{o}F. However, their 28-day strengths were approximately the same. These results indicate that both temperature and humidity will affect the short-term and the long-term strength of concrete.

Carrasquillo et al. (1981) performed research investigating NSC of 4500 psi, medium-strength concrete of 8000 psi, and HSC of 11,000 psi with corresponding water-cement ratios of 0.70, 0.47, and 0.32, respectively at standard temperatures of 73 ^{o}F. The first curing condition involved continuous curing in a moist room with humidity ranging from 95 to 100 percent until 2 hours before testing. The second curing condition involved moist curing for 7 days before air storage at 50 percent relative humidity until 28 days. The third condition involved moist curing

for 28 days before air storage at 50 percent relative humidity for 95 days. For this test, NSC had a mean strength of 3330 psi, whereas the HSC had a mean strength of 10,210 psi. Results showed that drying affected the HSC much more than NSC, especially for the modulus of rupture. Figure 2.3 shows the strength ratio (dry/moist) versus the drying period. It can be seen that the dry to moist strength ratio for the modulus of rupture was only 74 percent.

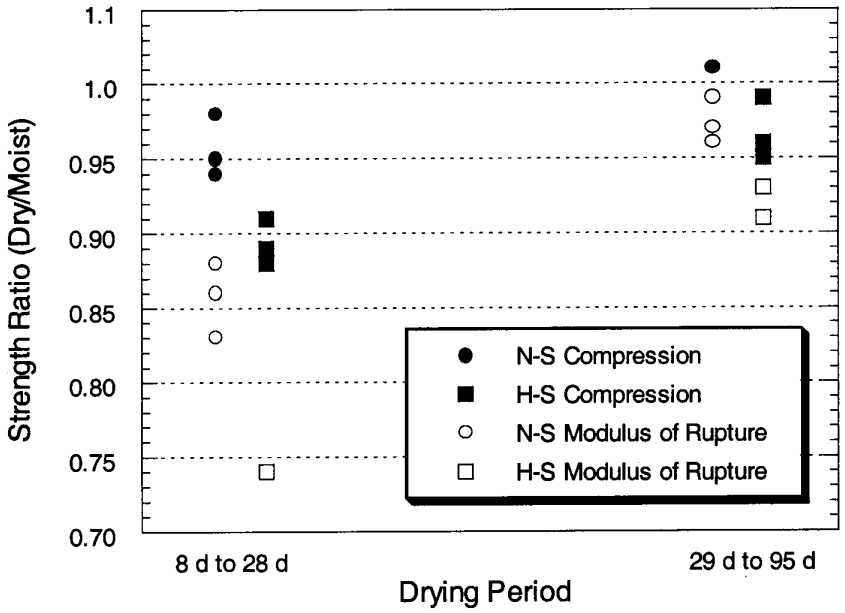

Figure 2.3. Ratio of Strength (Compression and Modulus of Rupture) after Drying to Strength for Continuous Moist Curing for NSC and HSC (Meeks and Carino 1999).

All the research studies cited show that high temperatures and low humidity reduce the long-term compressive and flexural tensile strength of HSC, with a larger reduction for the flexural strength. One limit of the results found in the literature was that none of the studies evaluated common mixture proportion and field curing conditions for HSC prestressed bridge girders made with Type III cement in the state of Texas.

2.4.5.3 Effect of Curing on Hydration

Kern et al. (1995) conducted a research program with the objective of evaluating the efficiency of different curing methods. Curing efficiency was defined as "the ability to keep the water in the concrete to guarantee high quantities of chemically bound water and thus to guarantee a high degree of hydration" (Kern et al. 1995), and curing efficiency was quantified as the ratio between the degree of hydration for a certain curing condition and the degree of hydration for 7 days under water curing at 68 ^{o}F. Both water retaining methods and water adding methods were studied. For the water adding methods, three curing conditions were studied. The first curing condition involved ponding the surface; the second curing method involved covering the surface with vapor-proof coverings, and the third curing condition involved wetting the surface by spraying water. The specimens were 8-inch cubes. Cubes were removed from their molds 24 hours after casting. Efficiency of curing was determined at 1, 3, and 7 days. It was determined that the curing efficiency was far better, especially for the first 7 days of curing, when moist coverings were used. For 1-day curing, the efficiency was approximately the same. It was concluded that evaporation occurred at the surface of the uncured specimens and thus the quantity of chemically bound water decreased in contrast with the cured specimens that showed an increase in the chemically bound water. This supports the fact that curing is extremely essential, especially for low water-cement ratios.

Bentz et al. (1997) conducted a study to determine the effects of relative humidity on hydration. The temperature was fixed at 77 ^{o}F, and the relative humidities were chosen as 90 percent, saturated, and sealed. The main conclusion was that different curing environments result in a significant effect on cement hydration. The saturated curing condition was determined to be the best method. It was also concluded that the sealed condition may be adequate for water-cement ratios greater than 0.4. Water-cement ratios lower than 0.4 for the sealed condition resulted in a large reduction in the degree of hydration.

2.5 PREDICTING CONCRETE STRENGTH

2.5.1 Background

The maturity method is widely used in predicting concrete compressive strength. In general, concrete goes through three periods (Pinto and Hover 1999). The first period is the dormant period, in which the concrete is a plastic and workable mixture. The second is the setting period, in which the concrete becomes stiff and unworkable. The third period is the hardening period, in which the concrete becomes rigid. Figure 2.4 illustrates these three periods.

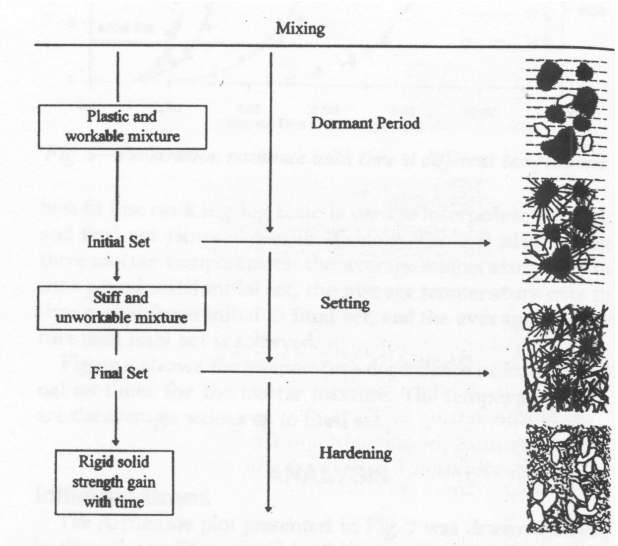

Figure 2.4. Schematic Description of Setting and Hardening of Cement Pastes (Pinto and Hover 1999).

The most critical period is the setting period, during which the concrete transitions from a fluid state to a rigid state (Pinto and Hover 1999). As soon as concrete loses it plasticity and becomes unworkable it leaves the dormant period and enters the setting period. This transition is where concrete stops behaving as a liquid and starts to behave as a solid. As hydration continues, the concrete gains the ability to support external loads. As the concrete gains strength and is able to support these external loads, it transfers from the setting period and to the hardening period.

Because the predicted strength of concrete using the maturity method is based on the hydration temperature profile, it is important to understand the five different phases of the concrete hydration (Gross and Burns 1999). In the first phase, which represents initial mixing of concrete, heat rapidly develops for a short period. This results in a minor increase in temperature. In the second phase, the concrete remains inactive in its plastic state for several hours. In this phase, the temperature remains relatively constant. In the third phase, the cement reacts vigorously with water and heat rapidly develops until it reaches a maximum rate. In this phase, the temperature increases significantly. In the fourth phase, the heat of hydration slows, with the temperature increasing until it reaches a maximum value at the end of this phase. In the fifth and last phase, the heat generation slows, and the concrete loses heat until it reaches equilibrium with the environment. For this phase, the temperature decreases until it reaches the ambient temperature. These phases are illustrated in Figure 2.5.

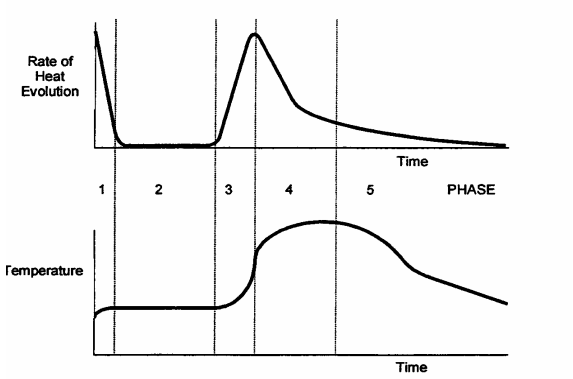

Figure 2.5. Heat Evolution and Concrete Temperature during Hydration (Gross and Burns 2000).

To measure the hydration temperature, temperature sensors can be embedded in to the structural element at certain critical locations. Critical locations correspond to those that give minimum and maximum hydration temperatures. These sensors can then be programmed to monitor the temperatures at certain intervals of time to allow determination of the time-temperature profile. These profiles can be used to determine the maturity index, which is then used to predict the concrete strength. Thermistors and thermocouples are devices used to measure the hydration temperatures.

The maturity equation is widely used due to its simplicity. The maturity index, M, is:

$$M = \sum (T - T_0)\Delta t \qquad (2.18)$$

where T is the hydration temperature, T_0 is the datum temperature, and Δt is the change in time. This equation represents the area between the concrete hydration temperature profile and the datum temperature, the temperature below which concrete cannot hydrate and is commonly reported to be 14 ^{o}F (Carino and Lew 2001). Figure 2.6 illustrates a schematic representation of the temperature history and shows the temperature-time factor.

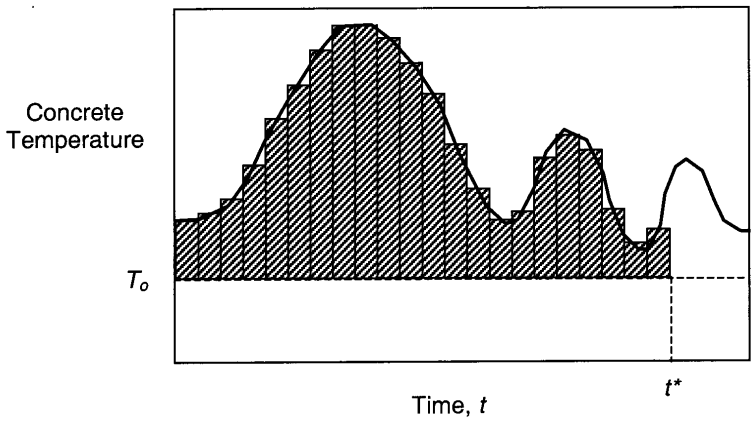

Figure 2.6. Schematic of Temperature History and the Maturity Index Computed According to the Nurse-Saul Equation (Carino and Lew 2001).

2.5.2 Application

Meyers (2000) performed an investigation of the applicability of the maturity method for high performance concrete (HPC) bridge decks. He monitored six bridge decks in Texas and investigated different mixture designs. Three critical locations were monitored in the decks using thermocouples. The first location was at the thickened slab curb; the second location was at the centerline of the deck steel, and the third location was at the support between panels. Critical locations correspond to locations that give minimum and maximum temperature development. The centerline of the deck steel resulted in the lowest temperature profile, mainly

due to the reduced concrete mass. The study found that the deeper the placement of the thermocouple, the higher the hydration temperature. Field mixture designs were tested in the laboratory. Three 4x8 inch cylindrical specimens were tested in compression at ages of 1, 3, 7, 14, 28, and 56 days, and the average strength of the three specimens at each testing day was found. The cylinders were moist-cured until the testing age. The specified compressive strength versus the field maturity at 7, 14, and 28 days gave conservative results when compared to the laboratory curve produced at 1, 3, 7, 14, 28, and 56 days. The researchers noted that higher cement contents resulted in higher hydration temperatures. Results were conservative even though the maximum hydration temperature of 100 ^{o}F was exceeded. The research indicated that the maturity method could be used for HPC.

An application of the maturity concept to determine the in-situ strength of concrete was conducted by Mukerjee in 1985 (noted by Meeks and Carino 1999). He determined the strength of field-cured concrete after correlating the maturity, which is a function of age and temperature, to strength. Thermocouples were inserted into the test sections of the slab, and additional cylinders were cast. Test tubes were installed in the slab beside the thermocouples in order to be able to remove these cylinders and test them knowing that they will have the same maturity. Results showed that the actual strengths determined by testing the cylinders were close to the predicted strengths by applying the maturity concept. Therefore, Mukerjee concluded that the maturity method was applicable for field structures.

Another application of the maturity concept to determine the in-situ strength of concrete using the maturity method was conducted by Carino (1984). The main research objective was to determine the accuracy of the maturity method in predicting concrete strength. Thermocouples were inserted into the test sections of the slab, and additional cylinders used to create the laboratory maturity curves were cast. Test tubes were installed in the slab beside the thermocouples in order to determine in-situ strength. Results showed that the actual in-situ strengths were very close to the predicted strengths by applying maturity concept.

Carino and Tank (1992) conducted research to validate the applicability of the maturity method in predicting the concrete strength while curing. Many variables were considered to

determine their effects on concrete strength, including the type of cement (I, II, and III), the curing temperature (40, 73, and 104 ^{o}F), the water-cement ratio (0.45 and 0.60), admixtures, and pozzolanic additions. Results showed that a three-parameter hyperbolic function developed in the study accurately modeled the strength gain under isothermal curing, and thus the maturity method could be used successfully for concretes with various constituents.

Kjellsen and Detwiler (1993) noted that the maturity method is inaccurate in predicting the long-term strength of concrete. Long-term strengths typically correspond to strengths exceeding 40 percent of the 28-day strength. The maturity method gives higher values of strength for higher curing temperatures because of a higher hydration profile. The research found that the maturity functions overestimated the effect of temperature on the long-term concrete strength.

A large number of research studies showed that higher initial curing temperatures result in lower later strengths. Byfors (1980) concluded that the maturity functions can be applied only at lower temperatures. This is because these functions do not consider the reduced long-term strengths due to high initial temperatures. Thus, it was concluded that there is no direct relationship between strength and the maturity. The functions developed are useful in predicting the short-term strength of concrete, and there is a further need to develop functions that predict the long-term strength of concrete based on the maturity method. Many researchers tried to explain the reason behind the resulting lower long-term strength when higher initial temperatures (Kjellsen and Detwiler 1993). However, there is general agreement that rapid hydration due to high initial temperatures obstruct the diffusion of hydration products into the bulk cement paste matrix. At higher temperatures, dense shells of hydration products form and act as diffusion barriers. Researchers agree that raising the initial temperature rapidly results in larger internal stresses, which lead to an increase in porosity and cracking. This in turn will reduce the strength potential of the concrete.

3 EXPERIMENTAL PROGRAM

3.1 RESEARCH OBJECTIVES

The main objective of this experimental research program was to determine appropriate allowable stresses for HSC prestressed bridge girders. Because field exposure (curing) conditions influence the compressive and flexural strength of HSC, an investigation was needed to determine strength adjustment factors for various exposure (curing) conditions. These strength adjustment factors were then applied to the data from the study reported by Hueste et al. (2003b) prior to making final design recommendations. In addition, the data from this experimental program were used to evaluate the applicability of the maturity method in predicting the concrete compressive and flexural strengths for different exposure (curing) conditions. After the curing factors were determined and applied to the data from the first phase of this study, a parametric study and reliability analysis was performed. The parametric study was conducted to evaluate the impact of the proposed allowable stresses on the design in terms of economy and span length. An evaluation of the safety of the proposed allowable stresses was then conducted by applying structural reliability theory. The following sections describe the experimental program.

3.2 EXPERIMENTAL RESEARCH PLAN

This study focuses on the compressive and flexural strength of HSC. Representative values of these mechanical properties are needed for recommending appropriate stress limits for design of HSC prestressed girders. The effect of field curing conditions on these properties must be considered prior to evaluating the stress limits for HSC prestressed members. Concrete strength is mainly influenced by mixture constituents (type of cement, aggregates, and admixtures), mixture proportions, size and shape of the specimens, concrete age, testing conditions, and curing conditions. This experimental program provides compressive and modulus of rupture data for standard concrete specimens exposed to varying environmental conditions for three different HSC mixtures.

3.2.1 Precaster Selection

Researcher selected three precasters that manufacture HSC prestressed bridge girders in Texas for this study (labeled as Precasters A, B, and C). These precasters are the same as those selected and used in the first phase of this study (Hueste et al. 2003b). Selection of these precasters was mainly based on their regular production of HSC prestressed bridge girders. Other issues, such as production capacities and geographical locations were also considered. Mechanical properties of the plant-produced HSC were determined in the first phase of this study. However, these specimens were exposed to field conditions for approximately 24 hours and then were transported to the laboratory and cured under standard laboratory conditions (73 ^{o}F and 100 percent relative humidity). Because actual girders are typically not exposed to these well defined exposure (curing) conditions and because it has well established that both temperature and humidity influence the mechanical properties of concrete, an investigation was required to determine the influence of temperature and humidity on the mechanical properties of HSC mixtures produced by precast plants in Texas.

3.2.2 Selection of Environmental Exposure Conditions

The first phase of this research program evaluated the mechanical properties of HSC from three precasters. The specimens evaluated in the first phase of this research program were exposed to laboratory curing conditions 24 hours after casting. As noted earlier, the exposure (curing) conditions can significantly alter the mechanical properties of concrete. As such, to provide more reliable recommendations on the design of HSC bridge girders, strength adjustment factors for concrete exposed to various field exposure (curing) conditions are needed. The research in the first phase only investigated specimens that were cured in the laboratory for 24 hours after casting. This study investigated the influence of different curing conditions on the compressive strength and modulus of rupture (flexural tensile strength) of HSC specimens. Because the objective is to determine adjustment factors for different exposure (curing) conditions, specifically for the samples evaluated in the first phase of this research program, this study used typical concrete materials and proportions used in the first study. To properly

characterize the broad range of field exposure conditions found in Texas, the exposure conditions shown in Table 3.1 were investigated.

Table 3.1. Exposure Conditions Investigated in This Study.

		Humidity	
		Low	100%
Temperature	High	-	(2)
	Room	(4)	(1), (3)

(#) represents different exposure regimes.

Because the investigation focuses on bridge girders and the temperature of these girders is elevated at early ages due to hydration reactions, samples exposed to exposure (curing) conditions 2, 3, and 4 were placed into an elevated temperature room for the first day to simulate the higher early temperatures in bridge girders. When determining the internal temperature for actual girders, thermocouples were inserted inside the structural members as soon as casting took place. The concrete hydration temperature was then recorded. The increase in the hydration temperature depends on several factors, including the ambient temperature, the mixture constituents and proportions, the size of the member, and how deep the temperature sensor is inserted. Figure 3.1 shows the hydration temperature field profiles obtained from Precaster B. As shown, the peaks range approximately from 105 to 147 ^{o}F.

Because the specimens cast in the laboratory are much smaller than the actual structural members, the hydration temperature profile will be lower for a given ambient temperature. A lower hydration temperature profile would not be expected to yield the same strength as that corresponding to the actual field profile. Thus, elevated heat curing for 1 day at a higher temperature and 100 percent humidity was used to obtain more representative temperature profiles that are in the range of the actual measured field temperature profiles. The constant temperature and humidity rooms available at Texas A&M University provided a maximum

temperature of 107 °F at 100 percent relative humidity. This curing condition was used for the first 24 hours for curing conditions 2, 3 and 4. The specimens undergoing curing conditions 3 and 4 were then transported to different environmental rooms approximately 24 hours after the concrete was cast.

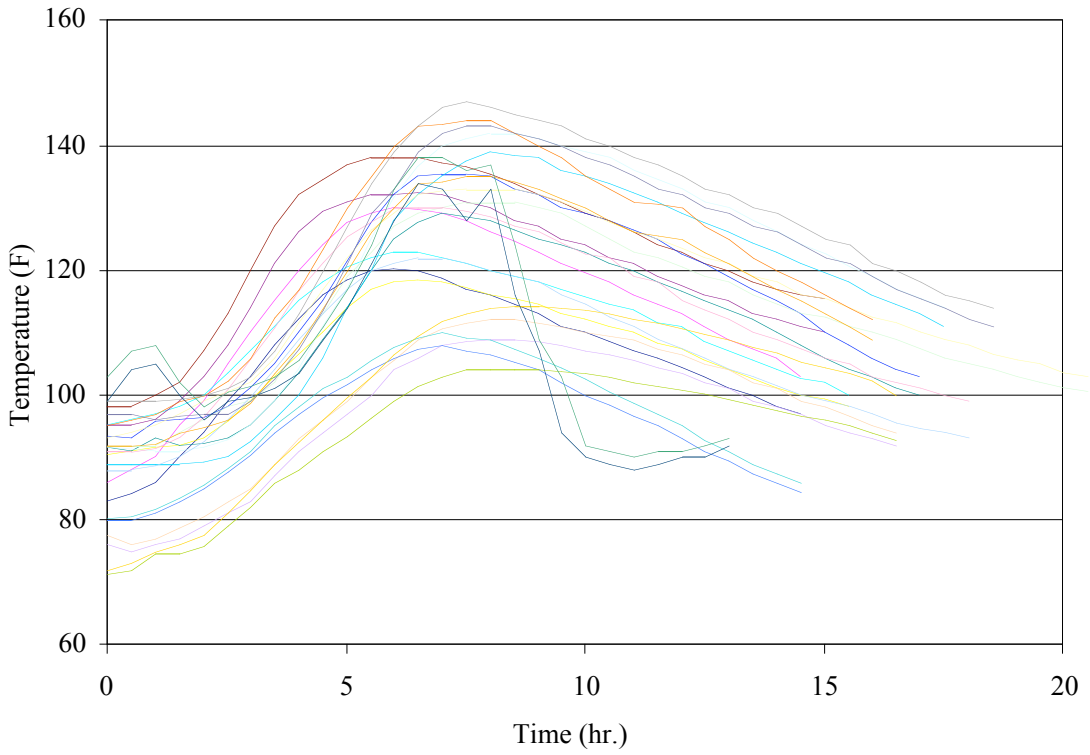

Figure 3.1. Field Hydration Temperature Profiles for Precaster B.

The environmental room conditions selected to mimic different field exposure (curing) conditions included the following:

(1) Standard: Continuous 73 °F and 100 percent relative humidity. This represents standard laboratory curing conditions following ASTM C 192/C 192M-98 (ASTM 1998a).

(2) Field 1: Continuous 107 °F and 100 percent relative humidity (HH). This exposure represents summer field conditions. This is the upper temperature

available in the environmental rooms and is reasonable because it represents typical high temperatures in Texas.

(3) Field 2: 107 ^{o}F and 100 percent relative humidity for one day followed by 73 ^{o}F and 100 percent relative humidity (RH). This represents moderate field conditions with a higher temperature for the first day due to the early heat of hydration. This curing condition was mainly chosen to determine the effect of the elevated one-day heat on the concrete compressive and flexural strengths when compared to standard laboratory conditions.

(4) Field 3: 107 ^{o}F and 100 percent relative humidity for 1 day followed by 73 ^{o}F and 30 percent relative humidity (RL) exposure. This was selected to represent field conditions with moderate temperature and low humidity.

3.2.3 Experimental Plan

Table 3.2 summarizes the experimental plan followed in this research program. For each precaster, 100 beams and 100 cylindrical specimens were cast for a representative HSC mixture for each precaster. Eight specimens of each type were used for monitoring the hydration temperatures. For each curing condition up to 1 day, the hydration temperature was monitored using two beams and two cylinders. The average temperature profiles were then determined for each pair of beams and cylinders. For each precaster and for each curing condition, testing was conducted at the ages of 1, 3, 7, 14, 28, and 56 days for both compression strength and modulus of rupture. Three specimens were tested for each age in order to reduce the effect of variability of test results by determining the batch average.

Table 3.2. Summary of the Experimental Plan.

Precaster	Curing Type	Test Ages											
		Compressive Strength						Modulus of Rupture					
		1	3	7	14	28	56	1	3	7	14	28	56
A	Standard	x	x	x	x	x	x	x	x	x	x	x	x
	HH	x	x	x	x	x	x	x	x	x	x	x	x
	RH	x	x	x	x	x	x	x	x	x	x	x	x
	RL	x	x	x	x	x	x	x	x	x	x	x	x
B	Standard	x	x	x	x	x	x	x	x	x	x	x	x
	HH	x	x	x	x	x	x	x	x	x	x	x	x
	RH	x	x	x	x	x	x	x	x	x	x	x	x
	RL	x	x	x	x	x	x	x	x	x	x	x	x
C	Standard	x	x	x	x	x	x	x	x	x	x	x	x
	HH	x	x	x	x	x	x	x	x	x	x	x	x
	RH	x	x	x	x	x	x	x	x	x	x	x	x
	RL	x	x	x	x	x	x	x	x	x	x	x	x

Standard = Standard Laboratory Conditions (73 ^{o}F and 100 percent Humidity continuously)
HH = High Temperature and High Humidity (107 ^{o}F and 100 percent Humidity continuously)
RH = Room Temperature and High Humidity (107 ^{o}F and 100 percent Humidity for 1 day, then 73 ^{o}F and 100 percent Humidity)
RL = Room Temperature and Low Humidity (107 ^{o}F and 100 percent Humidity for 1 day, then 73 ^{o}F and 30 percent Humidity)
x = Tested (3 specimens)

3.3 MATERIALS

The materials used in this testing program were representative materials used by precast plants in Texas. Each participating plant provided information on their suppliers. The suppliers provided cement, sand, coarse aggregate, and chemical admixtures to fabricate the specimens. All precasters used Type III cement and as such, this cement type was used to produce the HSC mixtures.

The two coarse aggregate types used were crushed limestone and coarse river gravel. Natural river sand was used for the fine aggregate. ASTM C566 (1997b), "Standard Test Method for Total Evaporable Moisture Content of Aggregate by Drying," was used to determine the moisture content of the coarse and fine aggregates on the day of casting. Table 3.3 summarizes the characteristics of the fine and coarse aggregates used in the testing program. TxDOT provided the absorption and specific gravity values for all aggregates.

Table 3.3. Properties of Fine and Coarse Aggregate.

Precaster	Description	Absorption (%)	Specific Gravity	Moisture Content (%)
A	Fine Aggregate (NRS)	0.66	2.63	5.39
	Coarse Aggregate (CRG)	1.09	2.59	1.17
B	Fine Aggregate (NRS)	0.89	2.60	3.69
	Coarse Aggregate (CRG)	1.97	2.62	1.83
C	Fine Aggregate (NRS)	0.34	2.62	3.59
	Coarse Aggregate (CL)	1.40	2.65	2.18

CL = Crushed Limestone
CRG = Coarse River Gravel
NRS = Natural River Sand

High range water reducers (HRWR) and retarders were used by all precasters and were incorporated into the mixtures evaluated in this program. The HRWR reduces the amount of water required for the mixture and to improve the concrete workability and dispersion of the cement grains, which results in higher strengths. Set retarding admixtures were used to delay the setting time of concrete to prevent early setting. Table 3.4 summarizes the properties of the admixtures.

Table 3.4. Admixture Characteristics.

Precasters	Admixtures	Types	% Solids	Specific Gravity
A	Retarder	Pozzolith 300R	43	1.24
	HRWR	Rheobuild 1000	43	1.20
B	Retarder	Daratard	50	1.17
	HRWR	Daracem	40	1.20
C	Retarder	NR Boral	43	1.22
	HRWR	SP150	43	1.22

The mixture proportions used for each precaster are shown in Table 3.5. These mixture proportions were selected because these are the precasters' typical mixtures for prestressed girders that require compressive strengths from 6000 to 9000 psi. In addition, these proportions were used for at least some of the sample collections in Phase 1 of this research project (Hueste et al. 2003b). Moisture adjustments for the free water in the aggregates were made for all mixtures.

Table 3.5. Mixture Proportions.

Precaster	Coarse Agg (pcy)	Fine Agg (pcy)	Cement (pcy)	Water (pcy)	W/C	Retarder (oz/cwt)	HRWR (oz/cwt)
A	1989	1214	705	197	0.28	3.5	29.0
B	1998	1369	658	224	0.34	3.0	15.0
C	1837	1464	658	223	0.34	3.0	20.0

3.4 SAMPLE FABRICATION AND CURING

When preparing for mixing and casting the representative HSC mixture for each precaster, certain important issues were addressed. These issues included determining the appropriate mixture proportions, adjusting the mixture proportions, choosing the mixing process, and monitoring the conditions in the different temperature and humidity-controlled rooms. Proper casting is very important in order for the concrete samples to be in good condition for testing and thus give reliable results. Proper curing according to the experimental program was also critical to meet the objectives of this study. Specimen casting followed ASTM C31/C31M-98 (1998b). The following sections address all of these issues.

3.4.1 Mixing Procedure

All specimens were cast at Texas A&M University because it was necessary to transport the specimens to the temperature and humidity controlled rooms immediately after casting. Since the three precasters are several hours away from Texas A&M University, researchers decided to procure the fine and coarse aggregates used by each precaster and store them at a

nearby ready-mix plant. These aggregates were then used for making the concrete mixtures needed for this study.

Researchers planned to make all the specimens for each precaster from one concrete batch to avoid variations due to different batches. The volume of concrete needed for the 200 specimens exceeded the volume that could be mixed in the laboratory. The researchers were concerned about the possible extended transport times from the ready-mix plant to the University's laboratory and the potential for the concrete to lose its fluidity and workability. The ready-mix plant is approximately 30 to 45 minutes away from the laboratory and approximately 2 hours are needed to cast 100 beams and 100 cylinders. To avoid potential early setting and to determine the crew required to cast the concrete, the setting time of the concrete followed AASHTO T 197 (2002), "Time of Setting of Concrete Mixtures by Penetration Resistance" was evaluated prior to casting. The setting time was performed to determine whether it was acceptable to mix the concrete at the ready-mix plant or if it should be mixed at the University's laboratory. The setting time for a Type III cement paste with a water-to-cement ratio (w/c) of 0.28 was 104 minutes while that of a w/c of 0.34 was 147 minutes. Because the setting time of concrete was relatively short, it was decided to perform mixing at the University laboratory.

It is important to note that no retarder was used when performing the concrete setting test. Although retarders increase the setting time of concrete, it was expected that the ambient temperature would be higher than the laboratory temperature at which the setting test was performed, so the setting time should be less. Therefore, it was assumed that the increase in the setting time due to the use of a retarder is offset by the decrease in the setting time due to higher ambient temperatures.

The concrete mixing process used at the laboratory was as follows:

1. Samples of the coarse and fine aggregates were taken to the university laboratory on the day of casting to determine the moisture contents of both aggregates. Necessary water adjustments were made.
2. The coarse and fine aggregates were batched at the ready-mix plant and loaded in the ready-mix truck.

3. A portion of the water (approximately 60 percent of the total) was added to the ready-mix truck at the plant.

4. The aggregate and water mixture were transported to the University laboratory.

5. The retarder, mixed with three gallons of water that had been held back, was added to the drum and mixed for approximately 2 minutes.

6. The Type III cement was added gradually along with the remaining water.

7. The mixture was mixed for approximately 100 revolutions.

8. The HRWR, mixed with five gallons of water that had been held back, was then added.

9. The drum was then rotated until the HRWR took effect and the fluidity was visibly improved.

10. The slump was evaluated immediately after the concrete seemed visibly workable. If the slump was low, additional HRWR was added (with a small amount of water) up to the maximum amount used by the precaster.

3.4.2 Exposure Conditions

Four different temperature and humidity-controlled rooms maintained the four selected exposure conditions. For the 107 ^{o}F and 100 percent relative humidity moisture room, a steam humidifier was installed in addition to the existing sprayer to ensure 100 percent relative humidity at all locations in the moisture room. The researchers noticed that when the relative humidity was increased the temperature decreased. This is because the temperature of the added moisture was lower than the ambient temperature. The temperature was increased, and the moisture room was monitored to ensure stable conditions.

For the 73 ^{o}F and 30 percent relative humidity moisture room, a dehumidifier was installed. This dehumidifier reduces the room humidity by removing the moisture in the room and converting it to water. When the dehumidifier was installed, the temperature of the room decreased slightly, as a result of ice formation on the coils of the dehumidifier. Monitoring was done throughout the curing process to ensure stable conditions in all curing rooms.

In order to validate the curing procedure prior to casting a large number of samples, two samples (one cylinder and one beam) were cast, and the hydration temperatures were monitored using the selected thermocouples and data loggers. The recorded temperatures gave a reasonable representation of the recorded temperatures provided by the precasters for actual bridge girders.

Concrete strength depends, in part, on the curing or exposure conditions. Thus, it is important to be consistent with the curing methods and typical exposure conditions experienced by all precasters. After the cylindrical specimens were cast for the last two precasters, they were covered with plastic lids and transported to the moisture rooms. They were covered with plastic lids to prevent the cylindrical specimen tops from becoming oblique during transport. The lids were not used for the first casting (Precaster B). Beams were placed in the moisture rooms and then immediately covered with plastic sheets to prevent loss of moisture and also to prevent additional moisture in the room from setting on fresh concrete and weakening the top face of the specimens. A total of 75 beams and 75 cylinders were transported to the high temperature (107 ^{o}F) and high humidity (100 percent) moisture room and were subjected to elevated heat curing to stimulate field conditions for all precasters mixtures. The remaining 25 beams and 25 cylinders were transported to the normal temperature (73 ^{o}F) and high humidity (100 percent) moisture room for laboratory curing for all precasters' mixtures.

3.4.3 Specimen Fabrication

During casting, the ambient temperature was recorded. In addition, the air content and the slump were measured and recorded for each precaster. The main tools used in making the concrete test specimens included molds, tamping rods, vibrators, slump apparatus, air content apparatus, and temperature measuring devices following ASTM C 31/C 31M (1998). Beams were consolidated using an external vibrator with a 1-inch head. Finally, additional concrete was removed, and the surface was evened and smoothly flattened using a trowel. The total casting time of 100 beams and 100 cylinders took approximately 1 hour.

All specimens were demolded and labeled 1 day after casting took place except for the Precaster B. For Precaster B, demolding took a total of 5 days. However, this issue was

resolved for the last two castings. A total of 50 beam and 50 cylinder specimens were then transported to two moisture rooms (25 to each room) with different curing conditions. Three cylindrical specimens were randomly selected from each of the four moisture rooms 1 day before testing. The cylindrical specimen ends were ground using a grinding machine in order to remove the end imperfections and to improve the perpendicularity of each specimen. During grinding, specimens were kept moist by spraying water on them. The low-humidity specimens were not sprayed. Immediately after grinding, the specimens were placed back in their proper exposure rooms. Beams cured under standard laboratory conditions were placed in water saturated with calcium hydroxide. For each testing age, a total of 12 cylinders and 12 beams were tested, with three cylinders and three beams from each of the four moisture rooms. During testing, the specimens that were supposed to remain at 100 percent relative humidity were kept moist by spraying them with water.

3.5 MATERIAL TESTING

3.5.1 Early Age Concrete Characteristics

After the concrete was mixed, the slump was measured following AASHTO T 119 (2002); the unit weight was determined following AASHTO T 121 (2002), and the air content was determined following AASHTO T 152. The slump apparatus, shown in Figure 3.2, was used to determine the slump of fresh concrete. The unit weight apparatus, shown in Figure 3.3, was used to determine the unit weight of concrete. The air content apparatus, shown in Figure 3.4, was used to determine the percentage of air trapped in fresh concrete. The results obtained are presented in Chapter 4.

Figure 3.2. Slump Cone Apparatus.

Figure 3.3. Unit Weight Apparatus.

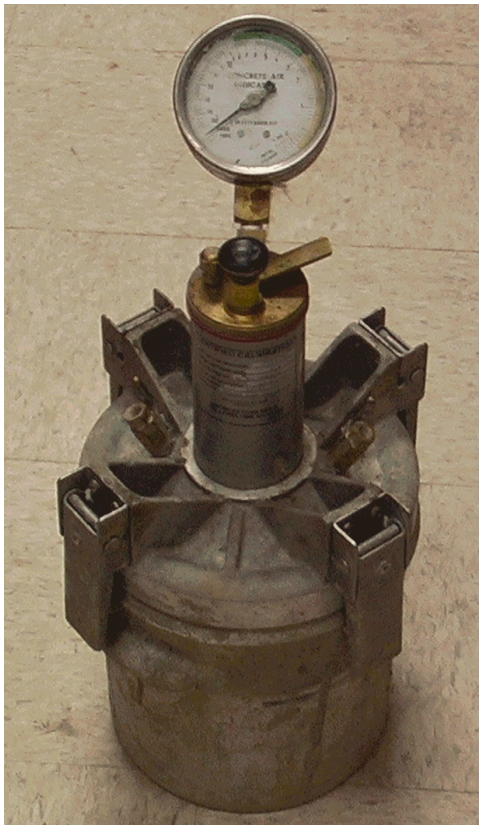

Figure 3.4. Air Content Apparatus.

Thermocouples connected to data loggers were used to record the internal temperature of the concrete specimens during hydration. The data logger used in the study was a HI98804 model manufactured by Hanna Instruments. This data logger, shown in Figure 3.5, contains four separate channels. The recorded data can either be printed or retrieved electronically using a software package included with the system. After the specimens were cast, the tip of the thermocouple was inserted into the center of the fresh concrete for both specimen types. The data logger was then set to record data at five-minute time intervals. One instrument was used for each curing condition, with two cylinder and two beam samples monitored in each room for a week.

Figure 3.5. Data Logger

3.5.2 Hardened Concrete Characteristics

3.5.2.1 Compressive Strength

The compressive strength values of the HSC samples were determined using 4x8 inch cylindrical specimens. This size was selected mainly because all precasters used this specimen size for testing, and it is consistent with the specimen size for the Phase 1 research.

A 500 kip MTS machine was used to test the samples for compressive strength. This machine is hydraulically controlled and can be used in displacement or load control mode. ASTM C39/C 39M-01 (2001) was followed when testing for concrete compressive strength. The loading rate was 35 psi/s, as specified by the standard. Testing was done at the ages of 1, 3, 7, 14, 28, and 56 days for all four different curing conditions. Three cylinder specimens were tested in compression for each curing condition, each precaster, and on each testing day. The acceptable range for three testing results was 7.8 percent.

Neoprene pads and steel rings were used together at the ends of the cylinders during the compression tests (see Fig. 3.6). Neoprene caps were used instead of sulfur caps because Hueste et al. (2003b) determined in Phase 1 that sulfur caps underestimated the compressive strength and did not give consistent results. Even though the specimens' ends were ground smooth, the neoprene pads helped eliminate the effect of the irregularities of the concrete surface during testing. ASTM C 2240-00 (2000) requires the neoprene pads to have a durometer hardness of 70 when testing for specimens with compressive strengths ranging from 4000 to 12,000 psi. The neoprene pads were changed whenever they were damaged or worn.

Figure 3.6. Neoprene Pad and Steel Retaining Ring.

Figure 3.7 shows a cylindrical specimen capped with neoprene pads in steel retaining rings and being tested in a 500 kip MTS machine. The preferred type of failure is a cone failure. Since the energy stored in the neoprene pads is released when the specimen breaks, a cone failure rarely occurs (Hueste et al. 2003b). Figure 3.8 shows a specimen with a cone type of failure.

Figure 3.7. Compressive Strength Test.

Figure 3.8. Compression Cone Failure.

The grinding wheel described earlier, shown in Figure 3.9, was used to grind the hardened cylindrical specimens in order to eliminate the specimen inclination such that all faces are perpendicular to each other. A jig was fabricated to help maintain perpendicularity between the cylinder sides and ends. Specimens were ground using silicon carbide grinding powder.

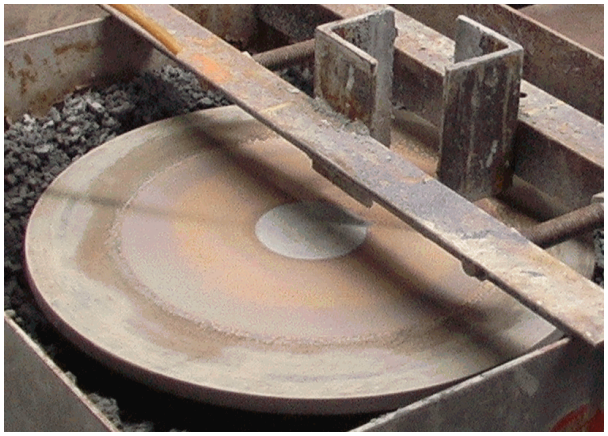

Figure 3.9. Grinding Wheel.

3.5.2.2 Modulus of Rupture

The flexural strength of HSC was determined using 6 x 6 x 20 inch prism specimens. This specimen is the smallest size permitted by the ASTM standard C 31/C 31M (1998b) for making and curing concrete test specimens in the field, yet meets all requirements for this study.

A 20 kip MTS machine was used to test for the modulus of rupture (MOR). This machine is hydraulically controlled and can be used in displacement or load control mode. ASTM C78-94 (1998c) was followed when testing for the MOR. Testing was done at the ages of 1, 3, 7, 14, 28, and 56 days for all four different curing conditions. Three specimens were tested for each curing condition on each testing day. All the beam specimens that were cured continuously under standard laboratory conditions were submerged in a saturated lime solution for 1 day before the testing age as specified by ASTM C78 (1998c). Beam specimens that were cured under different field conditions were not submerged in a lime bath prior to testing. A loading rate of 150 psi/min was used as specified by the standard. Figure 3.10 shows a beam specimen being tested in the 20 kip MTS machine. Figure 3.11 shows a typical flexural failure.

The load was applied at the third points of the beam. Before failure, the length of the beam was recorded and after failure the cross-sectional dimensions at three different locations along the length of the beam were recorded. The average cross-sectional dimensions were used to more accurately determine the actual dimensions used in calculating the MOR. The distance

from beam end to crack was also recorded. The modulus of rupture is calculated using the following equation.

$$R = \frac{PL}{bd^2} \qquad (3.1)$$

where R is the MOR (flexural strength, psi), P is the maximum load exerted on the beam (lb), L is the span length of the beam (inches), b is the average width of the beam (inches), and d is the average depth of the beam (inches). The acceptable range for two testing results is 16 percent based on the ASTM standard.

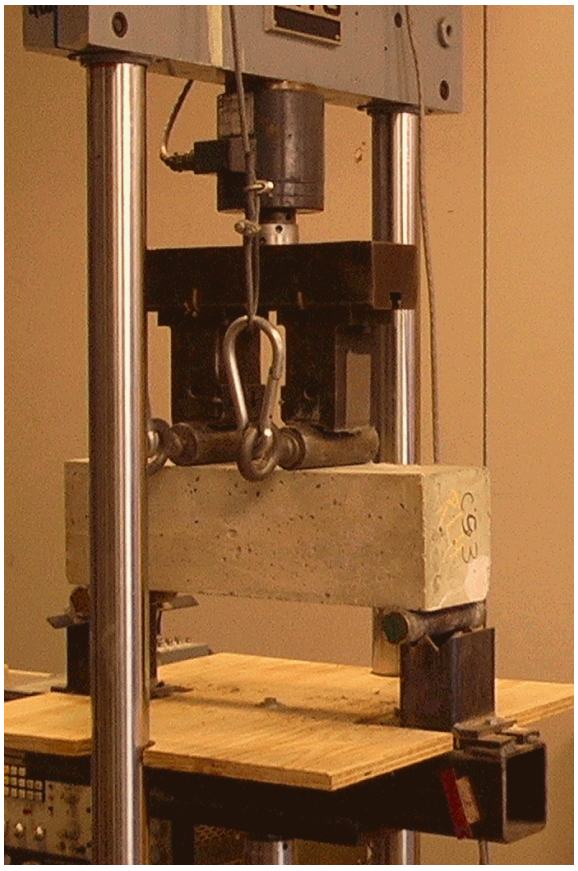

Figure 3.10. The Modulus of Rupture Test.

Figure 3.11. Flexural Failure.

4 EXPERIMENTAL RESULTS, ANALYSIS, AND DISCUSSION

4.1 GENERAL OVERVIEW

This section includes an analysis and discussion of the results obtained from the compressive strength and the MOR testing program of HSC. This includes an investigation of the concrete strength development for different early exposure (curing) conditions, determination of environmental exposure (curing) factors, statistical analysis of the effects of the variables and their interactions on the measured response, investigation of the goodness of fit of prediction formulas, and an investigation of the accuracy of the maturity method in predicting the concrete compressive strength and MOR for the different environmental exposure (curing) conditions.

4.2 ANALYSIS OF DATA

In this section, the equations and methodologies used for data analysis are presented and discussed.

4.2.1 Development of Strength with Time

The rate at which concrete develops strength and the strength potential that concrete can attain depends in part on the exposure (curing) conditions, including both the temperature and humidity. Strength development is often reported as a ratio of the strength at the age considered to the 28-day strength. The results for compressive strength development obtained from this study will be compared with those predicted by Equation (4.1), which was recommended by ACI Committee 209 (1992):

$$(f_c')_t = \frac{t}{a+\beta t}(f_c')_{28} \qquad (4.1)$$

where $(f_c')_t$ is the compressive strength at time t (days), $(f_c')_{28}$ is the compressive strength at 28 days, and a and β are constants. The parameters a and β for Type III cement and moist-cured concrete were used and are 2.3 and 0.92, respectively.

4.2.2 Statistical Data Analysis

The objective for performing a statistical analysis is to determine the effects of certain factors considered in this study on the measured response. These factors are the precasters, the exposure (curing) conditions, and the concrete age. The primary response variable is the batch average. The appropriate distribution to describe the batch average data was determined by plotting the data using a quantile plot. For this study, normal and lognormal distributions were evaluated. Differences between each data point within a batch and the batch were plotted for the normal distribution. Differences between the logarithm of each data point within a batch and the logarithm of the batch average were plotted for the lognormal distribution.

SAS (1999) software was used to perform the statistical data analysis. Because there are three factors considered, the model for the three-factor factorial design with interactions was applied. This analysis has one replication and, as a consequence, the three-way interaction is assumed not to exist. Details of this analysis can be found in many statistical books, such as Milton and Arnold (1995). Performing this statistical analysis determines which factors result in significant effects on the mean value of the variable. The statistic used to test for these effects is F_{Effect}, given by the following equation:

$$F_{Effect} = \frac{MS_{Effect}}{MS_{Error}} = \frac{\frac{SS_{Effect}}{DF_{Effect}}}{\frac{SS_{Error}}{DF_{Error}}} \qquad (4.2)$$

where F_{Effect} is the test statistic, MS_{Effect} is the mean square of the effect, MS_{Error} is the mean square of the error, SS_{Effect} is the sum of the squares of the effect, SS_{Error} is the sum of the squares of errors, DF_{Effect} is the number of degrees of freedom for the effects, and DF_{Error} is the number

of degrees of freedom for the errors. The F_{Effect} term has the distribution shown in Figure 4.1. The distribution shown is expressed using the probability density function (PDF). Large values for F_{Effect} indicate a small p-value, which is the shaded area on the right of the value of F_{Effect}, as shown. P-values below 0.05 (5 percent) are considered significant in this analysis and so any factor or interaction of factors resulting in a p-value less than 0.05 is significant.

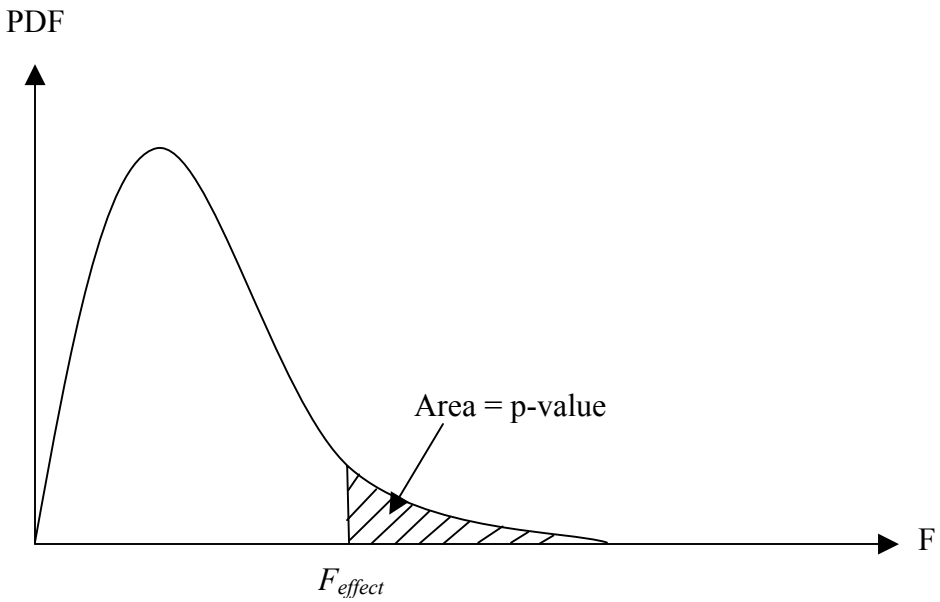

Figure 4.1. Probability Density Function for F.

The results of the statistical data analysis are summarized in an analysis of variance (ANOVA) table. Table 4.1 is a typical ANOVA table created by SAS. In this example, the logarithm of the batch average (denoted as LogBAvg) is the dependent variable. The factors and interaction of factors considered include: "Curing", "Precaster", "Age", "Precaster × Age", "Precaster × Curing", and "Curing × Age". Note that the term curing refers to the early exposure (curing) environmental condition.

The Pr>F column in Table 4.1 refers to the p-values for the tests of the corresponding effects. As shown, a p-value for "Curing" less than 0.05 indicates that the strength (which is logBavg) is influenced by the different exposure conditions. A p-value for "Precaster" less than 0.05 indicates that the strength is significantly different among precasters. A p-value for "Age" less than 0.05 indicates that strength is different among ages. A p-value for "Precaster × Age"

greater than 0.05 indicates that the compressive strength is not influenced differently for different ages among precasters. A p-value for "Precaster × Curing" less than 0.05 means that the strength is significantly influenced by the different exposure (curing) conditions among precasters. Finally, a p-value for "Curing × Age" less than 0.05 indicates that strength is significantly influenced by age for the different exposure (curing) conditions.

Table 4.1. Example of an ANOVA Table.

Source	DF	Sum of Squares	Mean Square	F Value	Pr > F
Model	41	0.31489099	0.00768027	32.69	<0.0001
Error	30	0.00704798	0.00023493		
Corrected Total	71	0.32193897			

R-Square	Coeff Var	Root MSE	LogBAvg Mean
0.978108	0.389006	0.015328	3.940177

Source	DF	Type III SS	Mean Square	F Value	Pr > F
Curing	3	0.003557	0.001186	5.05	0.006
Precaster	2	0.126429	0.063215	269.08	<0.0001
Age	5	0.158017	0.031603	134.52	<0.0001
Precaster x Age	10	0.001024	0.000102	0.44	0.9168
Precaster x Curing	6	0.009451	0.001575	6.70	0.0001
Curing x Age	15	0.016413	0.001094	4.66	0.0002

If it is desired to determine the variance among specific factors considered important in the analysis, such as among the field exposure (curing) conditions, a reduced model can be generated and tested. In order to test for the significance of the specific factors considered, results from the full model and the reduced model are used to determine a new p-value. The equation used in determining the new F statistic is:

$$F = \frac{\frac{SS_{Test}}{DF_{Test}}}{\frac{SS_{FullError}}{DF_{FullError}}} \tag{4.3}$$

where SS_{Test} is the difference between the sum of squares of effects for the full and the reduced model, DF_{Test} is the difference between the number of degrees of freedom of effects for the full and reduced model, and $SS_{FullError}$ and $DF_{FullError}$ are the sum of squares for the full model only.

The sum of squares for the full model represents all the variations observed in the data. Part of this variation is due to the effects of the conditions, and the other part is random. Since the $SS_{FullError}$ is purely random, it must be the denominator. The sum of squares for the full model consists of three parts: the variation that is a result of the reduced model, the variation that is the result of the difference (if any) between the reduced and the full model and some randomness. By computing SS_{Test} one is attempting to obtain only the difference part. However, some randomness is also obtained along with it, which cannot be excluded. Hence, the comparison to the MS_{Error} is completed.

4.2.3 Prediction Formulas

Many prediction formulas for the MOR have been developed and recommended. The goodness of fit of a number of prediction formulas was investigated by comparing them with the data obtained from this study for each of the four different exposure (curing) conditions. Table 4.2 is a summary of the recommended formulas under investigation.

Table 4.2. Summary of Prediction Formulas.

Reference	Formulas	Comments
AASHTO LRFD Specification (2000) and ACI Committee 318 (2002)	$f_r = 7.5\sqrt{f_c'}$	All ranges of strength (psi)
ACI Committee 363 (1997) and Carrasquillo et al. (1981)	$f_r = 11.7\sqrt{f_c'}$	$f_c' > 3000$ psi $f_c' < 12{,}000$ psi
Raphael (1984) and Ahmad and Shah (1984)	$f_r = 2.3 f_c'^{2/3}$	$f_c' < 12{,}000$ psi
Burg and Ost (1992)	$f_r = 12.4\sqrt{f_c'}$	For moist-cured Specimens (psi)
CEB-FIP (1993)	$f_r = 1.40 \frac{1 + 1.5(h_b / h_0)^{0.7}}{1.5(h_b / h_0)^{0.7}} \left(\frac{f_c' - 8^{2/3}}{10} \right)$	All ranges of strength (MPa)
Khayat et al. (1995)	$f_r = 0.23 + 0.12 f_c' - 2.18 \times 10^{-4} (f_c')^2$	All ranges of strength (MPa)
Cetin and Carrasquillo (1995)	$f_r = 940 (f_c')^{1/2}$	(f_c' in MPa) (f_r in kPa)

4.3 EARLY AGE CONCRETE CHARACTERISTICS

Table 4.3 shows the results obtained for the early age characteristics of concrete. The air content for precaster C was not evaluated.

Table 4.3. Early Age Concrete Characteristics.

Precaster	Slump (inch)	Unit Weight (lb/ft^3)	Air Content (%)
A	8.25	77.5	1.4
B	9.00	77.4	0.4
C	4.75	75.1	---

4.4 ANALYSIS FOR COMPRESSIVE STRENGTH

4.4.1 Development of Strength with Time

Table 4.4 is a summary of the ratio of the average compressive strength (from three samples) at different testing ages to the corresponding average 28-day compressive strength. These strength ratios are provided for all exposure (curing) conditions and precasters. Actual data for all compressive strength samples are shown in Appendix B.

The average 1-day compressive strength values under standard curing conditions for all precasters on average is 67 percent of the 28-day strength. The average 7-day compressive strength is 89 percent of the 28-day strength. Concrete subjected to 1-day elevated heat exposure resulted in higher strength ratios for the early ages. On average, concrete attained 97 percent of its 28-day strength at 7 days when continuously cured at 107 ^{o}F and 100 percent relative humidity (HH). This is because elevated temperatures accelerate the hydration process such that concrete gains strength more quickly at early ages. However, the 28-day strength is lower for the HH exposure condition when compared to concrete cured under standard laboratory conditions.

Elevated exposure with high initial temperatures for 1 day followed by curing at the standard temperature (73 ^{o}F) also results in earlier strength gains compared to standard curing

conditions. However, lower strength ratios were observed when compared with specimens continuously cured at high temperatures. For this study, the longer the concrete was cured under high temperature conditions, the faster the concrete gained compressive strength with time. However, the longer-term strength was lower. It is clear from this study that the rate of strength gain for all exposure conditions is higher than that predicted by ACI Committee 209 (1992). The prediction equation seems to provide a conservative prediction of strength gain when compared to the data from this study. One reason may be concrete mixtures' superplasticizer disperses the cement particles, resulting in a faster rate of hydration.

Table 4.4. Ratio of Compressive Strength to 28-Day Compressive Strength.

Precaster	Exposure Condition	Age					
		1 Day	3 Days	7 Days	14 Days	28 Days	56 Days
A	Standard	0.58	0.78	0.88	0.92	1.00	1.07
	HH	0.80	0.90	0.96	0.96	1.00	0.98
	RH	0.79	0.83	0.92	0.96	1.00	1.06
	RL	0.77	0.85	0.90	0.91	1.00	0.92
B	Standard	0.68	0.78	0.88	0.97	1.00	1.09
	HH	0.77	0.88	0.99	0.98	1.00	1.04
	RH	0.79	0.86	0.87	0.97	1.00	1.08
	RL	0.80	0.91	0.92	0.99	1.00	0.99
C	Standard	0.74	0.83	0.90	0.94	1.00	1.05
	HH	0.77	0.91	0.95	0.98	1.00	1.02
	RH	0.79	0.85	0.90	0.99	1.00	1.05
	RL	0.75	0.86	0.95	0.99	1.00	1.01
All Precasters	Standard	0.67	0.80	0.89	0.95	1.00	1.07
	HH	0.78	0.90	0.97	0.98	1.00	1.01
	RH	0.79	0.85	0.90	0.97	1.00	1.06
	RL	0.77	0.87	0.92	0.96	1.00	0.97
ACI 209 Predicted	Standard	0.31	0.59	0.80	0.92	1.00	1.04

Standard = Standard Laboratory Conditions (73 ^{o}F and 100 percent humidity continuously)
HH = High Temperature and High Humidity (107 ^{o}F and 100 percent humidity continuously)
RH = Room Temperature and High Humidity (107 ^{o}F and 100 percent humidity for 1 day, then 73 ^{o}F and 100 percent humidity)
RL = Room Temperature and Low Humidity (107 ^{o}F and 100 percent humidity for 1 day, then 73 ^{o}F and 30 percent humidity)

Figure 4.2 shows the development of compressive strength with time for all exposure (curing) conditions with a separate graph for each precaster. For precasters A and C, the compressive strength for samples cured under standard laboratory conditions resulted in higher strengths beyond 7 days compared to concrete subjected to continuous elevated heat exposure. Again, this supports the observation that elevated heat exposure lowers the long-term strength. For Precaster B, samples cured under standard laboratory conditions resulted in higher strengths beyond 14 days compared to concrete subjected to continuous elevated heat exposure.

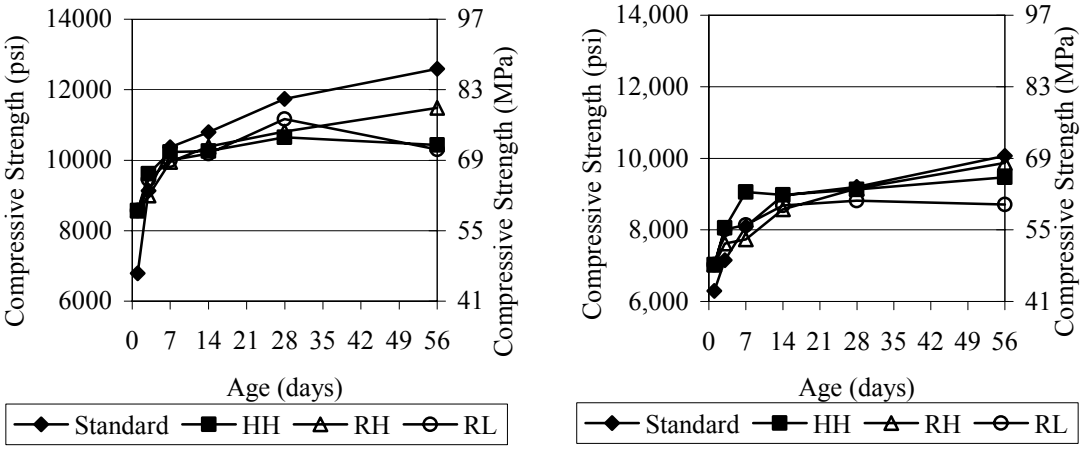

(a) Precaster A

(b) Precaster B

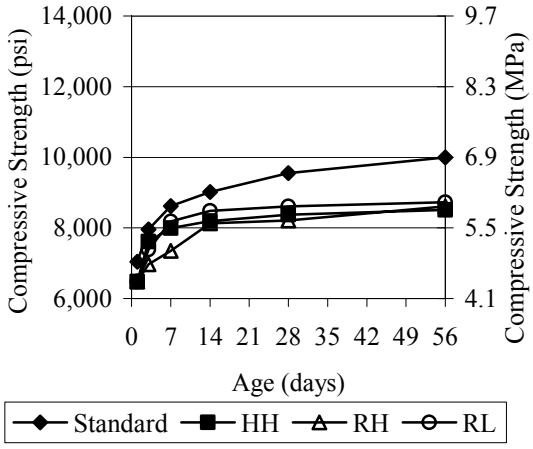

(c) Precaster C

Figure 4.2. Development of Compressive Strength with Time (by Precaster).

Figure 4.3 shows the development of compressive strength with time for all precasters, with a separate graph for each exposure (curing) condition. For all exposure conditions, it is

clear that the Precaster A mixture resulted in the highest compressive strength. This is because it has a lower water-cement ratio and a higher amount of the HRWR admixture that resulted in higher compressive strengths compared with the other two precasters. The mixtures from Precasters B and C had the same water-cement ratio, but different cement and admixture suppliers and different coarse aggregate types. In Figure 4.3(a), for standard curing conditions, the Precaster B mixture had the lowest strength, unlike the three field exposure conditions where the concrete from the Precaster C mixture resulted in the lowest strength. The elevated exposure temperature of the Precaster C mixture influenced the long-term strength more than it influenced Precaster B. In Fig. 4.3 (b), where the concrete was subjected to a continuous elevated temperature, Precaster C seems to give strengths that are significantly lower than Precaster B. However, smaller differences are observed up to 14 days in Fig. 4.3 (c) and (d) where the concrete was subjected to elevated heat exposure 1 day only. The strengths are lower for Precaster C at 28 and 56 days for the RH exposure (curing) condition. However, the strengths are similar for all ages for RL condition.

4.4.2 Determination of Exposure Factors

A standard laboratory curing environment is 73 ^{o}F and 100 percent relative humidity. All other exposure conditions represent field exposure with different temperature and humidity combinations. Because the early age exposure (curing) conditions affect the mechanical characteristics of the concrete, exposure (curing) factors, based on early age exposure (curing) conditions, may be necessary to better predict these longer term characteristics. Table 4.5 is a summary of the exposure (curing) factors determined for all precasters, exposure (curing) conditions, and ages.

The concrete compressive strength for each precaster was not highly influenced by the variations in field exposure conditions. The results indicate that curing concrete under standard conditions results in a higher longer-term strength compared to other exposure conditions used in this study. As shown, the 28-day exposure (curing) factors for all other exposure conditions are lower than 1.00 (0.86-0.99), except for the RH exposure (curing) condition of Precaster B. Cetin and Carrasquillo (1995) explained this by the relatively non-uniform precipitation of hydration

products, and coarsened pore-structure as a result of elevated heat exposure. The overall short-term strength for all precasters combined is higher for concrete exposed to higher temperatures. As shown, the 1-day exposure factor for the average of all precasters is 1.10. This increase in the short-term strength occurs because elevated heat exposure accelerates the chemical reactions during the early hydration process. However, this trend did not hold true for the Precaster C mixture, where the 1-day field exposure factor was 0.92. It should be noted that for 1-day, only one set of three samples was tested for all field exposure (curing) conditions. This is because all the field samples are subjected to the same elevated heat exposure condition for the first day.

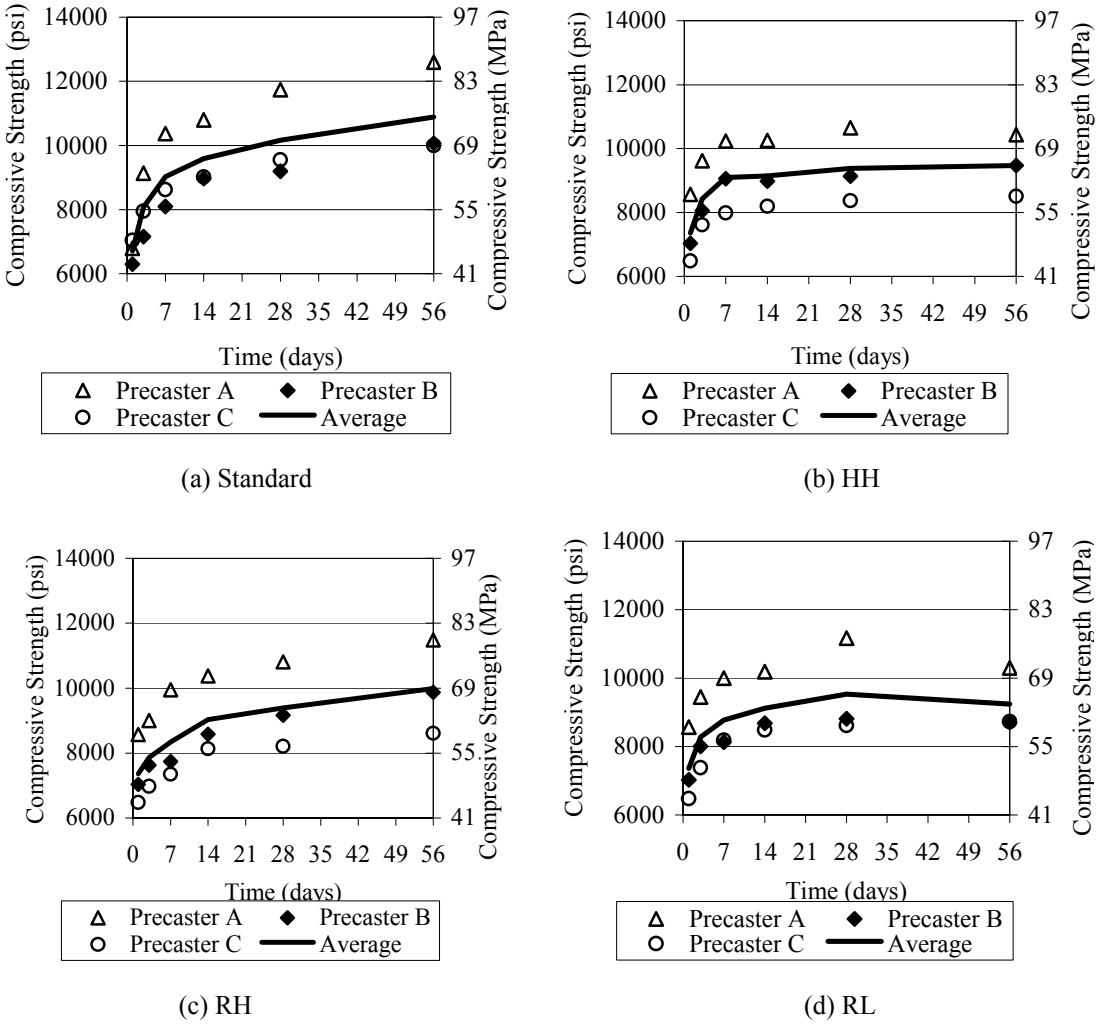

Figure 4.3. Development of Compressive Strength with Time (by Exposure Condition).

Table 4.5. Exposure (curing) Factors for Compressive Strength.

Precaster	Exposure Condition	Age					
		1 Day	3 Days	7 Days	14 Days	28 Days	56 Days
A	Standard	1.00	1.00	1.00	1.00	1.00	1.00
	HH	1.26	1.05	0.99	0.95	0.91	0.83
	RH	1.26	0.99	0.96	0.96	0.92	0.91
	RL	1.26	1.03	0.96	0.94	0.95	0.82
B	Standard	1.00	1.00	1.00	1.00	1.00	1.00
	HH	1.12	1.13	1.12	1.00	0.99	0.94
	RH	1.12	1.06	0.96	0.96	1.00	0.98
	RL	1.12	1.12	1.01	0.97	0.96	0.86
C	Standard	1.00	1.00	1.00	1.00	1.00	1.00
	HH	0.92	0.96	0.93	0.91	0.88	0.85
	RH	0.92	0.88	0.85	0.90	0.86	0.86
	RL	0.92	0.93	0.95	0.94	0.90	0.87
All Precasters	Standard	1.00	1.00	1.00	1.00	1.00	1.00
	HH	1.10	1.04	1.01	0.95	0.93	0.87
	RH	1.10	0.98	0.92	0.94	0.93	0.92
	RL	1.10	1.03	0.97	0.95	0.94	0.85

Standard = Standard Laboratory Conditions (73 ^{o}F and 100 percent humidity continuously)
HH = High Temperature and High Humidity (107 ^{o}F and 100 percent humidity continuously)
RH = Room Temperature and High Humidity (107 ^{o}F and 100 percent humidity for 1 day, then 73 ^{o}F and 100 percent humidity)
RL = Room Temperature and Low Humidity (107 ^{o}F and 100 percent humidity for 1 day, then 73 ^{o}F and 30 percent humidity)

In order to look more closely at the effect of different exposure (curing) conditions, the average exposure (curing) factors for all precasters are plotted in Figure 4.4 as a function of time. It is clear that elevated heat exposure specimens exhibit lower strengths relative to specimens cured under standard conditions.

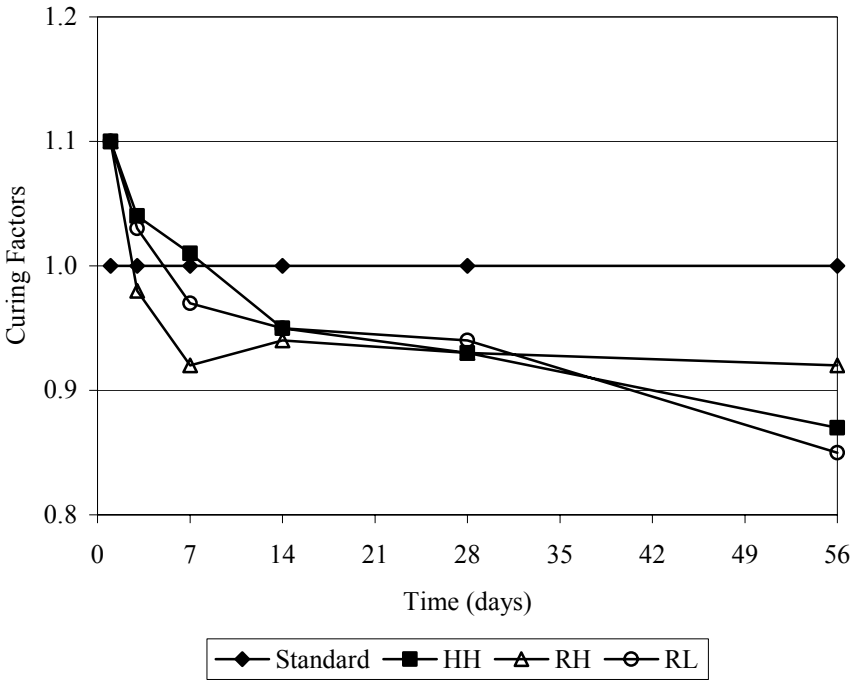

Figure 4.4. Average Compressive Strength Exposure Factors versus Time.

4.4.3 Statistical Data Analysis

4.4.3.1 Probability Distribution

Figure 4.5 shows the quantile plots for normal and lognormal distributions for the residuals. Both assumed distributions are reasonably linear; therefore, statistical analysis is valid for either distribution. Because the lognormal distribution was used in the earlier phase of this study, statistical data analysis for the compressive strength was performed based on the assumption of a lognormal distribution.

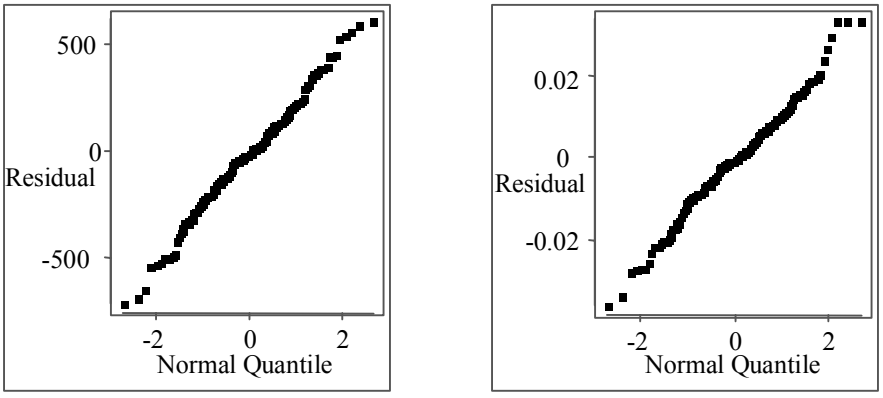

(a) Normal Distribution (c) Lognormal Distribution

Figure 4.5. Quantile Plots for Compressive Strength.

4.4.3.2 Analysis of the Full Model

Table 4.6 provides the ANOVA table, generated from SAS (1999), summarizing the results of the analysis for the full model where the mean logarithm of the batch averages for compressive strength is the primary response variable. The full model considers all exposure (curing) conditions, precasters, and ages in the analysis. It is clear by looking at the Pr>F column (p-values) that the logarithm of batch averages is significantly different among precasters, exposure (curing) conditions, concrete age, and the interaction of precaster with exposure (curing) conditions with age. The only interaction that was not significant was the interaction of precaster with age. To better visualize this significance, scatter plots of batch averages versus the factors tested are shown in Figure 4.6. These plots show how the batch averages are significantly different among ages, precasters, and exposure (curing) conditions.

Table 4.6. ANOVA Table of the Mean of the Logarithm of Batch Averages for Compressive Strength.

Source	DF	Sum of Squares	Mean Square	F Value	Pr > F
Model	41	0.31489099	0.00768027	32.69	<0.0001
Error	30	0.00704798	0.00023493		
Corrected Total	71	0.32193897			

R-Square	Coeff Var	Root MSE	LogBAvg Mean
0.978108	0.389006	0.015328	3.940177

Source	DF	Type III SS	Mean Square	F Value	Pr > F
Curing	3	0.003557	0.001186	5.05	0.006
Precaster	2	0.126429	0.063215	269.08	<0.0001
Age	5	0.158017	0.031603	134.52	<0.0001
Precaster x Age	10	0.001024	0.000102	0.44	0.9168
Precaster x Curing	6	0.009451	0.001575	6.70	0.0001
Curing x Age	15	0.016413	0.001094	4.66	0.0002

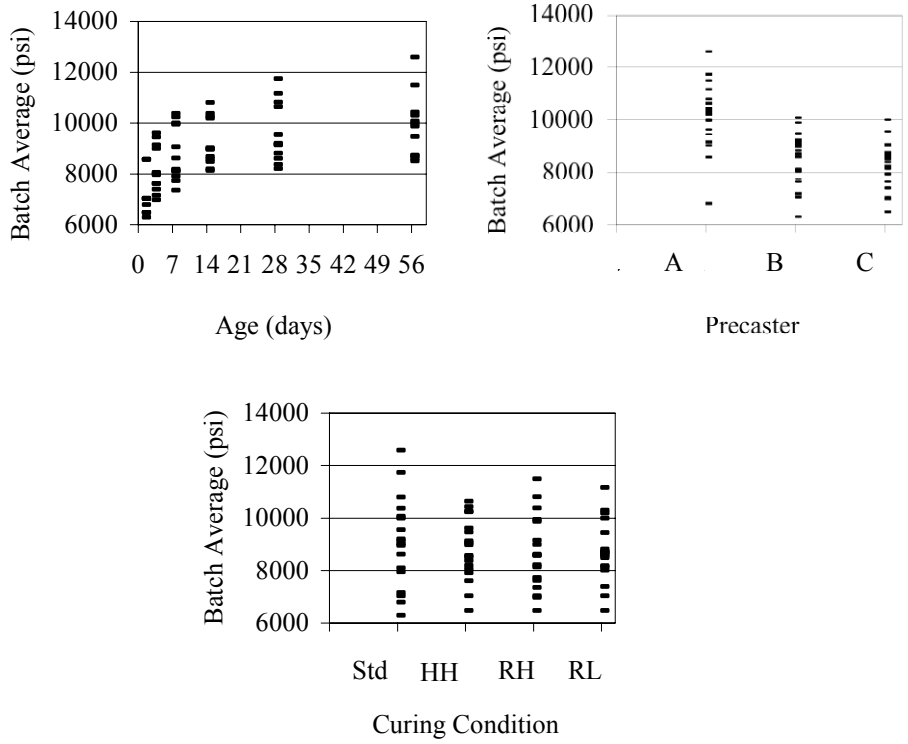

Figure 4.6. Scatter Plots of Batch Average for Compressive Strength.

4.4.3.3 Analysis of the Reduced Model

Based on the exposure (curing) factors reported in Table 4.5, the variations in the field exposure conditions seem to give an overall insignificant difference in strength for different precasters. In order to determine whether this is true, a reduced model was generated. In the reduced model, all the field exposure conditions were combined and tested. The reduced model considers all field exposure conditions, precasters, and ages in the analysis. This model is still a three-factor factorial model without three-way interaction, but the exposure (curing) factor now denoted by CC has just two conditions (standard laboratory curing and field exposure). Results from the full model and the reduced model were used to determine a new p-value. Table 4.7 shows the results of the reduced model. Using Equation 4.3, the F statistic is 2.128, corresponding to a p-value of 0.036, which is less than 0.05. This result shows that the difference among the field exposure conditions for compressive strength is actually significant.

Table 4.7. ANOVA (Reduced Model) of LogBAvg for Compressive Strength.

Source	DF	Sum of Squares	Mean Square	F Value	Pr > F
Model	25	0.30689041	0.01227562	37.52	<0.0001
Error	46	0.01504856	0.00032714		
Corrected Total	71	0.32193897			

R-Square	Coeff Var	Root MSE	LogBAvg Mean
0.953256	0.459042	0.018087	3.940177

Source	DF	Type III SS	Mean Square	F Value	Pr > F
CC	1	0.002597	0.002597	7.94	0.0071
Precaster	2	0.084916	0.042458	129.78	<0.0001
Age	5	0.158179	0.031636	96.70	<0.0001
Precaster x Age	10	0.001024	0.000102	0.31	0.9739
Precaster x CC	2	0.007102	0.003551	10.85	0.0001
CC x Age	5	0.011721	0.002344	7.17	<0.0001

4.4.3.4 Analysis of Three-way Interaction

Careful analysis of the exposure (curing) factors in Table 4.5 indicates that there may be a three-way interaction (Precaster × Curing × Age) among precasters, ages, and exposure (curing) conditions. In order to determine whether this is true, the three-way interaction analysis

was applied to the reduced model. The p-value corresponding to "Precaster × Curing × Age" was 0.0766, indicating that this interaction is not significant. To better judge if the three-way interaction is significant or not, this test was applied on the full model with each of the three cylinders within a batch as the Y-variable (measured response) instead of the logarithm of the batch average. This was done in order to be able to use the full model in testing for the significance. The p-value was found to be 0.0009, which is less than 0.05. Thus, the three-way interaction was found to be significant.

It is important to note that while neither method is completely accurate, the analysis provides useful information in evaluating the significance of the three-way interaction. The first method is less accurate because it presumes that the reduced model is correct. The fact that it is not significant could be due to using an SS_{error} from the reduced model, which is not purely random. The second method is not entirely accurate because the best measurement variable, the logarithm of batch averages, was not used in order to be able to include the three-way interaction. However, the distinction between individual cylinder measurements and batch averages is not likely related to the factors considered in this study. Thus, the second method more accurately reflects the existence of the three-way interaction. Since this method is more accurate, the researchers concluded that the three-way interaction does exist. Therefore, the exposure (curing) factors determined are significantly different for the interaction of ages, precasters, and exposure (curing) conditions and hence should be used separately. P-values only reflect the strength of the random data, are not fixed constants, and thereby cannot be accurately determined.

4.5 ANALYSIS FOR MODULUS OF RUPTURE

4.5.1 Development of Strength with Time

The MOR provides a measure of the flexural tensile strength. Table 4.8 is a summary of the ratio of the average MOR at the given testing ages to the 28-day average MOR for all exposure (curing) conditions and precasters. Actual data for all MOR samples are shown in Appendix B. As shown, the average one-day MOR for all precasters under standard exposure

(curing) conditions was 68 percent of the corresponding 28-day average MOR. The seven-day average MOR was determined to be 90 percent of the 28-day average MOR for standard curing conditions.

Table 4.8. Ratio of Average to 28-Day Average for MOR.

Precaster	Exposure (curing) Condition	Age					
		1 Day	3 Days	7 Days	14 Days	28 Days	56 Days
A	Standard	0.59	0.73	0.84	0.93	1.00	1.05
	HH	0.83	0.79	0.86	0.98	1.00	0.96
	RH	0.77	0.96	1.00	1.02	1.00	1.15
	RL	0.92	0.94	0.91	0.88	1.00	0.96
B	Standard	0.74	0.95	0.88	0.89	1.00	1.06
	HH	0.97	1.09	1.09	1.11	1.00	1.10
	RH	0.77	0.95	0.95	0.95	1.00	1.01
	RL	0.93	0.99	0.99	1.03	1.00	1.11
C	Standard	0.72	0.83	0.96	1.04	1.00	1.01
	HH	0.88	0.93	0.92	1.03	1.00	1.13
	RH	0.82	0.90	0.99	1.02	1.00	1.08
	RL	0.85	0.82	0.89	0.93	1.00	1.03
All Precasters	Standard	0.68	0.84	0.90	0.95	1.00	1.04
	HH	0.85	0.86	0.89	1.00	1.00	1.04
	RH	0.79	0.94	0.98	1.00	1.00	1.08
	RL	0.90	0.91	0.93	0.95	1.00	1.03

Standard = Standard Laboratory Conditions (73 ^{o}F and 100 percent humidity continuously)
HH = High Temperature and High Humidity (107 ^{o}F and 100 percent humidity continuously)
RH = Room Temperature and High Humidity (107 ^{o}F and 100 percent humidity for 1 day, then 73 ^{o}F and 100 percent humidity)
RL = Room Temperature and Low Humidity (107 ^{o}F and 100 percent humidity for 1 day, then 73 ^{o}F and 30 percent humidity)

Elevated heat exposure with a high 1-day initial temperature resulted in a higher MOR ratio compared to standard curing conditions. This may be because elevated heat exposure can result in concrete attaining most of its 28-day strength in the short term. Note that when calculating the overall MOR development for all precasters combined, the strength for the HH exposure condition for Precaster B was not used. This is because the 28-day average strength was lower than earlier ages because the specimens tested were not in perfect condition (i.e., slightly damaged).

Figure 4.7 shows the development of the MOR with time for all exposure (curing) conditions with each graph showing one of the precasters. It is clear that the MOR for all precaster mixtures cured under standard conditions resulted in higher MOR values beyond 7 days compared to concrete subjected to continuous elevated heat exposure. Again, this supports the observation that elevated heat exposure reduces the long-term strength. For all precasters, the RH exposure (curing) condition resulted in the second highest MOR values. The different field exposure conditions tended to give similar MOR values as a function of age for Precaster C. More variations in the MOR values for field exposure conditions were observed for Precasters A and B mixtures.

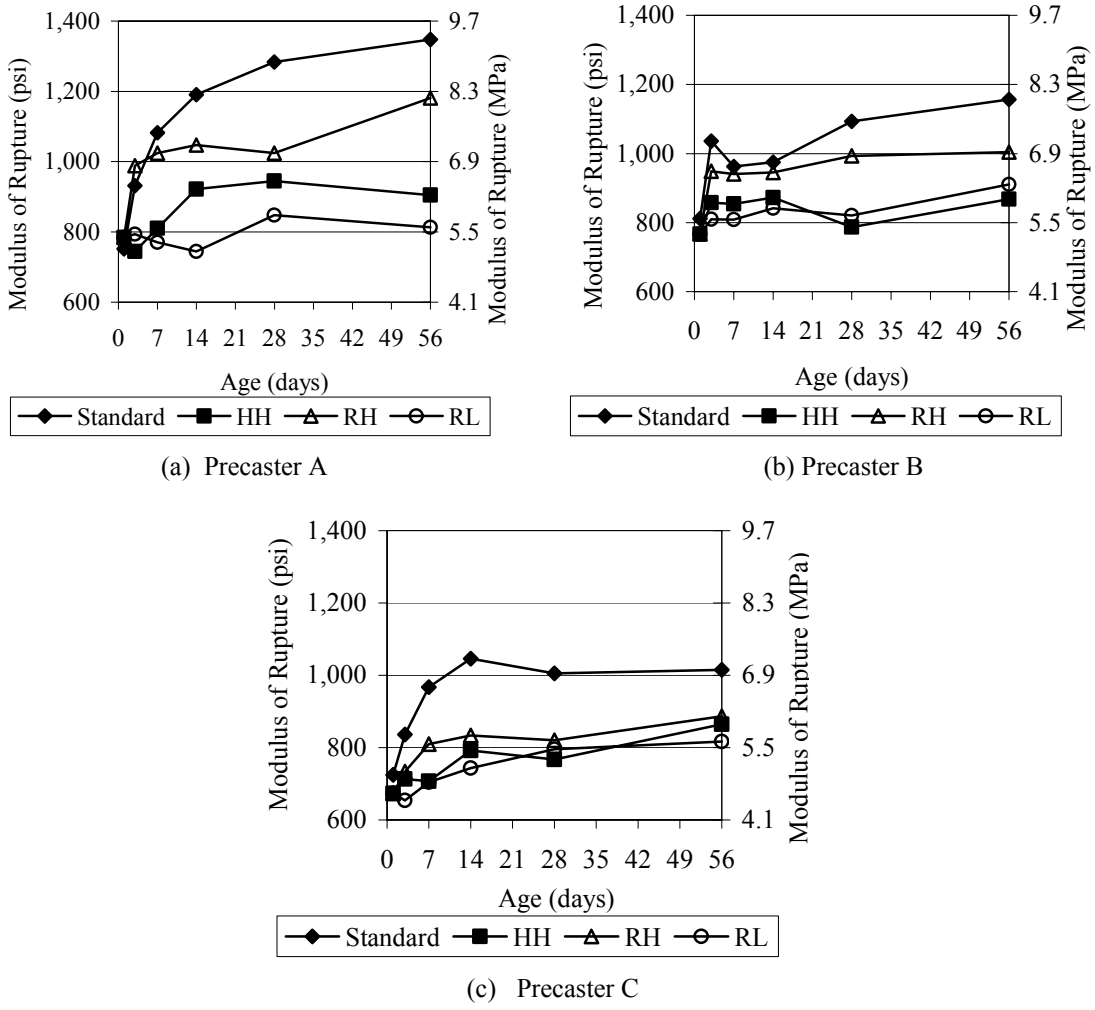

(a) Precaster A

(b) Precaster B

(c) Precaster C

Figure 4.7. Development of the MOR with Time (by Precaster).

Figure 4.8 shows the development of the MOR with time for all precasters for the different exposure (curing) conditions. In the graphs, for all four exposure (curing) conditions, it is clear that the concrete mixture for Precaster C had the lowest MOR with exceptions. For 100 percent RH, Precaster A concrete exhibits the highest MOR beyond 7 days. However, this is not the case for the low humidity condition (RL). This could be due to the lower water-cement ratio used for the Precaster A mixture compared to other precasters. Hydration may have ceased at an earlier age and lead to lower MOR values. It is clear that the high temperature and low humidity greatly reduced the MOR. The low humidity exposure condition could result in surface cracking of the specimens, thus reducing the MOR when compared to standard laboratory cured specimens where surface cracking is less likely due to the availability of moisture.

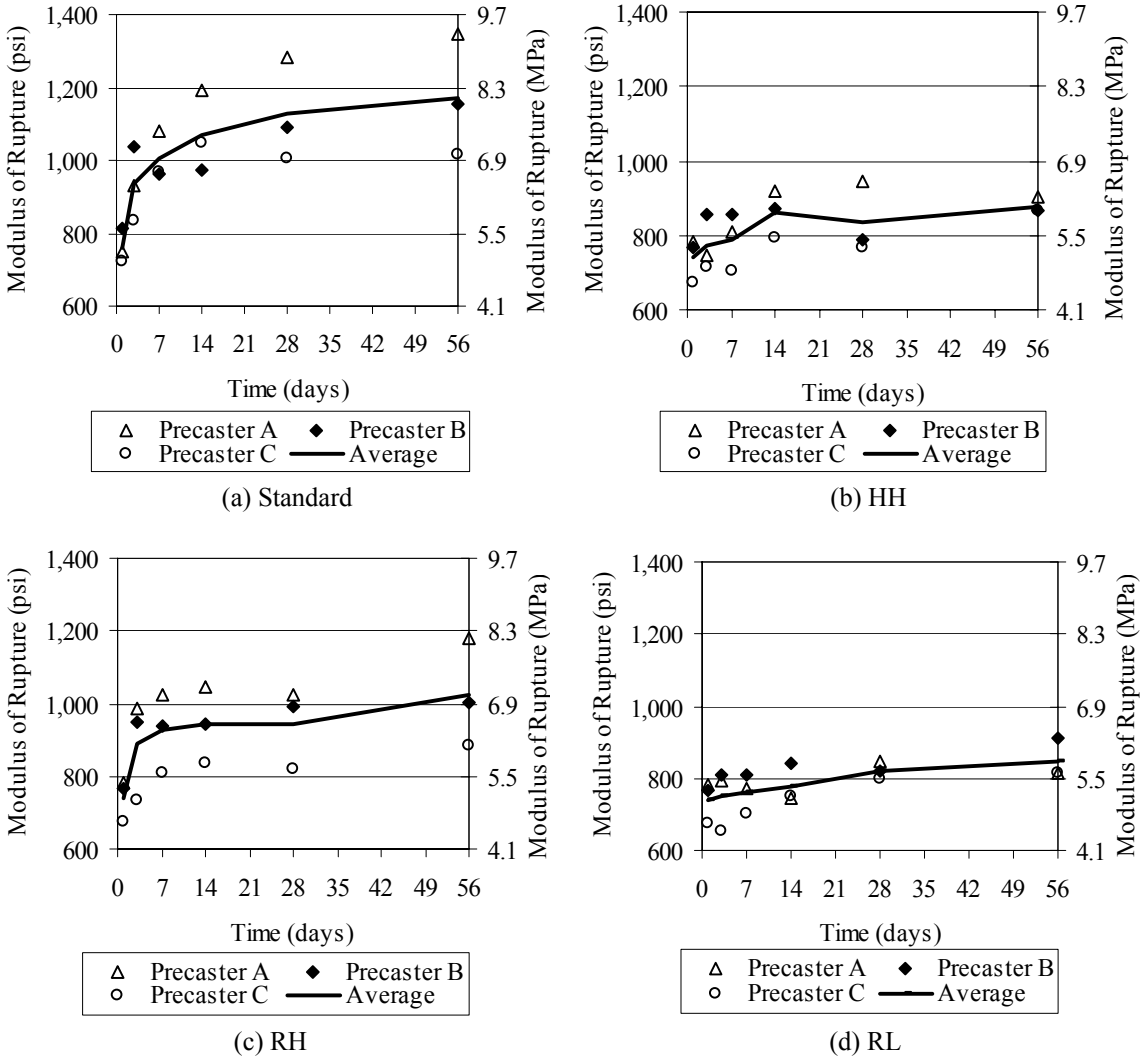

Figure 4.8. Development of the MOR with Time (by Exposure [Curing] Condition).

4.5.2 Determination of Exposure (Curing) Factors

The exposure (curing) factor is defined in this study as the ratio between the MOR values obtained based on field exposure conditions to that obtained based on standard laboratory curing conditions for the same age. Table 4.9 provides a summary of the exposure (curing) factors for the MOR determined for all exposure (curing) conditions and precasters. It is clear that the MOR is highly influenced by the different exposure (curing) conditions. Curing concrete under standard conditions resulted in a higher longer-term strength compared to other exposure (curing) conditions. As shown, the 28-day exposure (curing) factors for all exposure (curing) conditions (other than standard curing conditions) are lower than 1.00 (0.66 to 0.91). Exposing concrete to higher temperatures (107 ^{o}F) with 100 percent humidity resulted in reduction in the average MOR for all precasters and all ages compared to standard conditions. There are exceptions to this observation for Precaster A for the RH exposure (curing) condition at 1 and 3 days. Exposing concrete to a very low relative humidity (30 percent) and 73 ^{o}F after 1 day resulted in an overall reduction in the MOR compared to curing under standard conditions. Thus, both temperature and humidity seem to significantly influence the MOR of the concrete.

Table 4.9. Exposure (Curing) Factors for MOR.

Precaster	Exposure (Curing) Condition	Age					
		1 Day	3 Days	7 Days	14 Days	28 Days	56 Days
A	Standard	1.00	1.00	1.00	1.00	1.00	1.00
	HH	1.04	0.80	0.75	0.77	0.74	0.67
	RH	1.04	1.06	0.95	0.88	0.80	0.88
	RL	1.04	0.85	0.71	0.62	0.66	0.60
B	Standard	1.00	1.00	1.00	1.00	1.00	1.00
	HH	0.95	0.83	0.89	0.90	0.72	0.75
	RH	0.95	0.92	0.98	0.97	0.91	0.87
	RL	0.95	0.78	0.84	0.86	0.75	0.79
All Precasters	Standard	1.00	1.00	1.00	1.00	1.00	1.00
	HH	0.93	0.85	0.73	0.76	0.76	0.85
	RH	0.93	0.88	0.84	0.80	0.82	0.87
	RL	0.93	0.78	0.73	0.71	0.79	0.81
Overall	Standard	1.00	1.00	1.00	1.00	1.00	1.00
	HH	0.97	0.83	0.79	0.81	0.74	0.76
	RH	0.97	0.95	0.92	0.88	0.84	0.87
	RL	0.97	0.81	0.76	0.73	0.73	0.73

In order to evaluate the influence of different exposure (curing) conditions, the overall (all precasters) exposure (curing) factors are plotted in Figure 4.9 as a function of time. For all ages, the standard curing conditions resulted in the highest MOR. The RH exposure (curing) condition that differs from standard curing only in the first day, gave the second highest strength. The HH exposure condition had the third highest strength. Finally, the RL exposure condition had the lowest MOR, with exposure factors slightly lower than that for the HH condition. In general, high heat and low humidity result in lower MOR values.

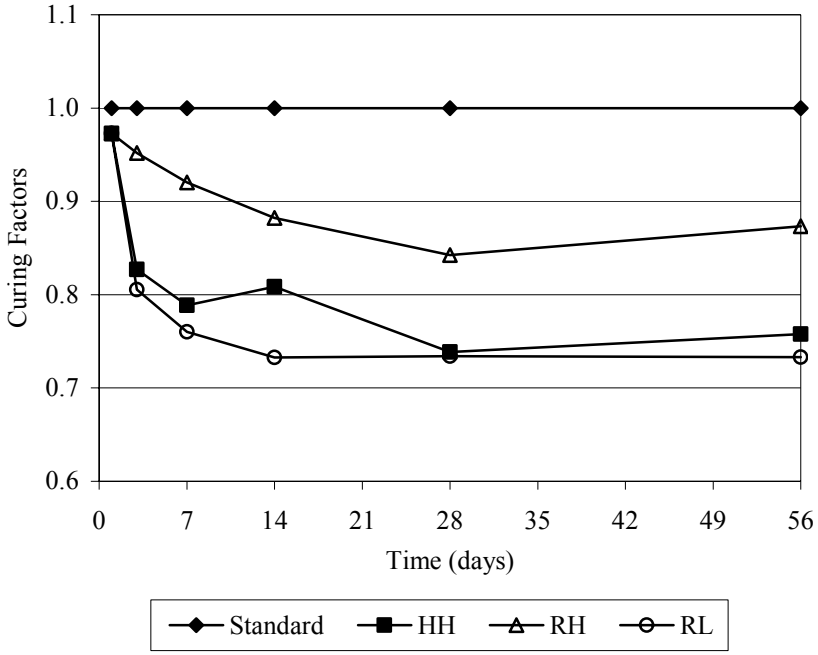

Figure 4.9. Average MOR Exposure (Curing) Factors versus Time.

4.5.3 Statistical Data Analysis

4.5.3.1 Probability Distribution

Figure 4.10 shows the quantile plots for normal and lognormal distributions for the batch averages. Both distributions are reasonably linear. Therefore, a statistical analysis can be performed based on either one. Because the lognormal distribution was used in the earlier phase of this study, the statistical data analysis for the MOR was performed based on the assumption of a lognormal distribution.

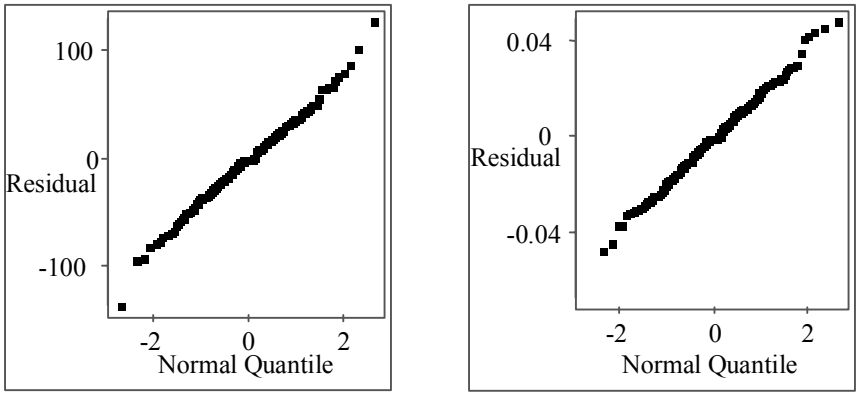

(a) Normal Distribution (c) Lognormal Distribution

Figure 4.10. Quantile Plots for MOR.

4.5.3.2 Analysis of the Full Model

Table 4.10 provides the ANOVA table, generated from SAS (1999), summarizing the results of the analysis for the full model where the logarithm of the batch averages for MOR is the primary response variable. It is clear from the Pr>F column (p-values) that the logarithm of batch averages is significantly different among precasters, exposure (curing) conditions, concrete age, and the interaction of precaster with exposure (curing) conditions and exposure conditions with age. The only interaction that was not significant was the interaction of precaster with age. To better visualize this significance, scatter plots of batch averages versus the factors tested are shown in Figure 4.11. These plots show how the batch averages are significantly different among ages, precasters, and exposure (curing) conditions.

Table 4.10. ANOVA (Full Model) of LogBAvg for MOR.

Source	DF	Sum of Squares	Mean Square	F Value	Pr > F
Model	41	0.32250841	0.00786606	12.99	<0.0001
Error	30	0.01817161	0.00060572		
Corrected Total	71	0.34068002			

R-Square	Coeff Var	Root MSE	LogBAvg Mean
0.946661	0.837460	0.024611	2.938814

Source	DF	Type III SS	Mean Square	F Value	Pr > F
Curing	3	0.12290881	0.040970	67.64	<0.0001
Precaster	2	0.05568975	0.027845	45.97	<0.0001
Age	5	0.09639795	0.019280	31.83	<0.0001
Precaster x Age	10	0.00812247	0.000812	1.34	0.2546
Precaster x Curing	6	0.01062269	0.001770	2.92	0.0229
Curing x Age	15	0.02876673	0.001918	3.17	0.0035

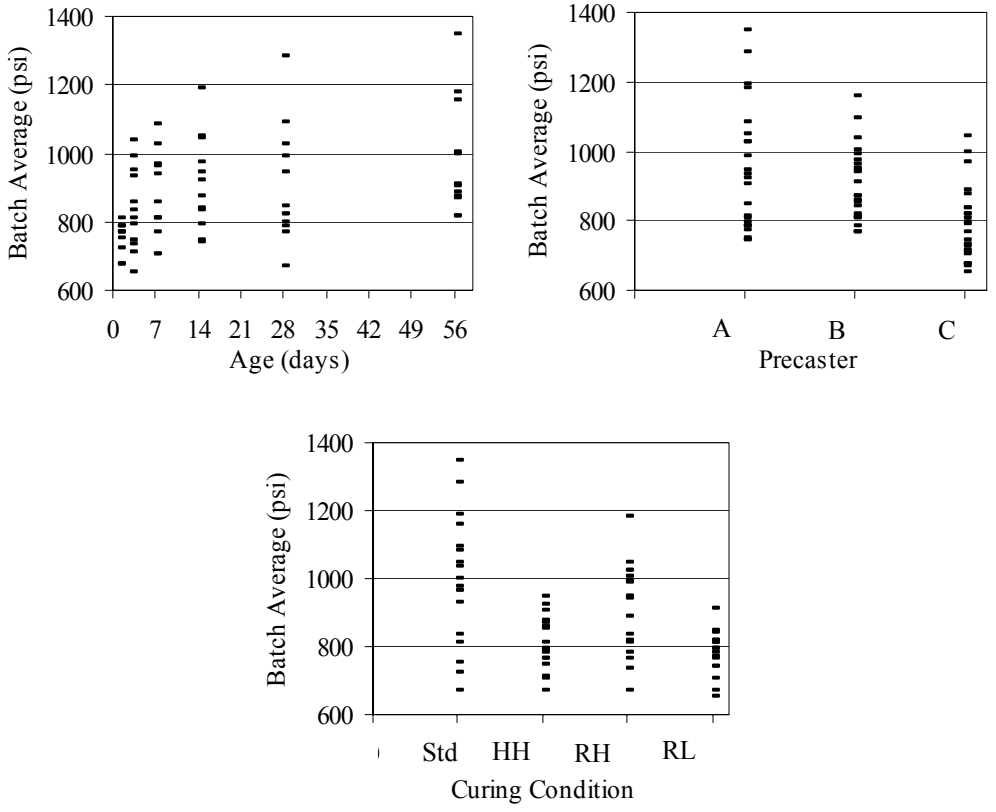

Figure 4.11. Scatter Plots of Batch Average for MOR.

4.5.3.3 Analysis of the Reduced Model

Based on the exposure (curing) factors reported in Table 4.9, the different field exposure conditions seem to have a significant effect on the MOR. In order to verify this observation, a reduced model was generated. In the reduced model, all the field exposure conditions were combined and tested as was done for the statistical analysis of the compressive strength data. Table 4.11 shows the ANOVA table for the reduced model. In order to test for the significance of the field exposure conditions, results from the full model and the reduced model were used to determine a new p-value. The F statistic (Eq. 4.3) after using both models was computed to be 6.06, corresponding to a p-value of 0.0000119, which is much less than 0.05. Thus, the test supports the observation that there is a significant difference among field exposure conditions for the MOR.

Table 4.11. ANOVA (Reduced Model) of LogBAvg for Flexural Strength.

Source	DF	Sum of Squares	Mean Square	F Value	Pr > F
Model	25	0.26377794	0.01055112	6.31	<0.0001
Error	46	0.07690208	0.00167178		
Corrected Total	71	0.34068002			

R-Square	Coeff Var	Root MSE	LogBAvg Mean
0.774269	1.391291	0.040887	2.938814

Source	DF	Type III SS	Mean Square	F Value	Pr > F
CC	1	0.086793	0.086793	51.92	<0.0001
Precaster	2	0.040610	0.020305	12.15	<0.0001
Age	5	0.107516	0.021503	12.86	<0.0001
Precaster x Age	10	0.008122	0.000812	0.49	0.8906
Precaster x CC	2	0.001671	0.000836	0.50	0.6099
CC x Age	5	0.015103	0.003021	1.81	0.1303

4.5.3.4 Analysis of Three-way Interaction

Analysis of the exposure (curing) factors in Table 4.9 indicates that there may be a three-way interaction (Precaster × Curing × Age) among precasters, ages, and exposure (curing) conditions. In order to determine whether this is true, the three-way interaction analysis was applied to the reduced model. The p-value corresponding to "Precaster × Curing × Age" was

0.9092, which indicates that the three-way interaction is not significant. To better judge if the three-way interaction is significant, this test was applied on the full model with each of the three cylinders within a batch as the Y-variable (measured response) instead of the logarithm of the batch average. The p-value was found to be 0.0008, which indicates that the three-way interaction is significant. As noted for the analysis of three-way interaction for the compressive strength, the second method is more accurate. Therefore, the three-way interaction does exist for the MOR as well.

4.6 RELATIONSHIPS BETWEEN MODULUS OF RUPTURE AND COMPRESSIVE STRENGTH

4.6.1 Strength Relationships

Figure 4.12 shows the MOR versus the compressive strength for all precasters with separate graphs for each exposure (curing) condition. Each graph includes data for all ages tested. The best-fit line to the data is also shown. All equations proposed in this study involving different relationships correspond to concrete strength values ranging from 6000 to 12,000 psi. It is clear that the MOR is proportional to the compressive strength. The standard curing conditions gave the lowest variation with a correlation coefficient (R^2) of 0.81. This is because other exposure conditions were initially subjected to elevated heat exposure, which probably resulted in non-uniform precipitation of hydration products, and a coarsened pore-structure. The RL exposure condition shown in Figure 4.12 (d) gave the shallowest slope. This might be because the low humidity (30 percent) forced the hydration process to slow down at an early age such that the MOR developed very low strength, whereas the compressive strength was not greatly influenced by the low humidity. Crack development could also influence the lack of MOR gain.

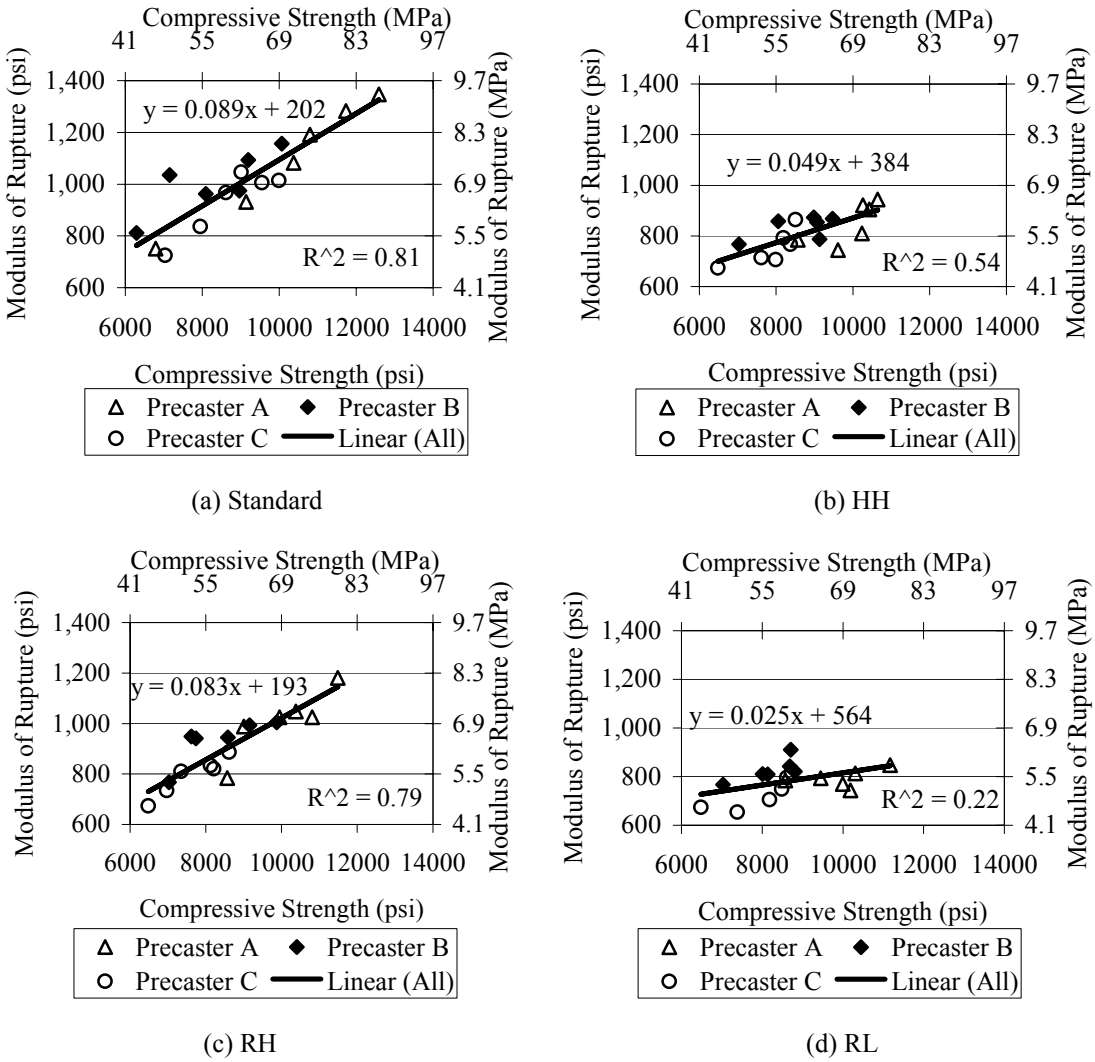

Figure 4.12. MOR versus Compressive Strength (by Exposure [Curing] Condition).

Figure 4.13 provides plots of the relative strengths (ratio of the MOR to corresponding compressive strength) versus the compressive strength for all precasters and ages with separate graphs for each exposure (curing) condition. All exposure (curing) conditions resulted in inversely proportional relationships. This is because the MOR develops more quickly in the short term relative to the rate of strength gain for the compressive strength.

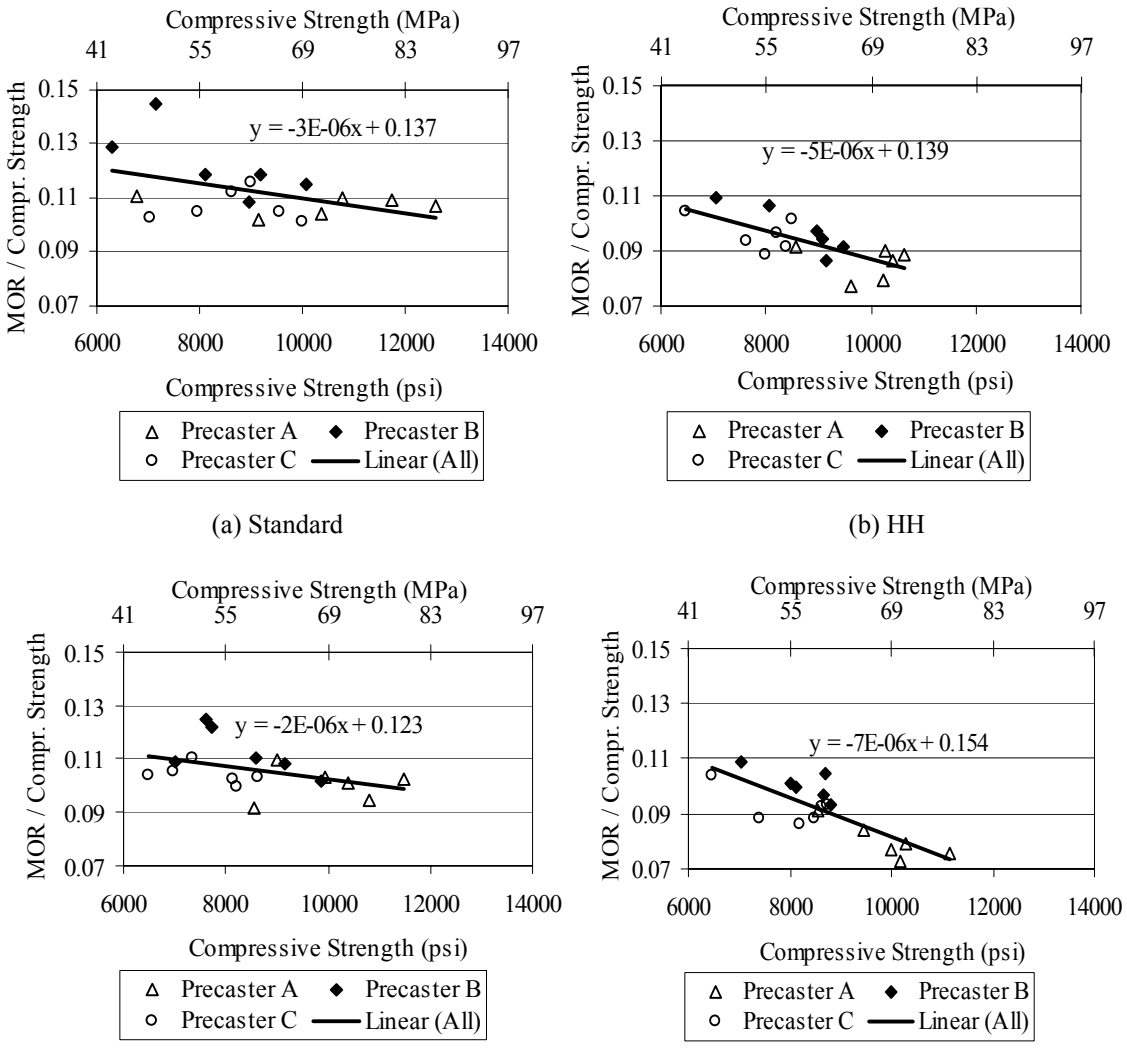

Figure 4.13. Relative Strength versus the Compressive Strength (All Exposure [Curing] Conditions).

Figure 4.14 provides plots of the MOR versus the square root of the corresponding compressive strength. These graphs are used to determine relationships for different exposure (curing) conditions. These relationships are determined by forcing the best-fit line to pass through the origin. Better relationships can be achieved by including a y-intercept. However, the square root model, which is used by the codes, clearly shows the difference in strength among the exposure conditions under investigation.

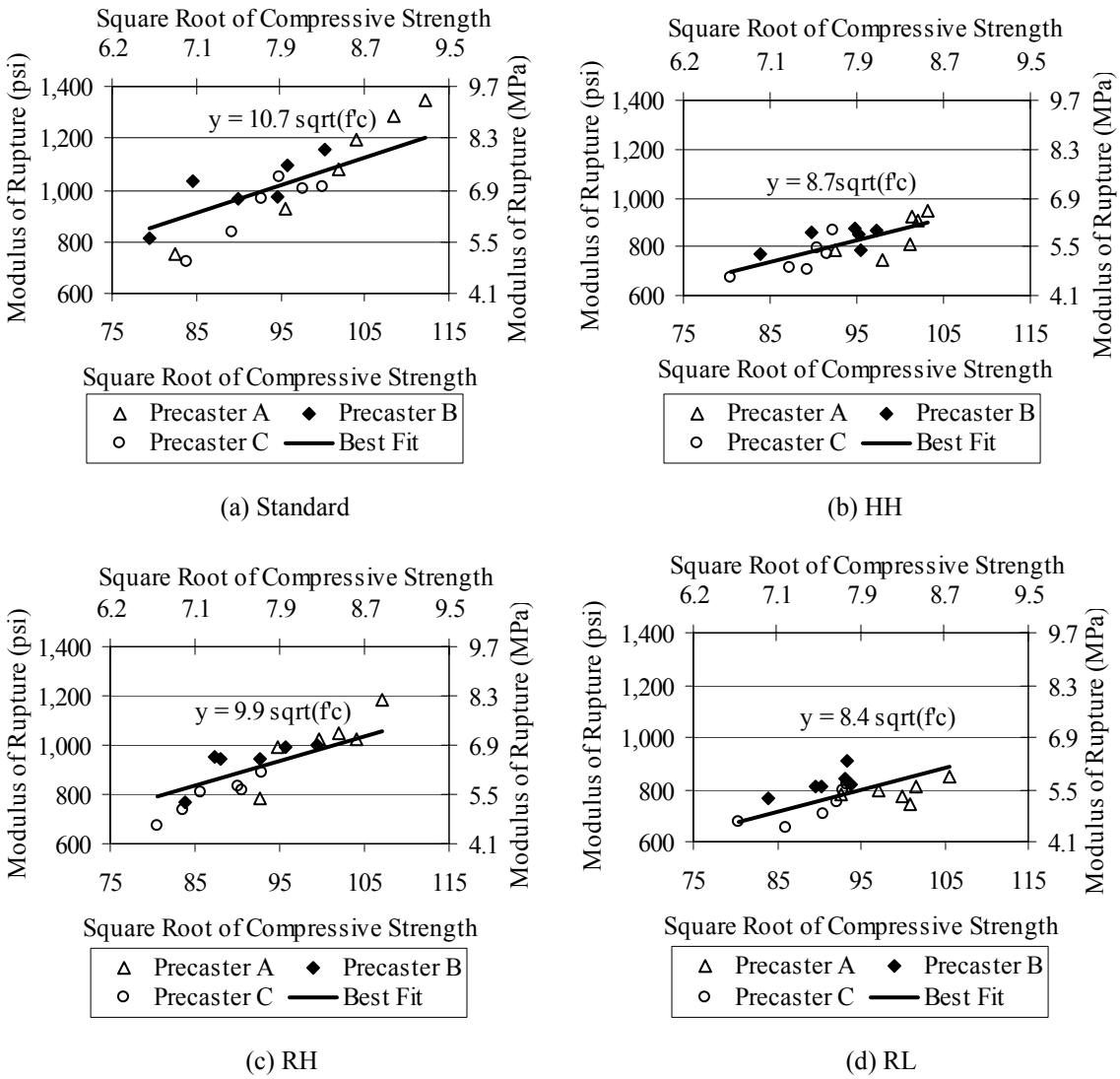

Figure 4.14. MOR versus Square Root of Compressive Strength (by Exposure [Curing] Condition).

4.6.2 Prediction Formulas

Figures 4.15 thru 4.18 provide a comparison of the MOR prediction formulas summarized in Table 4.2 to the data and best fit square root expression from this study for the different exposure (curing) conditions. Figure 4.15 shows the relationship between the MOR and compressive strength for concrete cured under standard conditions. The best-fit equation from this study for concrete cured under standard laboratory conditions is as follows.

$$f_r = 10.7\sqrt{f_c'} \tag{4.4}$$

where f_r is the MOR (psi) and f_c' is the compressive strength (psi). Raphael (1984) and Khayat et al. (1995) give the best f_r for the mixtures used in this study under standard curing conditions. The ACI 363 (1997) and the Burg and Ost (1992) formulas overestimate the data.

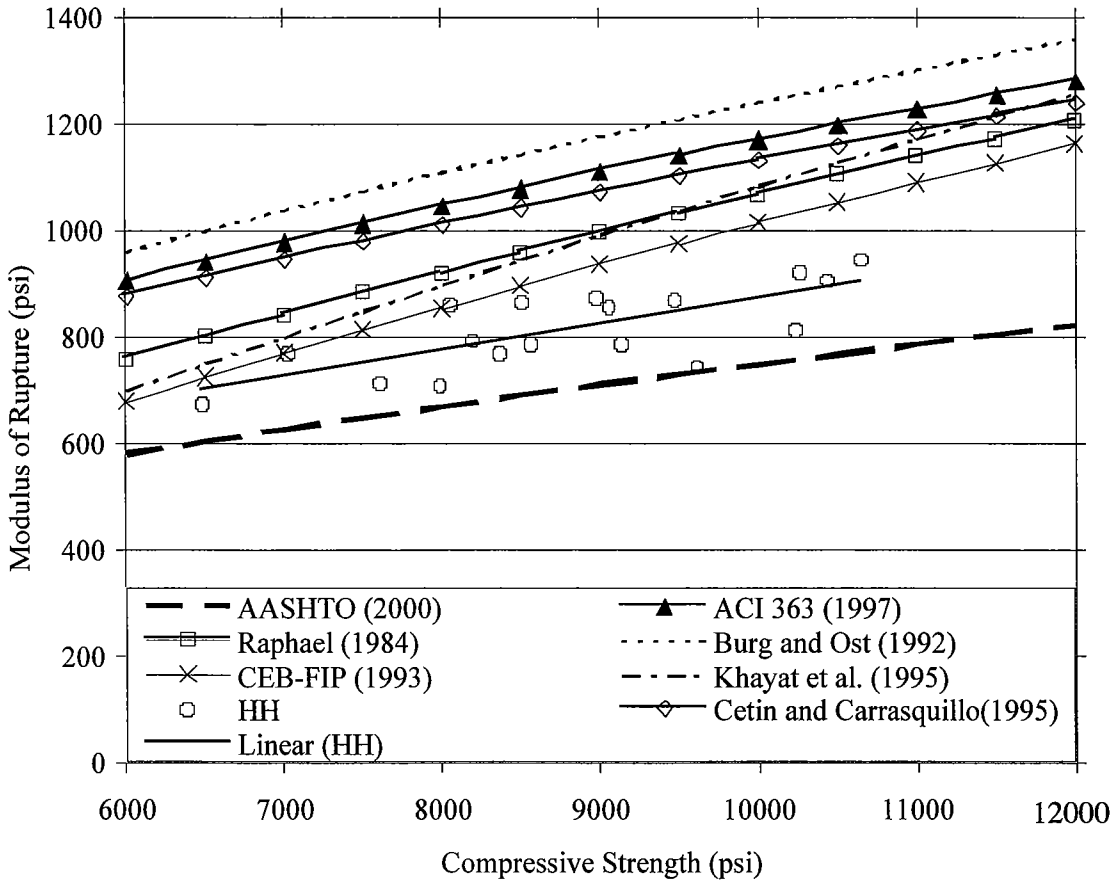

Figure 4.15. MOR versus Compressive Strength (Standard Curing).

Figure 4.16 includes the prediction formulas and the expression developed for concrete exposure conditions representing field exposure under high temperature and high humidity (HH). The best-fit expression determined in this study for concrete cured under these conditions is as follows.

$$f_r = 8.7\sqrt{f_c'} \tag{4.5}$$

For the HH exposure condition, all the prediction formulas overestimate the data except for the expression from the AASHTO LRFD Specification (2000), which provides a lower bound to the data. The CEB-FIP (1993) expression provides a close upper bound to the data.

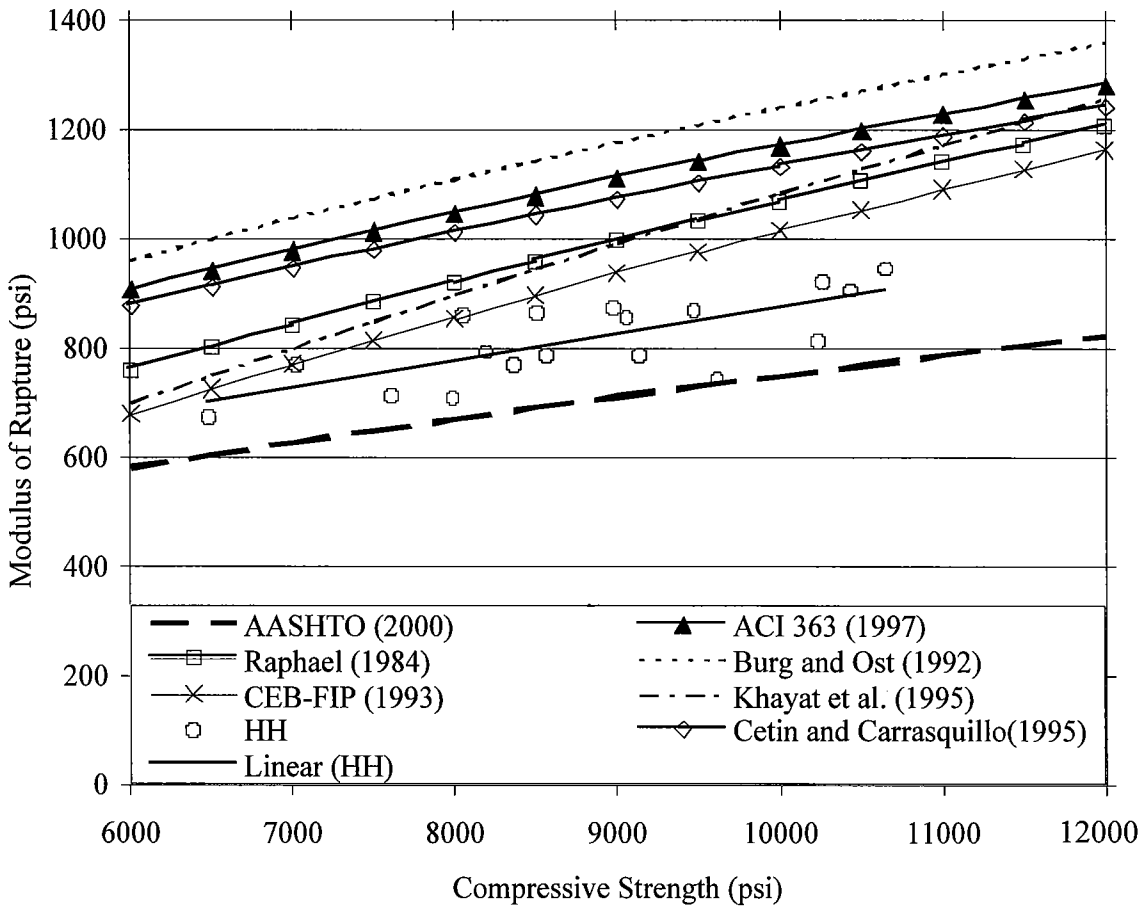

Figure 4.16. MOR versus Compressive Strength (HH Exposure).

Figure 4.17 includes the prediction formulas and the expression developed for the RH field exposure condition. The best-fit equation from this study for concrete cured under these conditions is as follows:

$$f_r = 9.9\sqrt{f_c'} \qquad (4.6)$$

The CEB-FIP (1993) formula gives the best prediction for concrete cured under such conditions. The ACI 363 (1997) and the Burg and Ost (1992) formulas overestimate the data. The AASHTO LRFD Specification (2000) formula underestimates the MOR because all the data points fall above it.

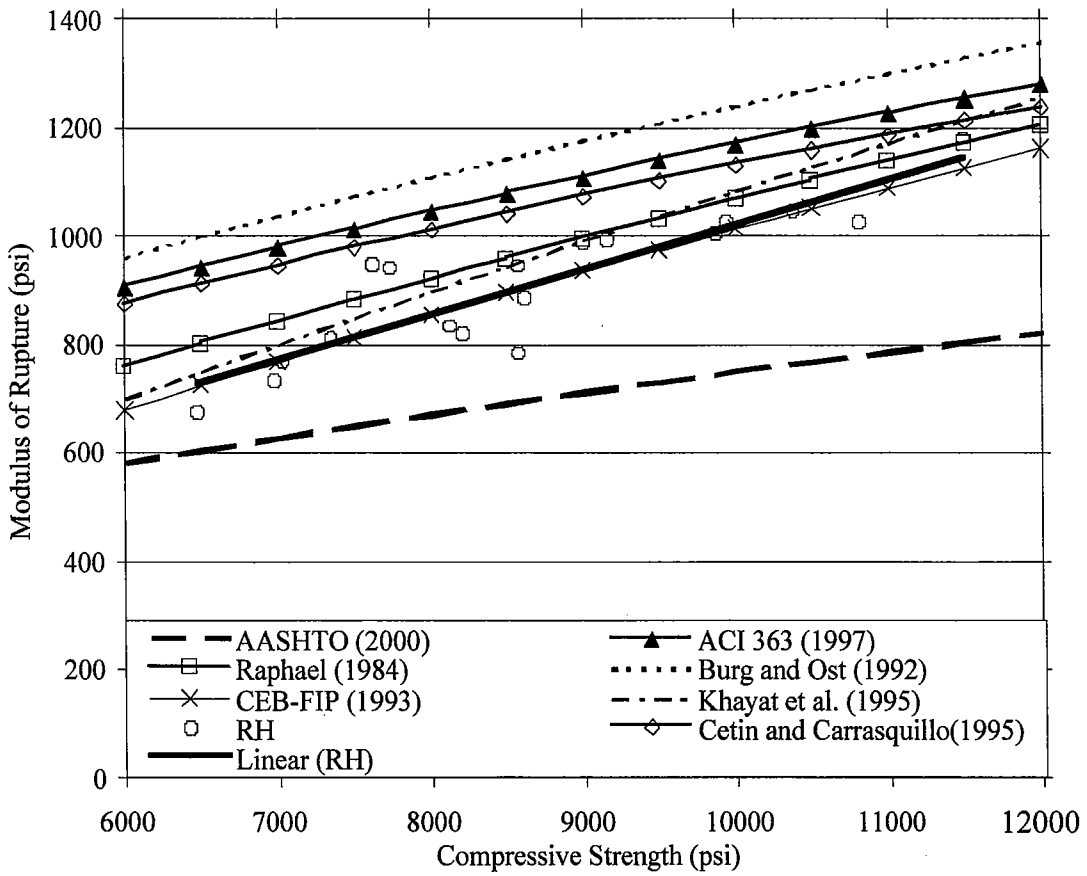

Figure 4.17. MOR versus Compressive Strength (RH Exposure).

Figure 4.18 includes the prediction formulas and the expression developed for the RL exposure condition. The best-fit equation from this study for concrete cured under these conditions is as follows.

$$f_r = 8.4\sqrt{f'_c} \tag{4.7}$$

All formulas seem to overestimate the data points except for the AASHTO LRFD Specifications (2000) formula that is a lower bound to nearly all the data points. This exposure condition resulted in the lowest strength relationship and so it represents a worst case for the field exposure conditions considered in this study. Thus, only the AASHTO LRFD Specifications formula, which is the same as that of ACI 318 (2002), provides a conservative estimate of the MOR.

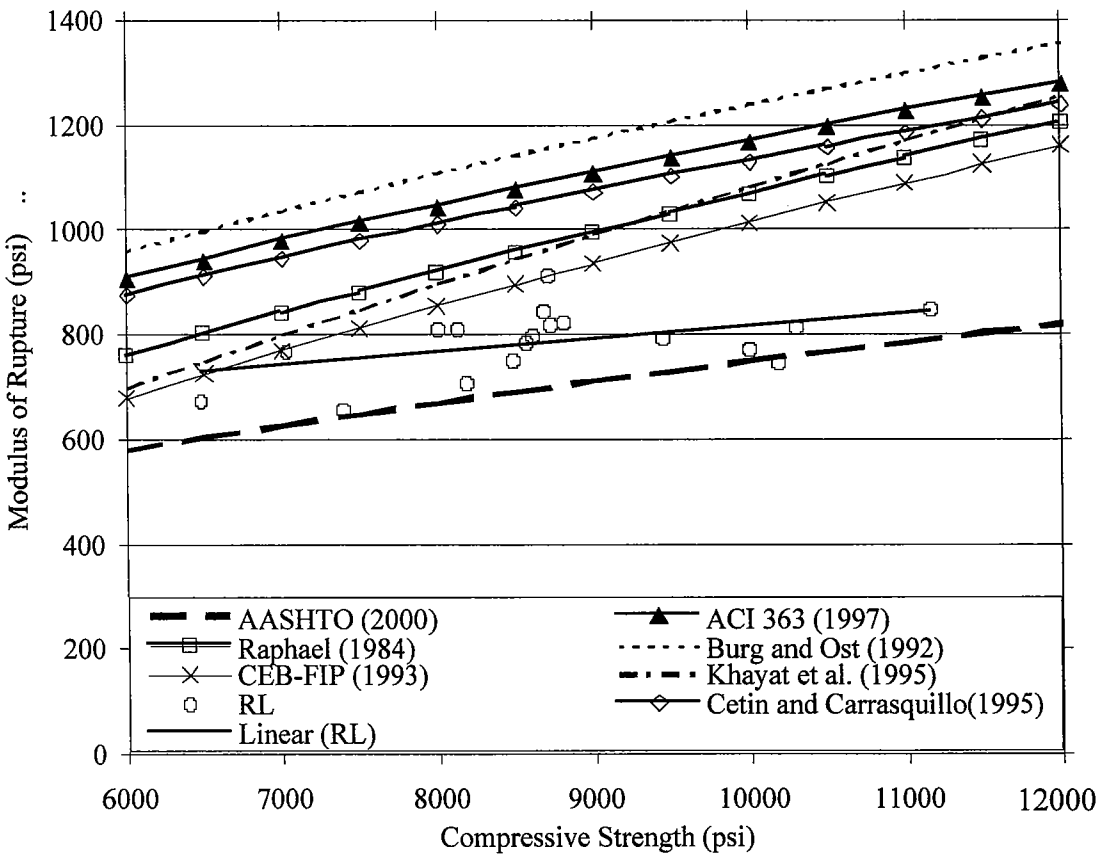

Figure 4.18. MOR versus Compressive Strength (RL Exposure).

4.7 THE MATURITY METHOD

The maturity method is used to predict concrete strength based on the concrete hydration temperature profile. This method is limited in accuracy because it does not account for the effect of humidity.

4.7.1 Hydration Temperature Profiles

As discussed earlier, the field exposure conditions involved subjecting the specimens to elevated heat exposure for one-day at a temperature of 107 ^{o}F and 100 percent relative humidity before transporting the specimens to rooms with different exposure (curing) conditions. The objective was to simulate a range of possible field exposure conditions at precast plants. The maximum hydration temperature depends mostly on the mass of the member. Since the specimens cast in the laboratory for this study are much smaller than bridge girders, the hydration temperature profile is expected to be lower for the specimens when cured at the same ambient temperature. Thus, specimens were subjected to elevated heat for 1 day to ensure that the hydration temperature profile is representative of the field profiles in the state of Texas. After approximately 1 day, the hydration process will slow down, and the internal temperature of the concrete will approach the ambient temperature.

For each exposure (curing) condition, the hydration temperatures were monitored in two beams and in two cylinders. The average temperature profiles for the beams and for the cylinders were used. The temperature profiles for each of the two beams were very close to each other. This was also the case for the two cylinders. Thus, using the average temperature profile is reasonable. The temperature profiles in Figures 4.19, 4.20, and 4.21 represent the hydration temperature profiles for specimens cast using the mixture proportions for Precasters A, B and C, respectively. The temperature profiles for the beams and cylinders were plotted for each exposure (curing) condition. As can be seen, the hydration temperatures in the beams are slightly higher than those in the cylinders. This is mainly because the beams have more mass than the cylinders.

Beams cured at 107 ^{o}F for the first day reached peak temperatures ranging from 120 ^{o}F to 135 ^{o}F, whereas cylinders reached peak temperatures ranging from 112 ^{o}F to 130 ^{o}F. Beams cured at 73 ^{o}F reached peak temperatures ranging from 85 ^{o}F to 106 ^{o}F, whereas cylinders reached peak temperatures ranging from 79 ^{o}F to 93 ^{o}F. Thus, there was a significant difference in the hydration temperatures for different precasters with different mixtures proportions. Specimens from the Precaster C mixture resulted in the highest hydration temperature profiles. The heat of hydration in not measurable for all specimens under all exposure (curing) conditions at approximately the same age for the different mixtures: 30 hours (Precaster A), 34 hours (Precaster B), and 28 hours (Precaster C). At these times the internal temperature of the concrete reaches the ambient temperature. The temperature becomes nearly constant past the time shown in the graphs.

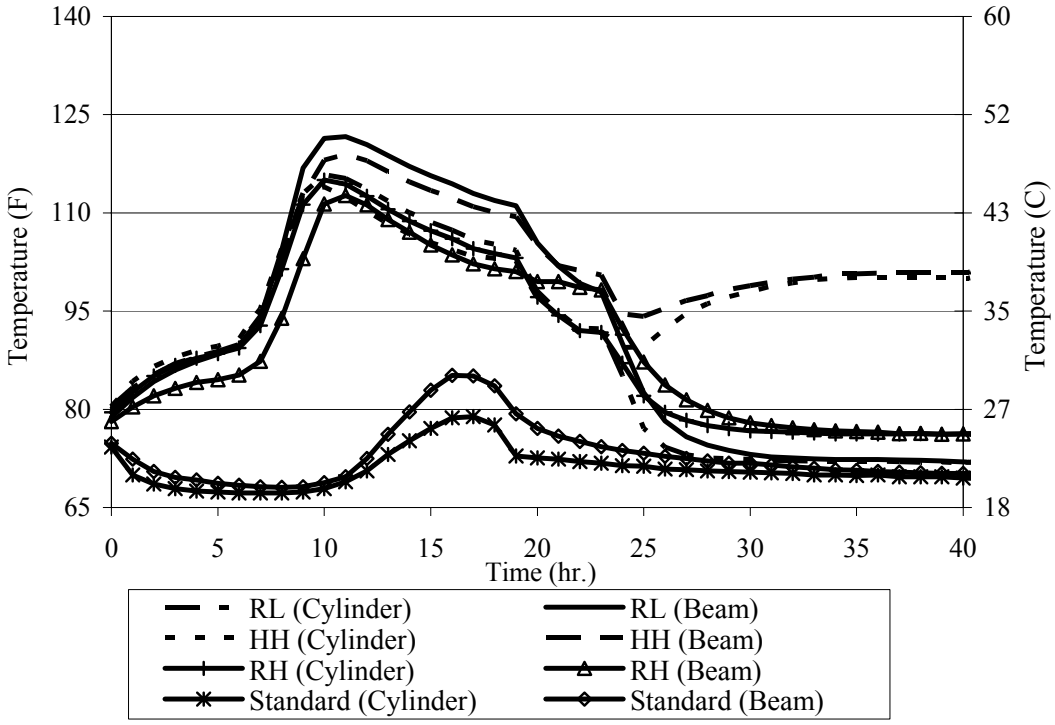

Figure 4.19. Temperature Hydration Profiles (Precaster A Specimens).

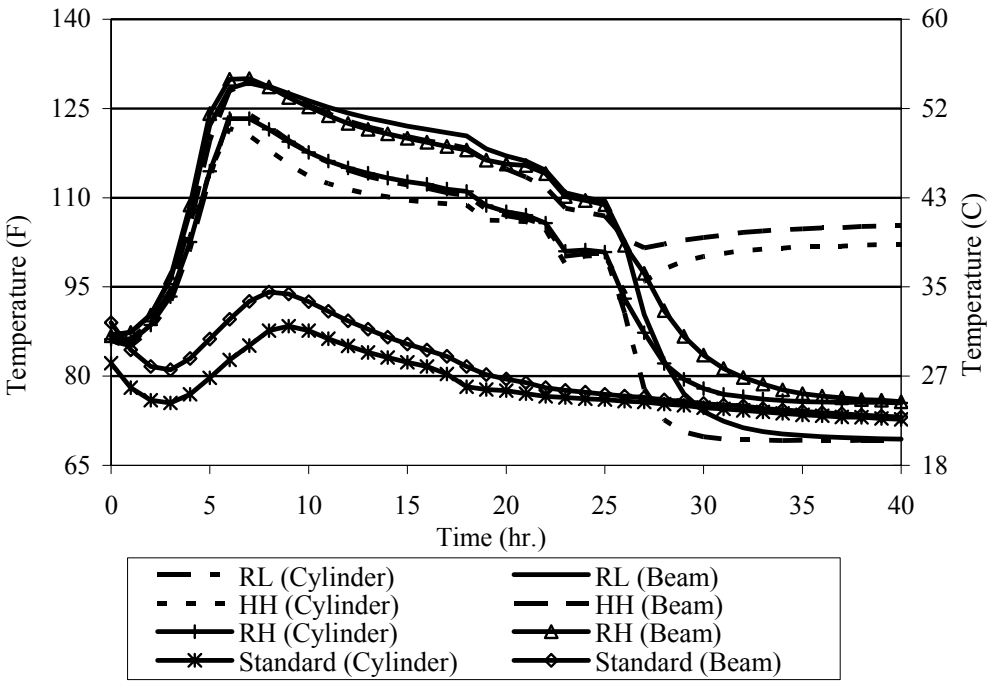

Figure 4.20. Temperature Hydration Profiles (Precaster B Specimens).

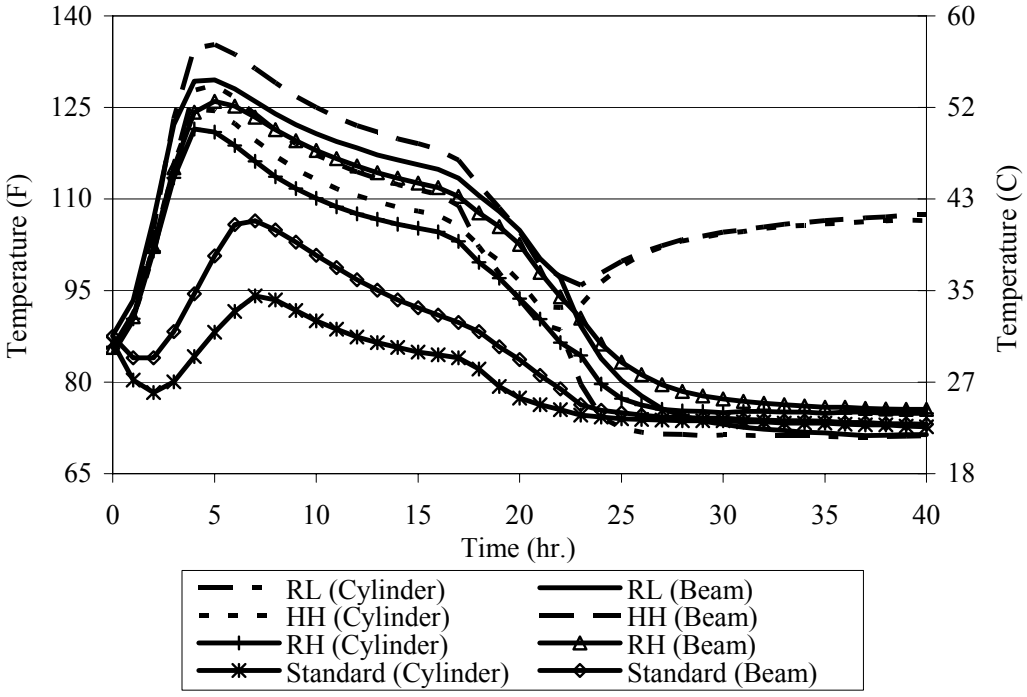

Figure 4.21. Temperature Hydration Profiles (Precaster C Specimens).

The success in representing different field exposure conditions can be evaluated in Figure 4.22. Actual hydration temperature data monitored in the field after casting of the girders were plotted. As discussed earlier, the hydration temperature in the member depends on the member mass, mixture constituents, constituent quantities, exposure conditions, and on the location of the thermocouple used to monitor the temperature. Thermocouples were placed at different locations inside the member. Only the minimum and maximum profiles were plotted for each period chosen. Figure 4.22 represents the highest and lowest actual field temperature profiles from Precaster B. Plotted are also the Precaster B specimen profiles determined for different exposure (curing) conditions in this study. As shown, all specimens exposed to "field" conditions resulted in hydration temperature profiles in between the actual field profiles. Thus, field exposure was successfully represented.

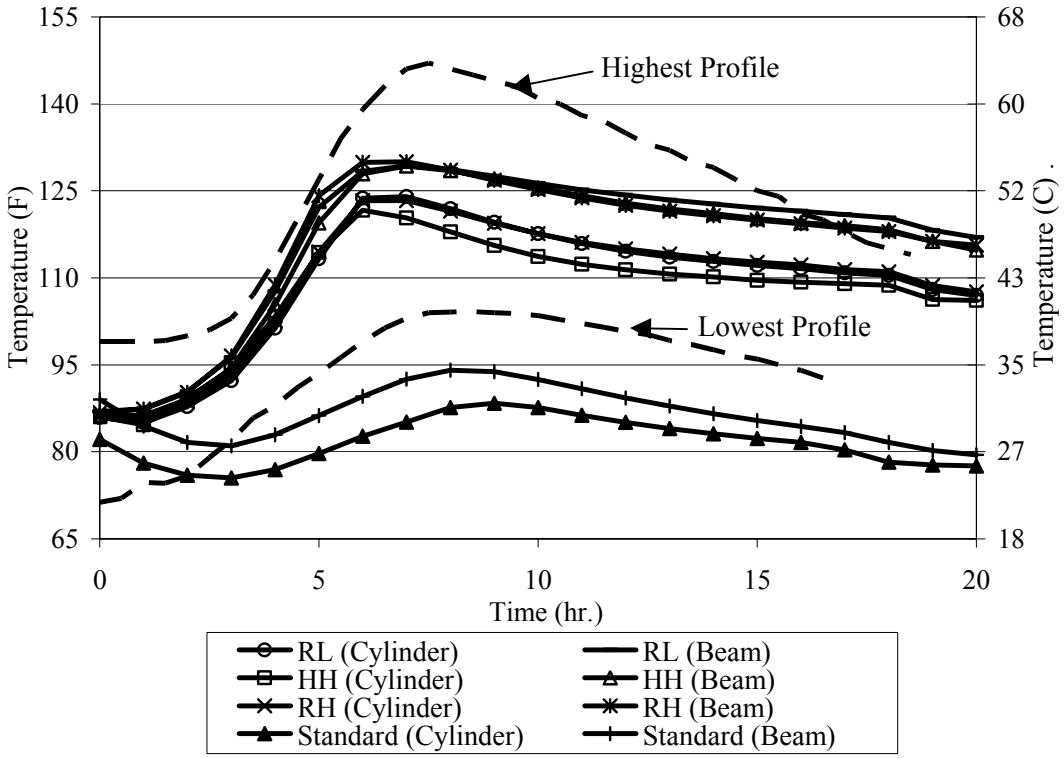

Figure 4.22. Specimens and Field Temperature Profiles (Precaster B).

4.7.2 Accuracy of the Maturity Method

4.7.2.1 Compression

Applying the maturity method involves determining the strength versus maturity index laboratory curve. This curve is based on concrete cured under standard exposure (curing) conditions. After the laboratory curve equation is determined, the strength of concrete cured under any other exposure temperature can be estimated by inserting the maturity index, determined from the hydration temperature profile, into the equation to find the corresponding strength. The accuracy of the maturity method for compression was evaluated for all precaster mixtures by comparing the actual strengths for different exposure conditions with the predicted strengths using the maturity method and determining the percentage error. Figure 4.23 represent the maturity laboratory curve for Precasters A, B, and C. The other points plotted represent the combination of compressive strengths and the corresponding maturity index determined for the field exposure conditions. The closer the points are to the laboratory curve, the more accurate the maturity method is in predicting the compressive strength. For compression, the maturity index determined from the area under the hydration temperature versus time profile for the cylinders was used. The datum temperature used was 14 ^{o}F.

Table 4.12 shows the percent accuracy of the maturity method in predicting concrete compressive strength for different precasters, exposure (curing) conditions, and ages. The maturity method predicted the concrete short-term compressive strength fairly well. The maximum prediction error for all exposure (curing) conditions for Precasters A and B was determined to be approximately 9 percent for the first seven days. However, for Precaster C, the maximum prediction error was approximately 17 percent for the first 7 days. The maturity method is not accurate in predicting the long-term strength beyond 7 days. This is because the maturity method is based on the hydration temperature profile, which means that the predicted strength is higher for higher temperatures. This means that the standard exposure (curing) conditions should then give a lower strength as predicted by the maturity method. However, the long-term strengths of specimens that were subjected to elevated heat exposure are actually lower than for standard curing conditions.

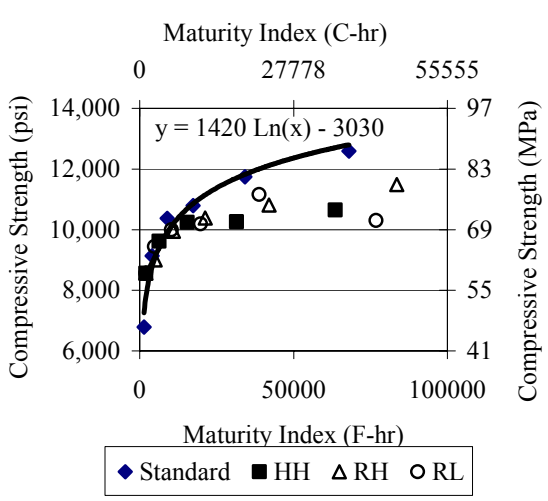

(a) Precaster A

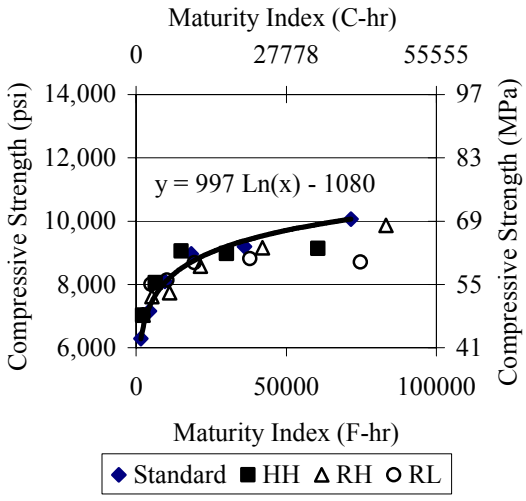

(b) Precaster B

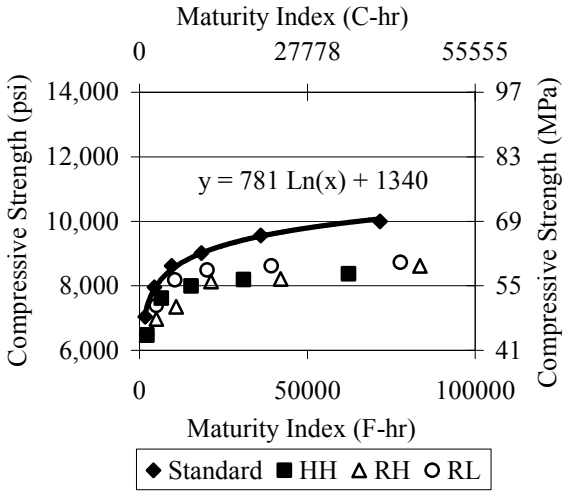

(c) Precaster C

Figure 4.23. Maturity Laboratory Curve and Actual Strengths (Compressive Strength).

Table 4.12. Maturity Index and Percent Error of the Maturity Method for Compressive Strength.

Exposure Condition	Age (days)	Precaster A		Precaster B		Precaster C	
		Maturity Index (°F-hr)	% Error	Maturity Index (°F-hr)	% Error	Maturity Index (°F-hr)	% Error
HH	1	2035	8.87	2234	6.02	2237	13.6
	3	6279	2.13	6383	4.97	6593	7.82
	7	15422	4.43	14989	6.11	15390	11.0
	14	31466	14.1	30163	2.50	31023	15.0
	28	63554	19.3	60521	8.39	62288	19.0
	56	127730	31.3	121236	11.8	124817	23.5
RH	1	2035	8.87	2283	5.71	2125	13.0
	3	5026	1.05	5269	2.06	5064	14.7
	7	10939	2.55	11136	6.14	10954	17.1
	14	21313	7.39	21434	3.32	21319	12.3
	28	42061	12.1	42031	4.10	42051	17.6
	56	83557	14.0	83224	3.50	83513	18.3
RL	1	2054	8.71	2272	5.78	2235	13.6
	3	4843	4.30	4973	7.51	5005	8.19
	7	10295	1.16	10231	0.12	10531	4.78
	14	19804	8.43	19429	0.96	20132	7.01
	28	38822	7.50	37842	7.00	39335	11.5
	56	76857	25.9	74667	16.1	77740	16.1

4.7.2.2 Flexure

The maturity method was not intended for use in predicting the MOR. Even so, the maturity method was used to determine if the MOR could be reliably estimated. Figure 4.24 presents the maturity laboratory curve for precasters A, B, and C.

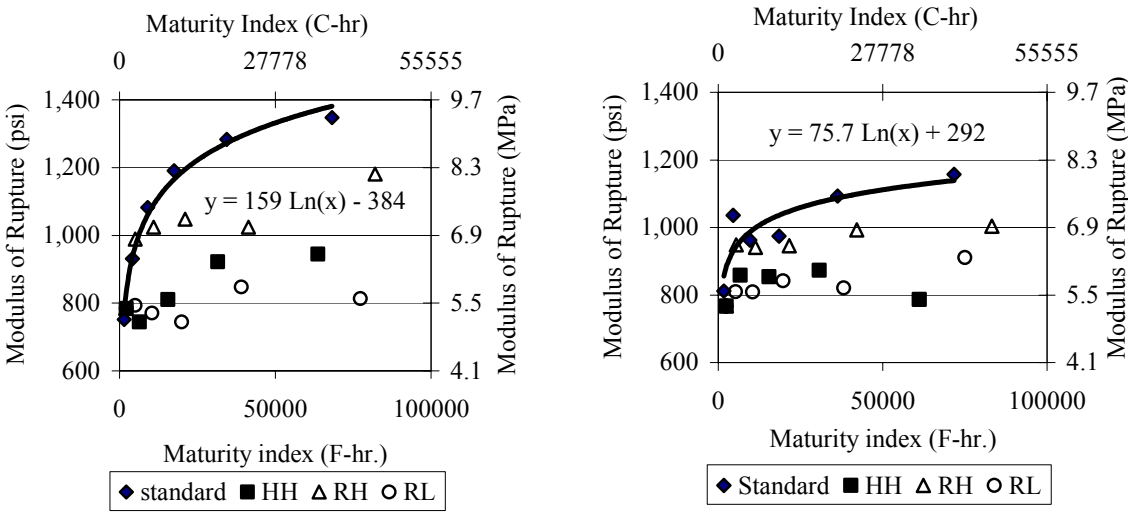

(a) Precaster A

(b) Precaster B

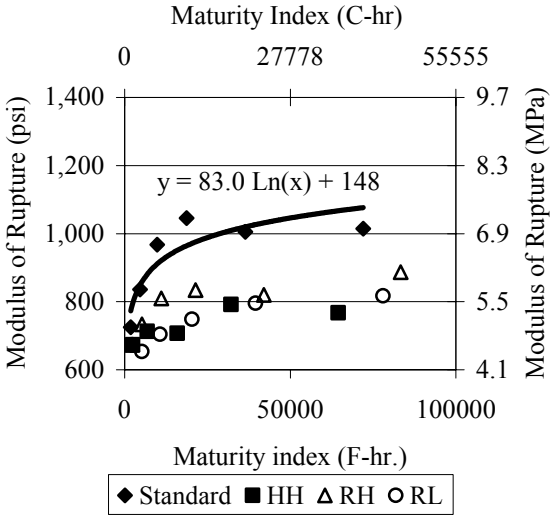

(c) Precaster C

Figure 4.24. Maturity Laboratory Curve and Actual Strength (for MOR).

Table 4.13 shows the percent accuracy of the maturity method in predicting the MOR for different precasters, exposure (curing) conditions, and ages. As shown, the percentage error is large, ranging from 2.2 to 72.3 percent. Therefore, the maturity method cannot predict the MOR of HSC.

Table 4.13. Maturity Index and Percent Error of the Maturity Method for the MOR.

Exposure Condition	Age (days)	Precaster A		Precaster B		Precaster C	
		Maturity Index (^{o}F-hr)	% Error	Maturity Index (^{o}F-hr)	% Error	Maturity Index (^{o}F-hr)	% Error
HH	1	2134	6.06	2426	15.0	2448	18.1
	3	6408	35.2	6734	11.8	6875	23.6
	7	15,510	41.5	15,453	19.7	15,948	34.6
	14	31,554	36.6	30,682	23.1	32,135	27.5
	28	63,642	45.1	61,137	43.2	64,509	39.1
	56	127,818	63.6	122,053	35.8	129,256	30.1
RH	1	1995	4.69	2446	15.1	2272	17.2
	3	5008	2.16	5494	0.46	5255	17.0
	7	10,900	6.44	11,349	6.22	11,121	13.7
	14	21,064	14.1	21,622	10.9	21,436	17.0
	28	41,384	27.1	42,169	10.6	42,067	25.8
	56	82,006	19.4	83,262	14.6	83,328	22.8
RL	1	2152	6.24	2464	15.2	2356	17.6
	3	4965	21.8	5235	16.1	5163	31.1
	7	10,429	40.7	10,480	22.8	10,707	30.3
	14	19,989	59.5	19,695	23.7	20,325	29.7
	28	39,107	52.5	38,125	32.9	39,561	29.0
	56	77,344	72.3	74,984	25.4	78,033	32.5

5 EVALUATION OF TENSILE STRESS LIMITS

5.1 GENERAL OVERVIEW

The focus of this study is to evaluate potential modifications to the allowable stress limits for the design of HSC prestressed bridge girders in Texas. Parametric studies conducted in Phase 2 of this research project (Hueste and Caudros 2003) indicated that the allowable tensile stress at service can limit the maximum span lengths for both AASHTO Type IV and Texas U54 HSC bridge girders. In addition, this is a stress limit that had some potential to be increased based on the testing of plant produced HSC samples in Phase 1 of this study (Hueste et al. 2003b). Therefore, the focus of this research was to determine whether the allowable tensile stress had a potential to be increased based on both the Phase 1 testing and the evaluation of exposure effects on strength described in this report.

The parametric study discussed in Chapter 6, along with the larger parametric study in Phase 2 (Hueste and Cuadros 2003), showed that HSC prestressed bridge girder designs are often controlled by the compressive stress limits. In addition, Phase 1 of this study showed that for HSC produced by Texas precasters, the actual concrete compressive strength at service is typically greater than specified, where the ratio of the actual to specified $f'c$ ranged from 1.01 to 1.89 (Hueste et al. 2003b). Note that the Phase 1 results did not consider field exposure conditions. For this study, the compressive stress limit was maintained as 0.45 $f'c$ as specified in the LRFD Specification. The reason for this is that the current limits for the compressive stresses were established to limit excessive creep, camber, or other local strains. The compressive stress limits for sustained loads (0.4 $f'c$ to 0.45 $f'c$) are generally in the linear range of behavior for NSC. An increase in the stress limit to 0.6 $f'c$ is allowed for load cases including transient loads. These limits were developed for NSC, and more studies are needed to evaluate whether these limits are applicable to HSC. Assuming that the same coefficients are appropriate for the compressive stress limits for HSC prestressed members, it is not conservative to assume an overstrength will be provided in the design phase, because production practices may change among precasters over time, and this overstrength is not a requirement. Potentially, the actual strength gain can be utilized by tailoring designs based on strength data for a typical concrete

mixture used by the selected precaster. However, the precaster may not be identified in the initial design stage and so this may not always be practical.

5.2 DETERMINATION OF APPROPRIATE EXPOSURE FACTORS

In Phase 1 of this study (Hueste et al. 2003b), specimens were cast at the precast plant, left at the plant to cure for 24 hours and then were transported back to the laboratory and placed in standard laboratory curing conditions. In order to evaluate whether the current allowable tensile stress at service may be adjusted for HSC prestressed girders in Texas, the data from the first phase of this study requires adjustment to reflect potential strength reductions due to field exposure conditions. In order to properly adjust for the mechanical properties obtained from the earlier phase of this study, it is important to determine which exposure condition considered in this study best reflects the exposure condition for the Phase 1 testing. Once this is established, exposure (curing) factor adjustments based on the appropriate exposure condition can be applied.

5.2.1 Selection of Appropriate Mixture Proportions

In this phase, typical mixture proportions were chosen for each precaster to evaluate strength under different exposure (curing) conditions. These mixture proportions were selected from among those used in Phase 1 of this study. The adjustments to the data to reflect different exposure conditions should be applied to Phase 1 specimens that were made from the same mixture proportions and that used the same aggregate type used in this study. The water-cement ratio and the aggregate type are especially critical in influencing the concrete strength when the cement type is unchanged. Table 5.1 includes a list of batches from Phase 1 sample collections that match the mixture proportions and aggregate type used for this study on exposure (curing) effects. The collection identifier includes two numbers, reflecting that two batches were tested for each collection. A total of six collections were made for each precaster. Precaster A uses varying mixture proportions, but recommended the use of a typical lower water-cement ratio (0.28) mixture for this study to be most representative of their standard mixture proportions. Phase 1 included collections for this water-cement ratio, as well as higher water-cement ratios.

Therefore, not all samples could be included for Precaster A. Precaster B changed from crushed limestone to river gravel for the coarse aggregate towards the end of Phase 1 testing. Therefore, only two collections matched the aggregate used in this study, where the current aggregate type was used.

It is important to note that the field temperature varied on different casting days for the earlier phase. From this study, it was determined that different ambient temperatures for the first day influence the concrete strength. The specimens under the RH exposure condition were subjected to elevated heat exposure for one day before they were cured under standard conditions. Because most of the first day ambient temperatures for the Phase 1 specimens lie between the RH and the standard curing conditions, it is also important to separate the appropriate batches from Phase 1 into those subjected to lower temperatures and those subjected to higher temperatures for the first day of exposure, and then test for which exposure condition considered in this study best reflects the exposure conditions in Phase 1. Therefore, Phase 1 specimens subject to one day ambient temperatures lower than 90 ^{o}F were considered separately than those with temperatures greater than 90 ^{o}F. Mechanical properties determined for specimens subject to first day temperatures lower than 90 ^{o}F) should be more consistent with those for specimens in this study that were subject to standard curing conditions. Mechanical properties determined for specimens cured for the first day at temperatures greater than 90 ^{o}F should be more consistent with the RH exposure condition. If this is true, then exposure (curing) factor adjustments can be applied separately for both cases. Table 5.1 shows the distribution of the Phase 1 batches among the different one-day ambient temperature ranges. Note that no MOR data were provided for collections A13-A14, B11-B12, and C13-C14.

Table 5.1. Summary of Appropriate Mixture Proportions.

Precaster	Mixture Proportions (All)	Mixture Proportions (T < 90 °F)	Mixture Proportions (T > 90 °F)
A	A11-A12, A13-A14, A15-A16, A17-A18	A13-A14 (88 °F)	A11-A12 (92 °F) A15-A16 (90 °F) A17-A18 (91 °F)
B	B13-B14, B15-B16	B15-B16 (79 °F)	B13-B14 (91 °F)
C	C3-C4, C7-C8, C9-C10, C11-C12, C13-C14, C15-C16, C17-C18	C3-C4 (61 °F) C7-C8 (72 °F) C9-C10 (63 °F) C11-C12 (68 °F) C13-C14 (88 °F) C17-C18 (77 °F)	None

5.2.2 Determination of Appropriate Exposure (Curing) Factors

To determine which exposure condition from this study best reflects the exposure condition considered in Phase 1, the strength data for the Phase 1 specimens was compared to the strength data from this study at ages of 7, 28, and 56 days. Plots were made with the x-axis corresponding to the strength obtained for each of the exposure conditions considered in this study and the y-axis corresponding to the strengths obtained for the exposure condition considered from Phase 1. Therefore, each data point represents the strength for a Phase 1 specimen versus the corresponding strength for a specimen from this study for concrete having the same materials, mixture proportions, and ages. A line of equality was plotted in each graph to visually evaluate which exposure condition best reflects the earlier phase. However, an evaluation was also performed analytically by finding a relative prediction error, as follows.

$$RPE = \frac{1}{n}\sum_{i=1}^{n}\left(\frac{f'}{f} - 1\right)^2 \qquad (5.1)$$

where f is the value of material property (compressive strength or MOR) obtained from testing, and f' is the predicted value. In this study f' is the material strength value obtained from Phase 1.

Relative prediction errors were calculated for all considered batches for both compressive strength and the MOR (flexural strength). Plots of the compressive and flexural strengths obtained from the previous study versus the compressive and flexural strengths obtained from this study for the four different exposure conditions are shown in Figures 5.1 and 5.2. All appropriate mixture proportions were used for these plots. Figures 5.3 and 5.4 show similar plots for mixture proportions with temperatures lower than 90 ^{o}F. Figures 5.5 and 5.6 is for mixture proportions with temperatures higher than 90 ^{o}F.

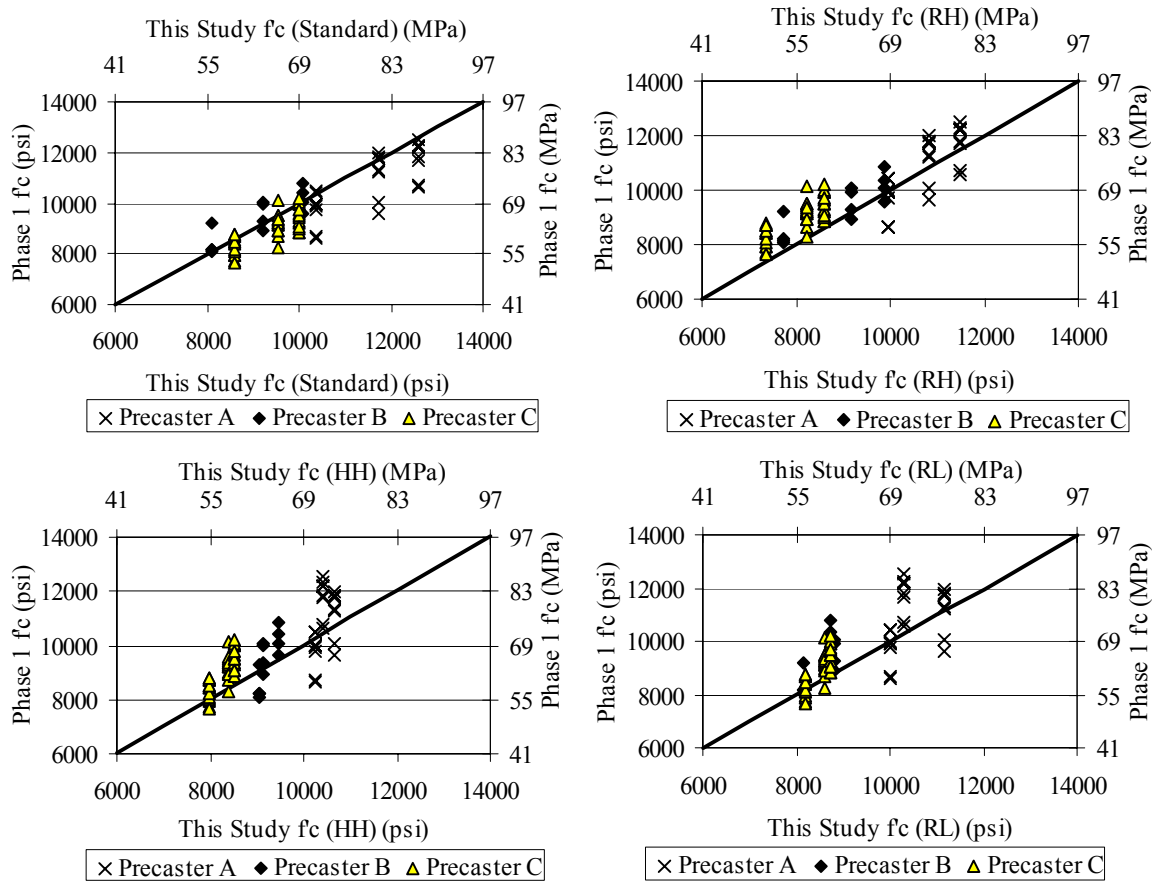

Figure 5.1. Equality Test for All Mixture Proportions – Compressive Strength.

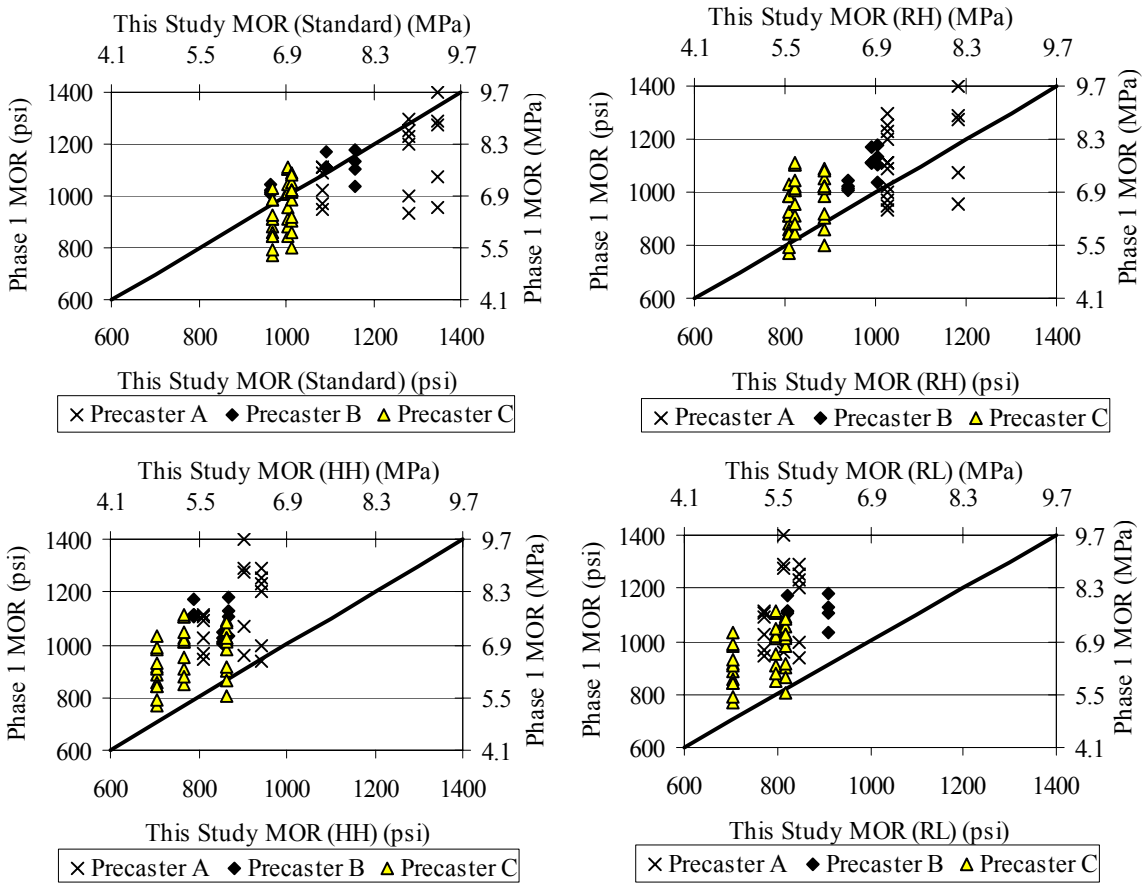

Figure 5.2. Equality Test for All Mixture Proportions – MOR.

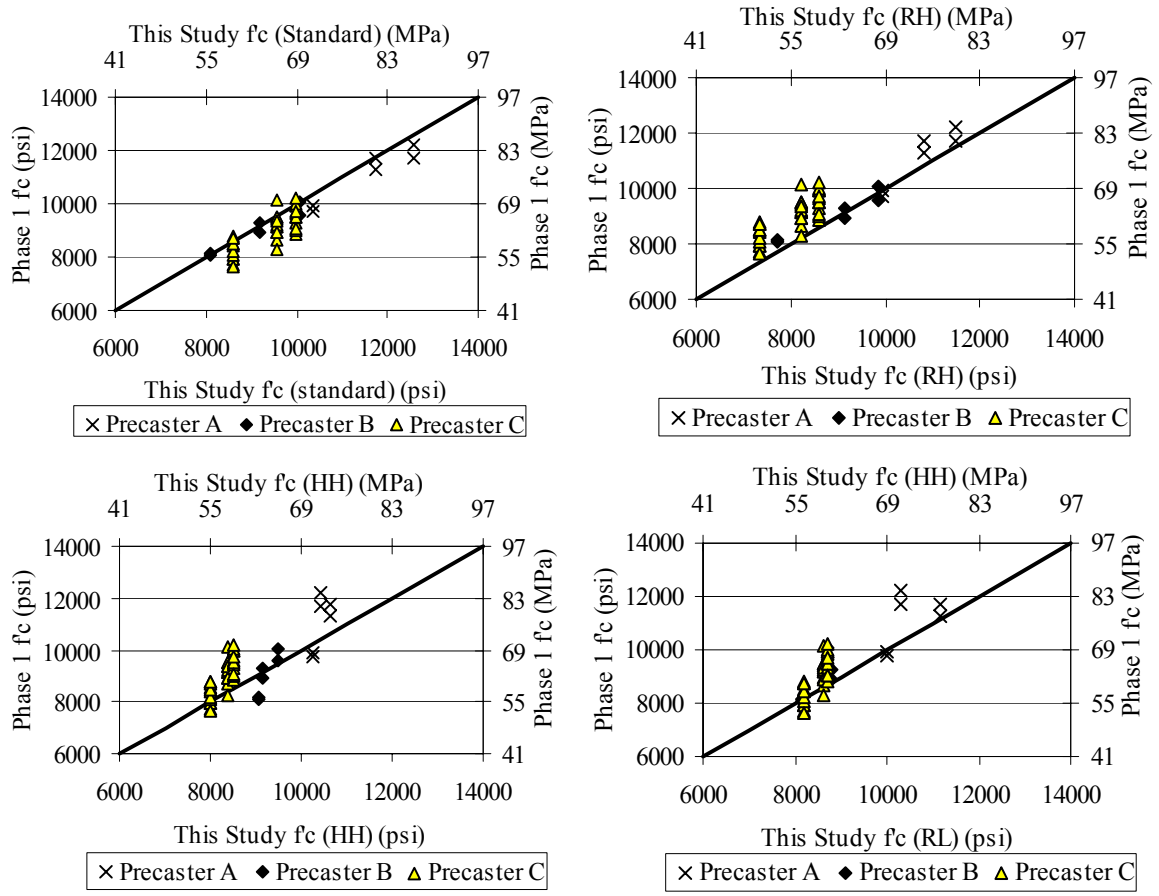

Figure 5.3. Equality Test for Mixture Proportions (Temperatures < 90 ^{o}F) – Compressive Strength.

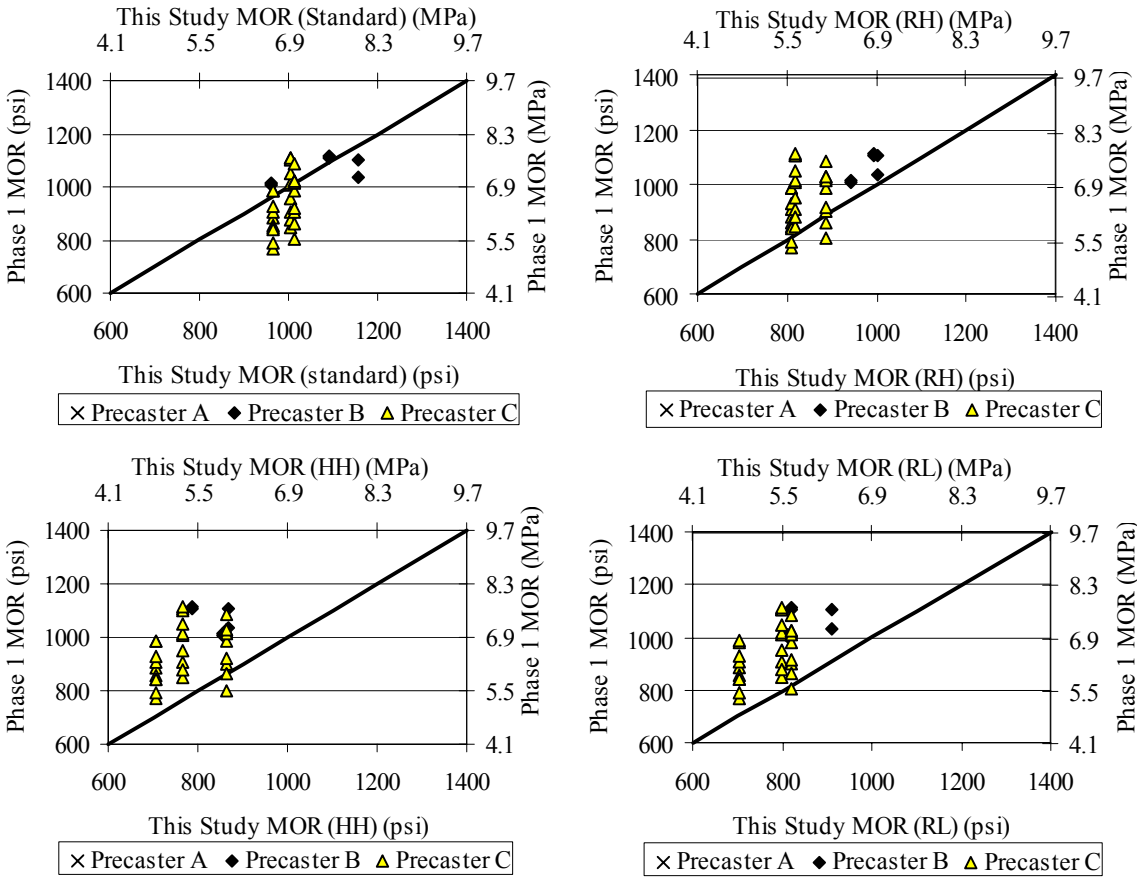

Figure 5.4. Equality Test for Mixture Proportions (Temperatures < 90 ^{o}F) – MOR.

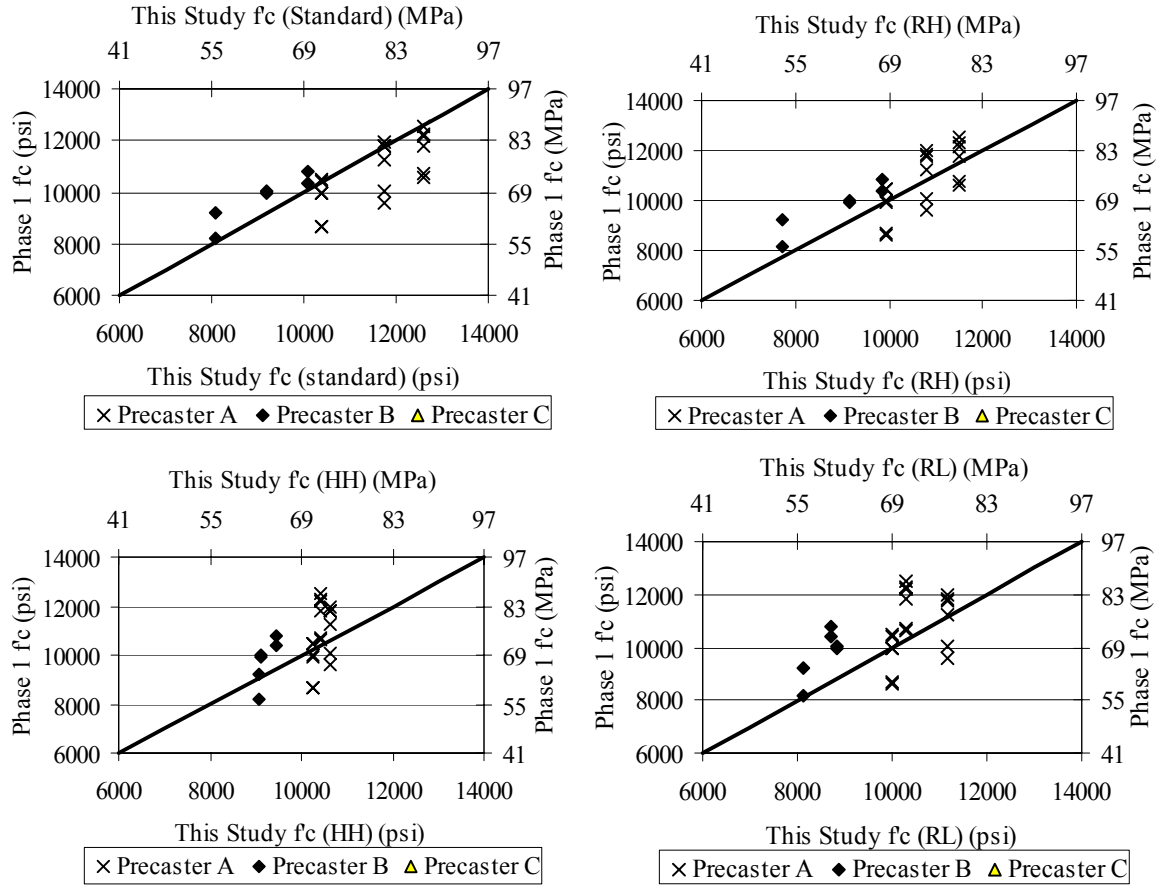

Figure 5.5. Equality Test for Mixture Proportions (Temperatures > 90 ^{o}F) – Compressive Strength.

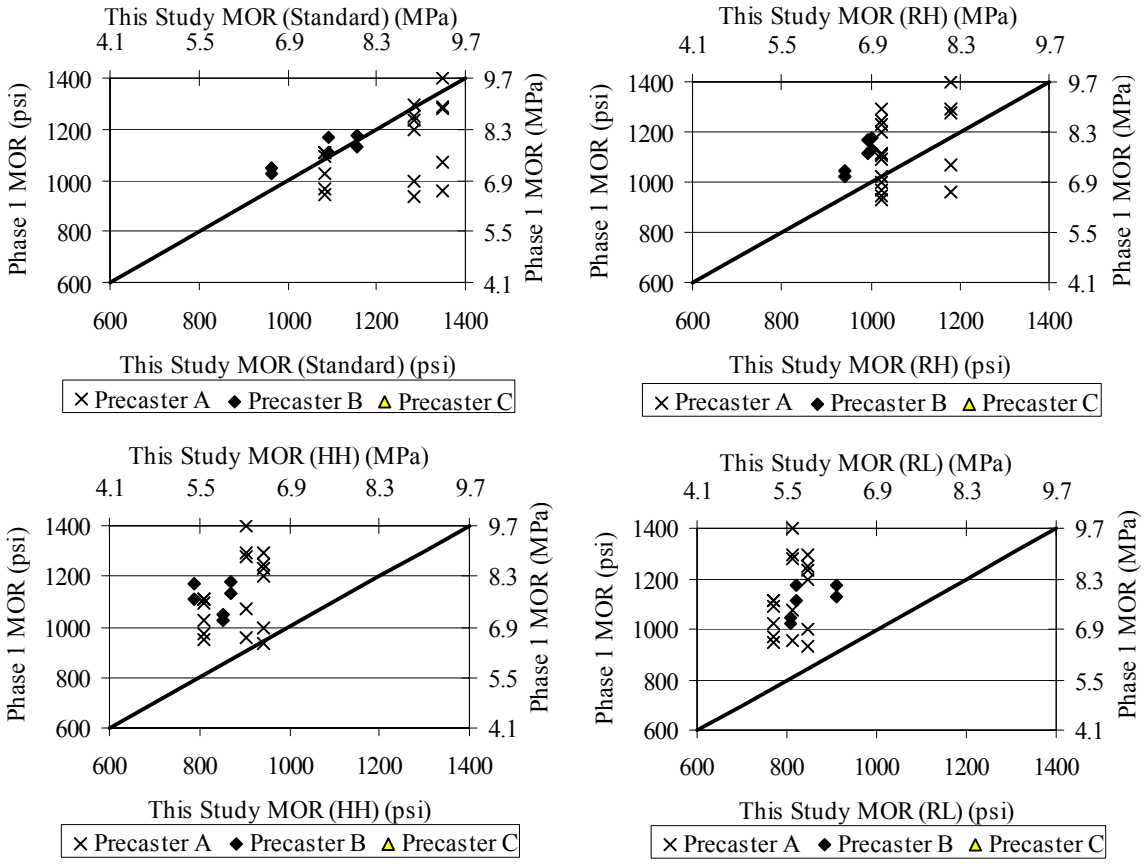

Figure 5.6. Equality Test for Mixture Proportions (Temperatures > 90 °F) – MOR.

From these plots, the standard curing condition and the RH exposure condition seem to best reflect the strength data from Phase 1 of this research program. Since it is difficult to determine which one of these two exposure conditions is more accurate in reflecting the earlier phase, the relative prediction errors were calculated. The results are shown in Table 5.2. When considering the appropriate mixture proportions for temperatures lower than 90 °F, the standard curing condition seems to result in the lowest prediction errors (percent) for both compressive and flexure strengths. This was expected because the low temperatures should reflect the standard curing condition better than the RH exposure condition where the temperature is 107 °F. When considering the appropriate mixture proportions for temperatures higher than 90 °F, the RH exposure condition resulted in the lowest prediction errors (percent) for both compression and flexure. This was expected because the high temperatures should reflect the RH exposure

condition better than the standard curing condition, where the temperature is 73 ^{o}F. Finally, when considering all the appropriate mixture proportions for all temperatures, the standard curing condition seems to result in the lowest prediction errors (percent) for both compressive and flexure strengths. This might be because there are a larger number of specimens subjected to temperatures lower than 90 ^{o}F than temperatures higher than 90 ^{o}F.

Table 5.2. Relative Prediction Errors for Compression and MOR.

Temperatures	Mechanical Property	Relative Prediction Errors (%)			
		Standard	RH	HH	RL
All Temperatures	Compression	7.77	9.56	9.31	8.74
	MOR	12.18	13.50	21.81	23.52
Temperatures < 90 ^{o}F	Compression	6.10	9.84	8.97	7.51
	MOR	11.09	13.24	19.85	19.65
Temperatures > 90 ^{o}F	Compression	10.54	8.55	10.30	11.30
	MOR	14.75	12.53	23.93	24.14

5.3 EVALUATION OF TENSILE STRESS LIMIT

5.3.1 Adjustment of Phase 1 Data

5.3.1.1 All Ambient Temperatures

The different temperature cases were all considered for recommendation of new allowable stresses. When all temperatures were considered, the exposure factors were calculated by considering the standard curing condition as the baseline. Thus, the exposure factor is the ratio between the strength obtained for each of the four exposure conditions investigated in this study to the strength obtained for the baseline exposure condition, which is standard laboratory curing in this case. From the statistical analysis, it was determined that the three-way interaction existed and so there was a significant difference among precasters, ages, and exposure conditions. Thus, different exposure factors were considered for different precasters, ages, and

exposure (curing) conditions. The strengths obtained in the previous phase of this study were then adjusted based on these exposure factors. The exposure factors shown in Table 4.5 were used in modifying Phase 1 compressive strength data. The exposure factors shown in Table 4.9 were used in modifying Phase 1 MOR data. Figure 5.7 shows the adjusted Phase 1 data results for all batches listed in Table 5.1 when samples exposed to all ambient temperatures were considered. The compressive and flexural strength data were adjusted for all four exposure conditions. The lower of the two lines shown represents the lower bound of the data. The other line represents the 95 percent lower bound to the data.

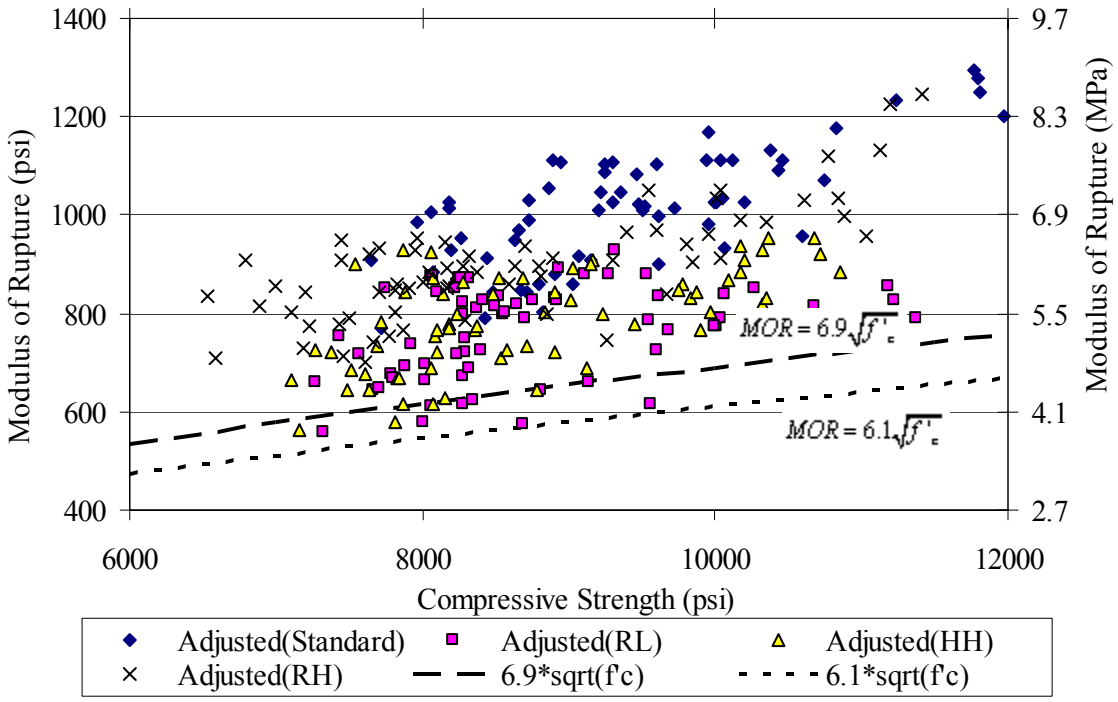

Figure 5.7. Adjusted Property Relationships (All Temperatures).

5.3.1.2 Lower Ambient Temperatures

When the batches with temperatures lower than 90 °F are considered, the standard curing condition was also found to be the exposure factor baseline. This was because the standard curing condition resulted in the lowest prediction errors (percent) for both compression and flexure. The strengths obtained in the previous phase of this study were then adjusted based on these exposure factors. Similarly, different exposure factors were considered for different precasters, ages, and exposure conditions. Figure 5.8 shows the adjusted Phase 1 data results for batches listed in Table 5.1 with temperatures lower than 90 °F. One of the two lines shown represents the lower bound of the data. The other line represents the 95 percent lower bound to the data.

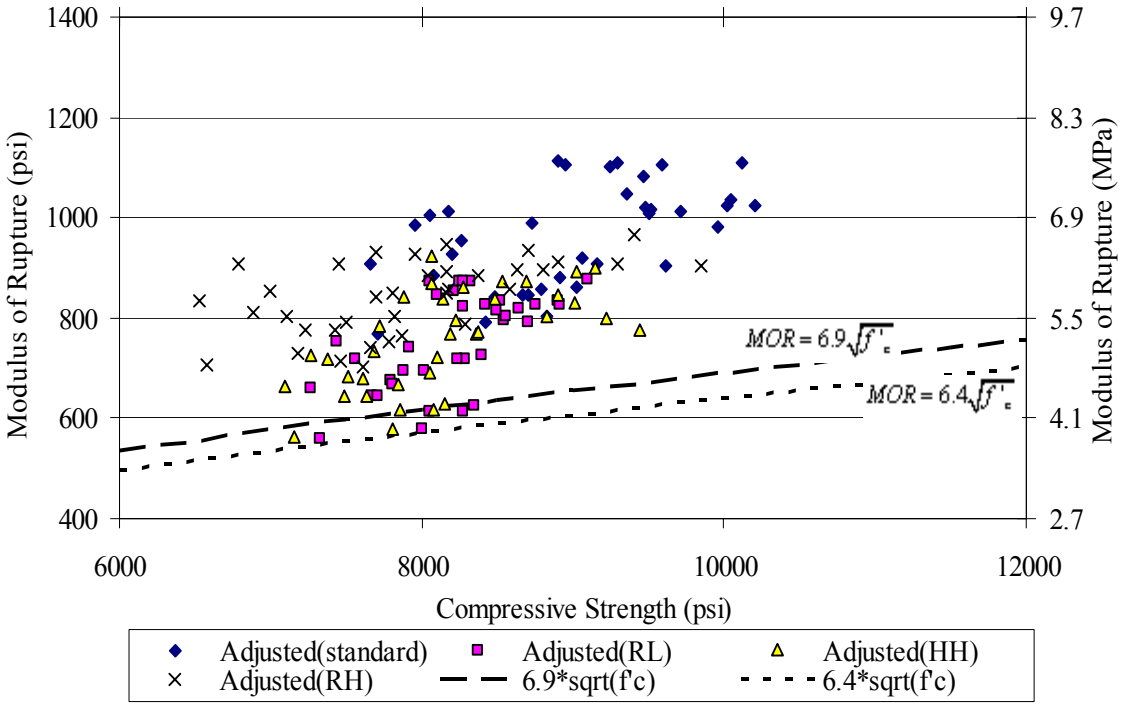

Figure 5.8. Adjusted Property Relationships (Temperatures < 90 °F).

5.3.1.3 Higher Ambient Temperatures

When the batches with temperatures greater than 90 °F were considered, the RH exposure condition was found to be the exposure factor baseline. The strengths obtained in the previous phase of this study were then adjusted based on these exposure factors. Similarly, different exposure factors were considered for different precasters, age, and exposure conditions. Figure 5.9 shows the adjusted Phase 1 data results for batches listed in Table 5.1 with temperatures greater than 90 °F. The lower line shown in the figure represents the lower bound of the data. The other line represents the 95 percent lower bound to the data.

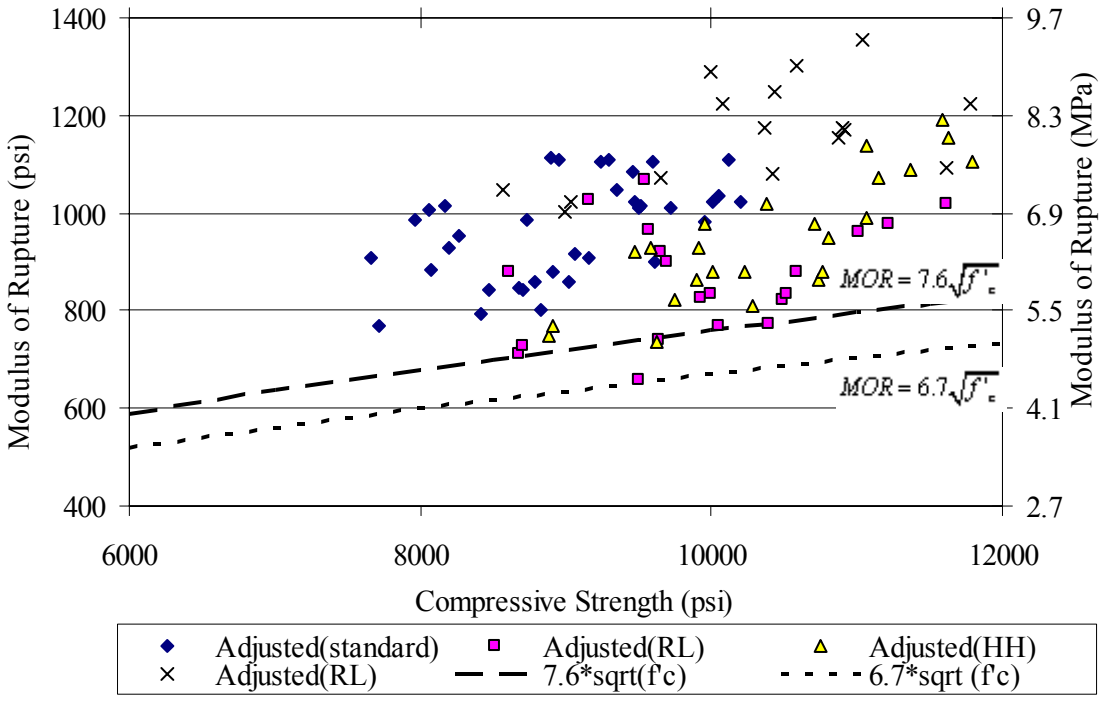

Figure 5.9. Adjusted Property Relationships (Temperatures > 90 °F).

5.3.2 Tensile Stress Limit for Design

Because the RH was the baseline exposure condition for batches with temperatures greater than 90 ^{o}F, the modified results were higher than the first two cases where the standard was the baseline. This was expected because the RH exposure condition resulted in strengths that are lower than the standard curing condition. Therefore, the exposure factors based on the RH exposure condition were higher, resulting in higher modified strengths. Because the temperature is different whenever casting takes place, it is impossible to recommend the two equations for batches that depend on the ambient temperature. It is more realistic to recommend one allowable stress equation that represents all ranges of ambient temperatures. Because the analysis of data considering all temperatures resulted in more conservative equations compared to other cases and because it covers all ranges of temperatures, recommendation will be based on this case. Based on the experimental results and the resulting data modified to account for all exposure conditions a modified tensile stress limit for design of Texas HSC for prestressed members is given in Equation 5.2

$$f_t = 7.0\sqrt{f_c'} \qquad (5.2)$$

where f_t is the allowable tensile stress (psi), and f_c' is the concrete compressive strength (psi). This simplified expression is slightly larger than the 95 percent lower bound to the data given in Figure 5.7. This limit is based on tests of small specimens, and size effects are also an important consideration that could not be addressed within the scope of this study.

5.3.3 Use of Other Exposure Factors

5.3.3.1 Use of Lowest Exposure Factor

Because the three-way interaction was significant among precasters, ages, and exposure conditions, the exposure factors used in modifying the strengths obtained from the earlier phase of this study, were different among ages, precasters, and exposure conditions. The possibility of using one exposure factor to modify all the data was also studied. Figure 5.10 shows the

modified results based on the lowest exposure factors for compression and MOR for the case when all temperatures were considered. The lowest exposure factors among exposure conditions, ages, and precasters for compression and flexure were found to be 0.82 and 0.60, respectively. From the graphs, it is clear that the lower bound for the data is lower than the tensile stress equation recommended by the ACI 318 code and the AASHTO LRFD specification, discussed in Section 4. The 95 percent lower bound equation shown is approximately the same as that recommended by the codes. It is clear that this is conservative when compared with the equation recommended based on different exposure factors for ages, precasters, and exposure conditions.

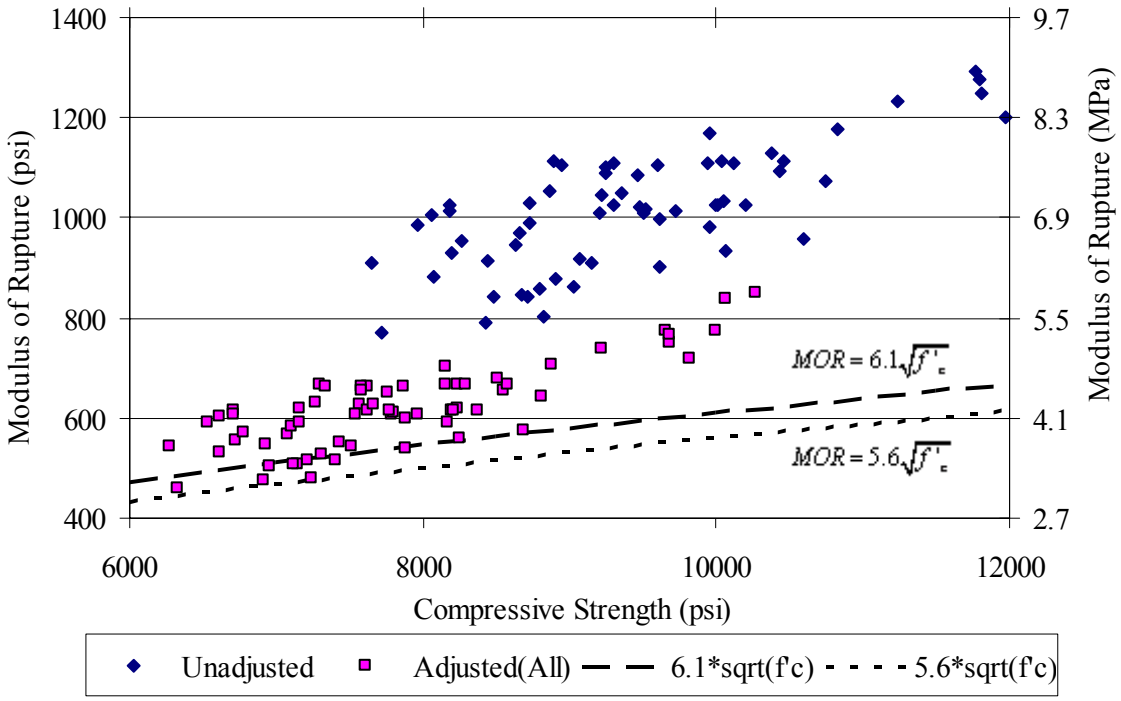

Figure 5.10. Adjusted Property Relationships Based on Lowest Exposure Factors.

5.3.3.2 Use of Average Exposure Factor

Figure 5.11 shows the modified results based on the average exposure factors for compression and flexure. The average exposure factors among exposure conditions, ages, and precasters for compression and flexure were 0.93 and 0.79, respectively. From the figure, it is clear that the allowable stress equations increased significantly. Recommending an allowable stress equation based on an average exposure factor may not be conservative because there is a large difference between the 0.79 average exposure factor and the 0.60 minimum exposure factor. Modifying the RL exposure condition by an average exposure factor of 0.79 instead of using the actual exposure factors of 0.71, 0.66, and 0.60 corresponding to the 7, 28, and 56 days overestimates the actual strength obtained at these days. Clearly, it is not safe to recommend an allowable stress equation based on an average exposure factor.

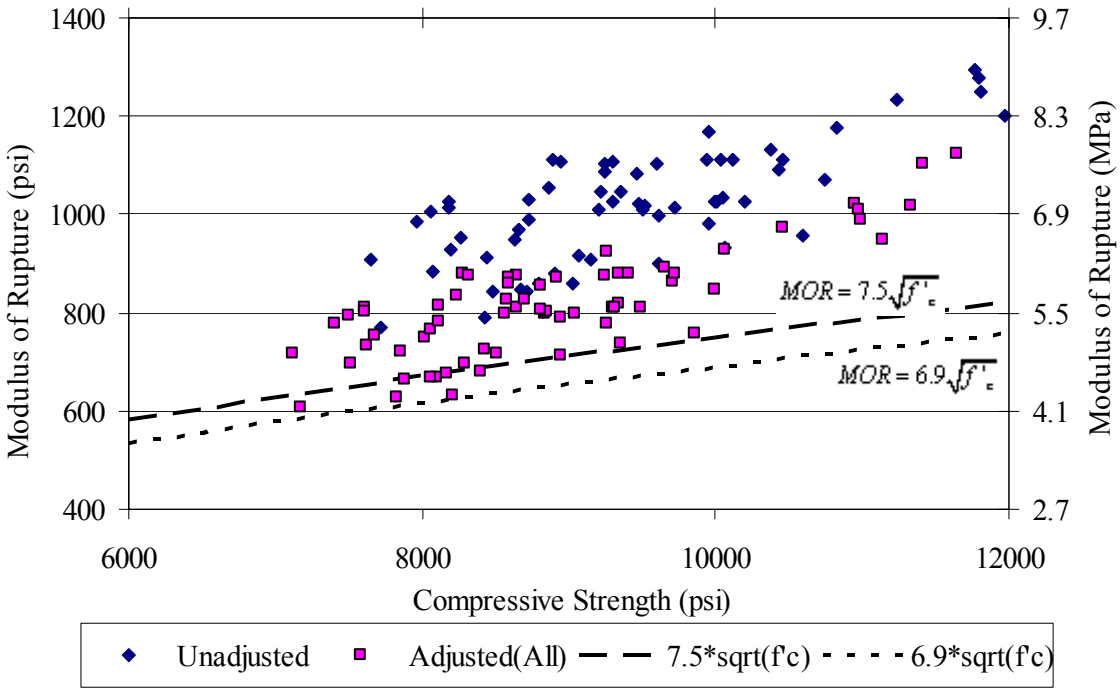

Figure 5.11. Adjusted Property Relationships Based on Average Exposure Factors.

6 PARAMETRIC STUDY AND RELIABILITY

6.1 GENERAL OVERVIEW

A parametric study was conducted to evaluate the impact of the modified tensile stress limit determined in Chapter 5 for the design of HSC prestressed girders by varying design parameters to determine the maximum span lengths that can be achieved under the current AASHTO design specification and when using the increased tensile stress limit. A reliability study was then conducted to compare the relative safety of the current and modified tensile stress limits by using statistical parameters to describe the load and resistance variables and then applying Monte Carlo simulation to determine the reliability indices for the designs obtained from the parametric study. The reliability indices for the designs based on current and modified tensile stress limits are compared.

6.2 PARAMETRIC STUDY

6.2.1 General

A parametric study was conducted to evaluate the impact of the modified tensile stress limit derived from the material testing in this study when applied to the design of HSC prestressed girders. The parametric study was performed for both the AASHTO Standard (1999) and LRFD (2000) Specifications. The specified concrete compressive strength and girders spacing were varied. The girder type considered was the Texas U54 beam section, because it is widely used in the design of bridges in the state of Texas. The diameters of the strands considered were 0.5 and 0.6 inch. The bridge girders were designed as simply supported beams to agree with TxDOT practices. The design parameters were selected to be consistent with the larger parametric study conducted for Phase 2 of this project by Hueste and Cuadros (2003). The allowable stress limits used in design are shown in Table 2.1. Design parameters can be found either in the larger parametric study conducted by Hueste and Cuadros (2003) or in the AASHTO Standard (1999) and LRFD (2000) Specifications. Additional design parameters are

also noted in Appendix D, where sample calculations are provided for a specific design. Table 6.1 summarizes the parameters and corresponding values evaluated.

Table 6.1. Summary of Design Parameters Evaluated.

Variable	Description and Selected Values
Codes	AASHTO Standard (1999) and LRFD (2000) Specifications
Girder Section	Texas U54
Concrete Strength	6000, 8000, 10,000, and 12,000 psi
Girder Spacing	8.5, 10, 11.5, 14.0, and 16.67 feet
Diameter of Strands	0.5 and 0.6 inch
Spans	Maximum spans ranged from 90 to 170 feet

For each combination of design specifications, concrete strength, girder spacing, and strand diameter, the maximum span length that can be achieved based on the flexural design considerations only by varying the number of strands in order to maximize the span lengths. Controlling limit states are the design criteria that limit the span length. In order for a design to be adequate, the ultimate flexural strength must be satisfied along the span. For service conditions, the allowable stresses that must be satisfied are the compressive and tensile stresses at release of prestressing at the beam ends, the compressive and tensile stresses due to sustained loads, and the compressive and tensile stresses at service under the total loads. The specified compressive strength of concrete at the time of initial prestress f'_{ci} was initially set at 0.75 f'_c and allowed to increase to the specified compressive strength f'_c at service if needed.

Minor differences occur between the designs in this study and equivalent cases for Phase 2 designs (Hueste and Cuadros 2003). The maximum difference between the two corresponding designs 0.8 feet, which is equivalent to 0.6 percent. This small difference is likely due to using a different number of iterations to refine the calculation of prestress losses. Results of the parametric study conducted for both the AASHTO Standard and LRFD Specifications will be discussed in the following sections.

6.2.2 AASHTO Standard Specification

6.2.2.1 0.5-Inch Diameter Strands

Table 6.2 shows the results of the parametric study for U54 girders with 0.5-inch strands following the AASHTO Standard Specification (1999). As expected, the modified tensile stress limit of $7\sqrt{f'_c}$ resulted in longer spans when the controlling limit state is tension at service due to total load at midspan. The increase in span lengths ranged from 0.9 to 2.2 feet, corresponding to an increase of 0.7 to 1.6 percent. The allowable concrete compressive strength under total sustained loads is the controlling limit state for most of the cases as long as the U54 girder can accommodate the strands required. Once no more strands can be accommodated (99 maximum), the tensile stresses at service due to total load becomes the controlling limit state. Therefore, the advantage of using the increased tensile stress limit takes place when using all 99 strand positions.

Figure 6.1 shows the maximum span lengths versus concrete strength for different girder spacings using the current and modified tensile stress limits for U54 girders with 0.5-inch strands. The new tensile stress limit results in longer maximum spans for the design using 10,000 and 12,000 psi, especially when using 99 strands. As shown, longer maximum spans can be attained with reduced girder spacing and higher concrete strength. Larger numbers of strands are required to attain maximum spans for higher concrete strengths and larger girder spacings. Because the maximum number of strands that the U54 girder section can accommodate is 99 strands, the use of 12,000 psi concrete for 0.5-inch diameter strands does not result in a significant increase in the maximum span length.

Table 6.2. Summary of Maximum Spans (AASHTO Standard Specification, Strand Diameter = 0.5 inch).

f'_c (psi)	f'_{ci} (psi)	Girder Spacing (feet)	$f_t = 6\sqrt{f'_c}$ (psi)		$f_t = 7\sqrt{f'_c}$ (psi)		Controlling Limit State	Difference in Span Length	
			Max. Span (feet)	No. Strands	Max. Span (feet)	No. Strands		(feet)	(%)
6000	4500	8.5	113.9	57	113.9	57	f (c) TDL	-	-
	4500	10.0	109.9	56	109.9	56	f (c) TDL	-	-
	4500	11.5	106.8	59	106.8	59	f (c) TDL	-	-
	4974	14.0	102.1	64	102.1	64	f (c) TDL	-	-
	5426	16.6	97.7	69	97.7	69	f (c) TDL	-	-
8000	6000	8.5	129.9	81	129.9	81	f (c) TDL	-	-
	6000	10.0	125.2	77	125.2	77	f (c) TDL	-	-
	6000	11.5	121.5	81	121.5	81	f (c) TDL	-	-
	6498	14.0	115.6	86	115.6	86	f (c) TDL	-	-
	6972	16.6	109.9	92	109.9	92	f (c) TDL	-	-
10,000	7500	8.5	140.2	97	141.3	94	f (c) TDL	1.1	0.8
	7500	10.0	135.9	96	136.8	93	f (c) TDL	0.9	0.7
	7500	11.5	130.2	99	131.5	96	f (t) TL	1.3	1.0
	7500	14.0	120.9	99	122.7	99	f (t) TL	1.8	1.5
	7500	16.6	112.8	99	114.5	99	f (t) TL	1.7	1.5
12,000	9000	8.5	141.9	99	144.1	99	f (t) TL	2.2	1.6
	9000	10.0	137.9	99	140.1	99	f (t) TL	2.2	1.6
	9000	11.5	131.4	99	133.4	99	f (t) TL	2.0	1.5
	9000	14.0	122.0	99	124.0	99	f (t) TL	2.0	1.6
	9000	16.6	113.9	99	115.7	99	f (t) TL	1.8	1.6

f(c) TDL = Compressive stresses due to total dead load at midspan.
f(t) TL = Tensile stresses at service due to total load at midspan.

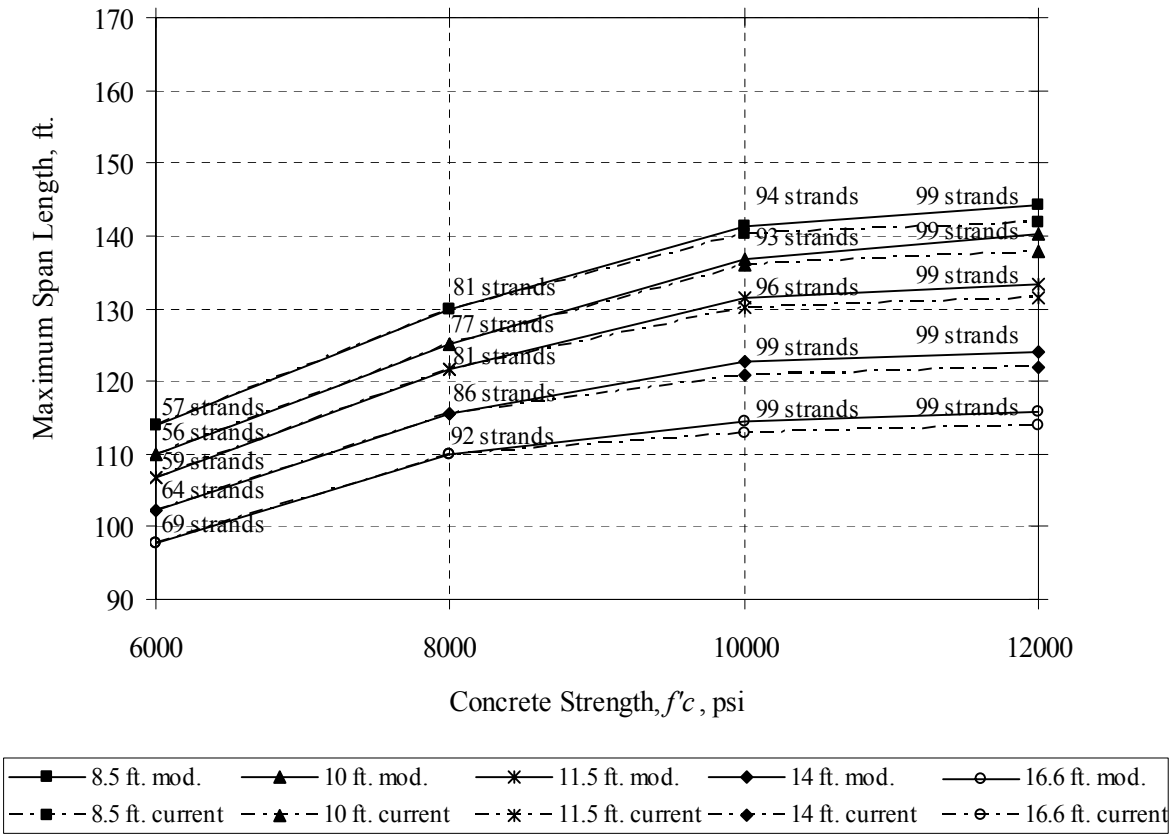

Figure 6.1. Maximum Span Length versus Concrete Strength for Different Tensile Stress Limits (AASHTO Standard Specification, Strand Diameter = 0.5 inch).

6.2.2.2 0.6-Inch Diameter Strands

Table 6.3 shows the results of the parametric study for U54 girders with 0.6-inch strands following the AASHTO Standard Specification. The modified tensile stress limit of $7\sqrt{f'_c}$ results in increases in span lengths ranging from 1.3 to 1.9 feet, corresponding to an increase of 1.0 to 1.5 percent. Again, tension at service load due to total load was the controlling limit state when 99 strands were used. The advantage of using the modified tensile stress limit is more prevalent when 0.5-inch diameter strands are used. When using the larger 0.6-inch diameter strands, the use of 99 strands is only needed for a concrete strength of 12,000 psi and girder spacing of 16.6 feet. Because the tensile stress at service is the controlling limit state when 99 strands are used, the benefit of using the new tensile stress limit was more prevalent for 0.5-inch diameter strands.

Table 6.3. Summary of Maximum Spans
(AASHTO Standard Specification, Strand Diameter = 0.6 inch).

f'_c (psi)	f'_{ci} (psi)	Girder Spacing (feet)	$f_t = 6\sqrt{f'_c}$ (psi)		$f_t = 7\sqrt{f'_c}$ (psi)		Controlling Limit State	Difference in Span Length	
			Max. Span (feet)	No. Strands	Max. Span (feet)	No. Strands		(feet)	(%)
6000	4500	8.5	115.0	41	115.0	41	f (c) TDL	-	-
	4500	10.0	111.1	41	111.1	41	f (c) TDL	-	-
	4727	11.5	108.0	43	108.0	43	f (c) TDL	-	-
	5161	14.0	103.4	46	103.4	46	f (c) TDL	-	-
	5699	16.6	99.4	50	99.4	50	f (c) TDL	-	-
8000	6000	8.5	131.7	56	131.7	56	f (c) TDL	-	-
	6025	10.0	127.2	56	127.2	56	f (c) TDL	-	-
	6400	11.5	123.4	58	123.4	58	f (c) TDL	-	-
	6914	14.0	117.8	63	117.8	63	f (c) TDL	-	-
	7448	16.6	112.7	67	112.7	67	f (c) TDL	-	-
10,000	8000	8.5	145.4	72	145.4	72	f (c) TDL	-	-
	7900	10.0	140.4	71	140.4	71	f (c) TDL	-	-
	8250	11.5	136.2	75	136.2	75	f (c) TDL	-	-
	8914	14.0	129.9	82	129.9	82	f (c) TDL	-	-
	9750	16.6	123.6	89	123.6	89	f (c) TDL	-	-
12,000	9491	8.5	156.7	90	156.7	90	f (c) TDL	-	-
	9441	10.0	151.5	89	151.5	89	f (c) TDL	-	-
	9810	11.5	145.8	93	145.8	93	f (c) TDL	-	-
	10,079	14.0	136.6	99	137.9	96	f (t) TL	1.3	1.0
	10,333	16.6	127.3	99	129.2	99	f (t) TL	1.9	1.5

f(c) TDL = Compressive stresses due to total dead load at midspan.
f(t) TL = Tensile stresses at service due to total load at midspan.

Figure 6.2 shows the maximum span lengths versus concrete strength for different girder spacing using the current and modified tensile stress limits for U54 girders with 0.6-inch strands. Typical to the designs for 0.5-inch diameter strands, longer maximum spans can be attained with reduced girder spacing and higher concrete strength. The concrete compressive strength can be fully utilized up to 12,000 psi because the maximum numbers of strands the girder can accommodate are rarely needed. As can be observed in Figure 6.2, there is little difference between designs based on the current and modified tensile stress limits. The differences are reflected by the dashed lines, which indicate the design using the current limit.

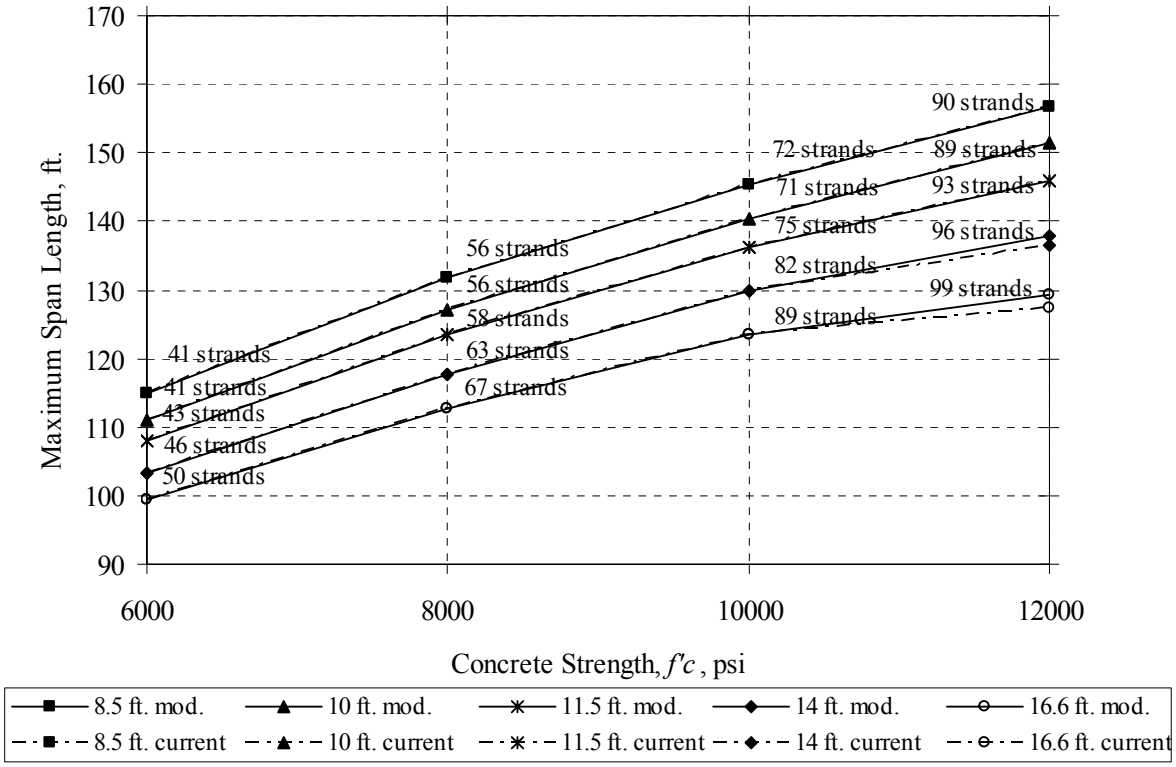

Figure 6.2. Maximum Span Length versus Concrete Strength for Different Tensile Stress Limits (AASHTO Standard Specification, Strand Diameter = 0.6 inch).

6.2.3 AASHTO LRFD Specification

6.2.3.1 0.5-Inch Diameter Strands

Table 6.4 shows the results of the parametric study for U54 girders with 0.5-inch strands following the AASHTO LRFD Specification (2000).

Table 6.4. Summary of Maximum Spans (LRFD Specification, Strand Diameter = 0.5 inch).

f'_c (psi)	f'_{ci} (psi)	Girder Spacing (feet)	$f_t = 6\sqrt{f'_c}$ (psi)		$f_t = 7\sqrt{f'_c}$ (psi)		Controlling Limit State	Difference in Span Length	
			Max. Span (feet)	No. Strands	Max. Span (feet)	No. Strands		(feet)	(%)
6000	4500	8.5	119.6	61	119.6	61	f (c) TDL	-	-
	4582	10.0	115.7	62	115.7	62	f (c) TDL	-	-
	4724	11.5	112.0	63	112.0	63	f (c) TDL	-	-
	5950	14.0	106.0	77	106.0	77	f (t) TL*	-	-
	5971	16.6	98.6	76	98.6	76	f (t) TL*	-	-
8000	6000	8.5	136.1	82	136.1	82	f (c) TDL	-	-
	6237	10.0	131.7	85	131.7	85	f (c) TDL	-	-
	6415	11.5	127.4	87	127.4	87	f (c) TDL	-	-
	7228	14.0	114.9	99	116.4	99	f (t) TL	1.5	1.3
	7347	16.6	107.5	99	108.9	99	f (t) TL	1.4	1.3
10,000	7500	8.5	144.2	99	146.2	99	f (t) TL	2.0	1.4
	7500	10.0	138.0	99	139.9	99	f (t) TL	1.9	1.4
	7500	11.5	132.5	99	134.3	99	f (t) TL	1.8	1.4
	7500	14.0	115.7	99	117.4	99	f (t) TL	1.7	1.5
	7500	16.6	108.2	99	109.8	99	f (t) TL	1.6	1.5
12,000	9000	8.5	145.4	99	147.7	99	f (t) TL	2.3	1.6
	9000	10.0	139.2	99	141.3	99	f (t) TL	2.1	1.5
	9000	11.5	133.6	99	135.7	99	f (t) TL	2.1	1.6
	9000	14.0	116.7	99	118.5	99	f (t) TL	1.8	1.5
	9000	16.6	109.2	99	110.8	99	f (t) TL	1.6	1.5

f(c) TDL = Compressive stresses due to total dead load at midspan.
f(t) TL = Tensile stresses at service due to total load at midspan.
f(t) TL* = Compressive stresses at the beam ends at release initially control the maximum number of strands that can be used followed by the maximum span being limited by tensile stresses at service due to total load at midspan.

Similar to the designs based on the AASHTO Standard Specification, the modified tensile stress limit for service condition resulted in longer spans when the controlling limit state is tension at service due to total load. The increase in span lengths ranged from 1.4 to 2.3 feet, corresponding to an increase of 1.3 to 1.6 percent. Figure 6.3 shows the maximum span lengths versus concrete strength for different girder spacings using the current and modified tensile stress limits at service. Differences between designs for the two stress limits can be observed by comparing adjacent dashed (current stress) and solid (modified stress) lines for a given girder spacing. The modified stress limit resulted in larger spans compared to the current limit especially when 99 strands are used. Again, it is clear that longer maximum spans can be attained with reduced girder spacing and higher concrete strength.

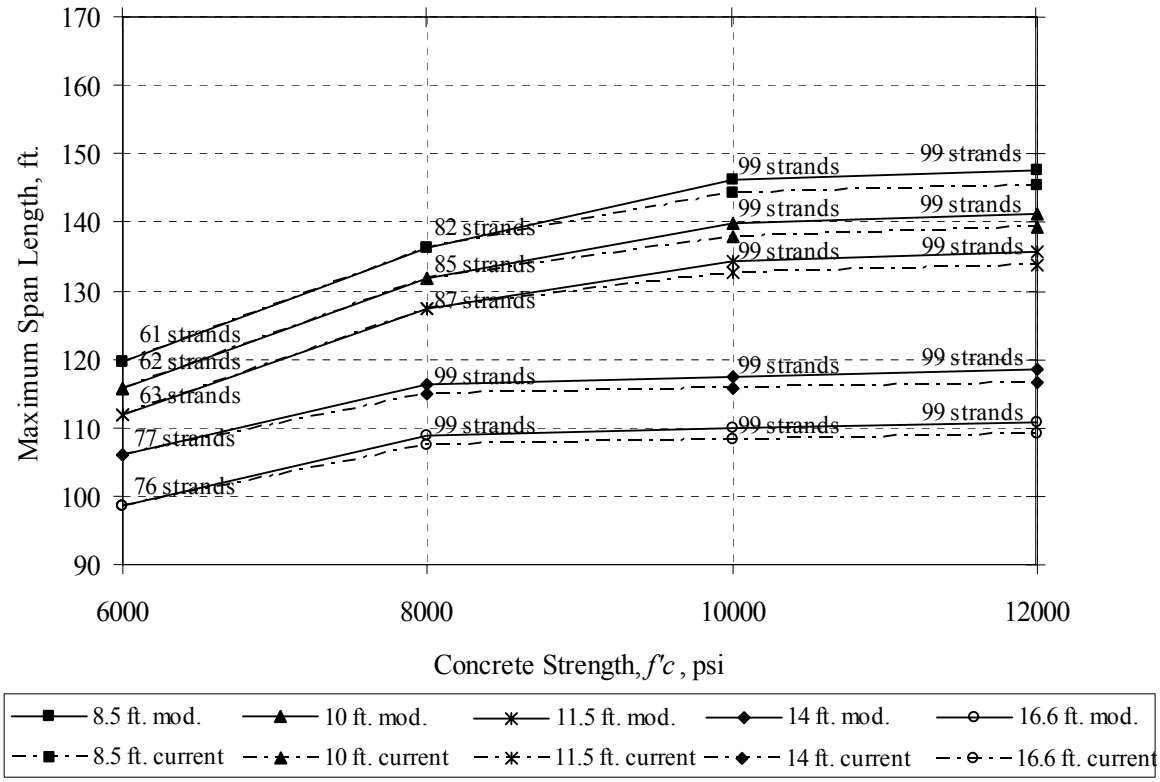

Figure 6.3. Maximum Span Length versus Concrete Strength for Different Tensile Stress Limits (LRFD Specification, Strand Diameter = 0.5 inch).

6.2.3.2 0.6-Inch Diameter Strands

Table 6.5 shows the results of the parametric study for U54 girders with 0.6-inch strands following the AASHTO LRFD Specification. The increase in span lengths was between 1.2 and 1.9 feet using the new stress limit, corresponding to an increase from 0.7 to 1.4 percent.

Figure 6.4 shows the maximum span lengths versus concrete strength for different girder spacings using the current and modified tensile stress limits. Typical for 0.5-inch diameter strand designs, longer maximum spans can be attained with reduced girder spacings and higher concrete strengths. It is clear that the concrete compressive strength can be effectively utilized up to 12,000 psi because 99 strands, which is the maximum number of strands the girder can accommodate, are rarely needed.

Table 6.5. Summary of Maximum Spans (LRFD Specification, Strand Diameter = 0.6 inch).

f'_c (psi)	f'_{ci} (psi)	Girder Spacing (feet)	$f_t = 6\sqrt{f'_c}$ (psi)		$f_t = 7\sqrt{f'_c}$ (psi)		Controlling Limit State	Difference in Span Length	
			Max. Span (feet)	No. Strands	Max. Span (feet)	No. Strands		(feet)	(%)
6000	4629	8.5	120.9	44	120.9	44	f (c) TDL	-	-
	4809	10.0	117.0	45	117.0	45	f (c) TDL	-	-
	4869	11.5	113.4	45	113.4	45	f (c) TDL	-	-
	5955	14.0	106.0	53	106.0	53	f (t) TL*	-	-
	5475	16.6	95.5	48	95.5	48	f (t) TL**	-	-
8000	6259	8.5	138.2	59	138.2	59	f (c) TDL	-	-
	6522	10.0	133.6	61	133.6	61	f (c) TDL	-	-
	6670	11.5	129.3	62	129.3	62	f (c) TDL	-	-
	7904	14.0	118.6	72	118.6	72	f (t) TL*	-	-
	7965	16.6	101.7	55	101.7	55	f (t) TL**	-	-
10,000	8173	8.5	152.8	77	152.8	77	f (c) TDL	-	-
	8546	10.0	147.8	80	147.8	80	f (c) TDL	-	-
	8916	11.5	143.2	83	143.2	83	f (c) TDL	-	-
	9954	14.0	127.7	93	127.7	93	f (t) TL*	-	-
	9777	16.6	110.0	68	110.0	68	f (t) TL**	-	-
12,000	9665	8.5	162.8	97	164.0	93	f (t) TL	1.2	0.7
	9920	10.0	156.0	99	157.5	96	f (t) TL	1.5	1.0
	10,146	11.5	149.7	99	151.6	99	f (t) TL	1.9	1.3
	10,315	14.0	129.8	99	131.6	99	f (t) TL	1.8	1.4
	10,390	16.6	121.3	99	122.9	99	f (t) TL	1.6	1.3

f(c) TDL = Compressive stresses due to total dead load at midspan.

f(t) TL = Tensile stresses at service due to total load at midspan.

f(t) TL* = Compressive stresses at the beam ends at release initially control the maximum number of strands that can be used followed by the maximum span being limited by tensile stresses at service due to total load at midspan.

f(t) TL** = Tensile stresses at the beam ends at release initially control the maximum number of strands that can be used followed by the maximum span being limited by the tensile stresses at service due to total load at midspan.

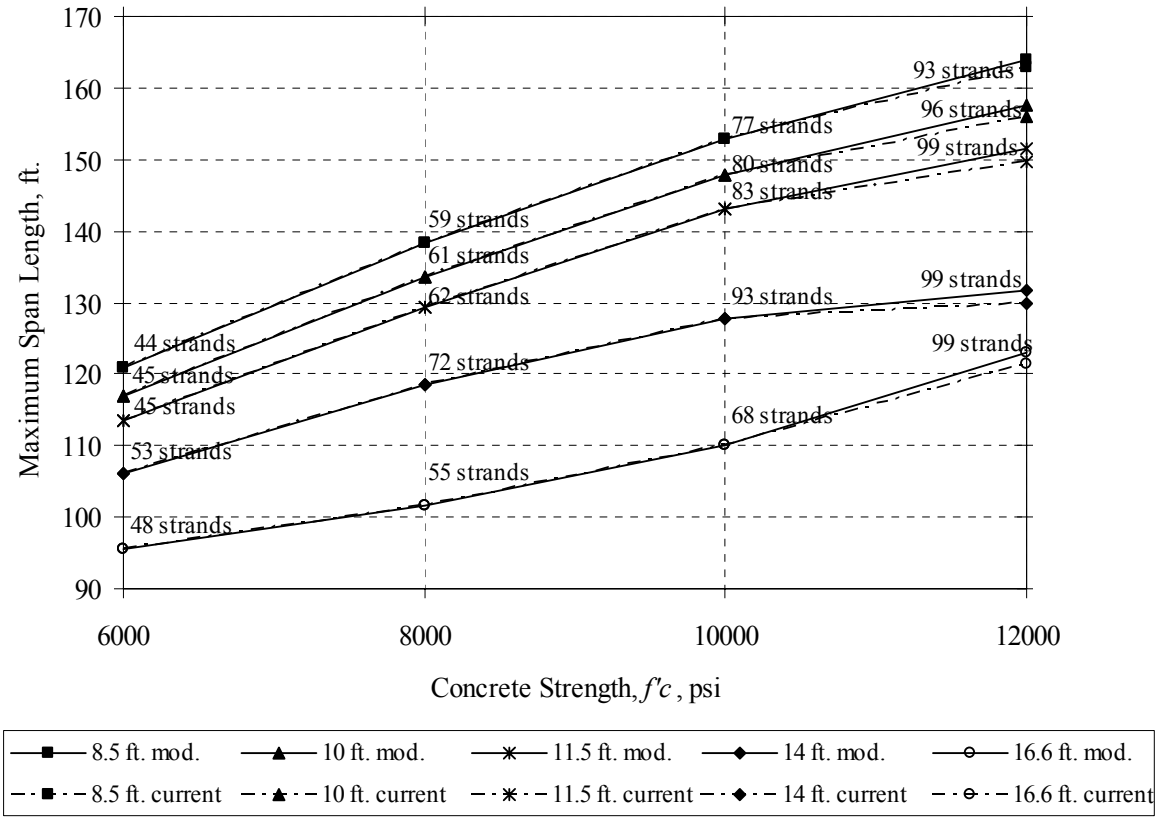

Figure 6.4. Maximum Span Length versus Concrete Strength for Different Tensile Stress Limits (LRFD Specification, Strand Diameter = 0.6 inch).

6.2.4 Summary

Figures 6.1 through 6.4 show that the advantage of using the modified tensile stress limit for U54 beams is greater for designs with 0.5-inch diameter strands compared to designs using 0.6 diameter strands. This is because the maximum numbers of strands is needed for more combinations of concrete strengths and girder spacings and therefore, the tensile stress at the service limit state governs for more cases.

Table 6.6 shows a comparison of designs using the AASHTO Standard and LRFD Specifications with the modified tensile stress limit. Overall, the Standard Specification seems more conservative. However, designs using the LRFD Specification result in smaller maximum spans for higher concrete strengths and larger girder spacings (14.0 and 16.6 feet).

Table 6.6. Comparison of Maximum Span Lengths for U54 Girders Using the AASHTO Standard and LRFD Specifications with Modified Tensile Stress Limit at Service ($f_t = 7\sqrt{f'_c}$).

f'_c (psi.)	Girder Spacing (feet)	0.5 inch Strands				0.6 inch Strands			
		Standard	LRFD	Difference		Standard	LRFD	Difference	
				(feet)	(%)			(feet)	(%)
6000	8.5	113.9	119.6	5.7	5.0	115	120.9	5.9	5.1
	10.0	109.9	115.7	5.8	5.3	111.1	117.0	5.9	5.3
	11.5	106.8	112	5.2	4.9	108	113.4	5.4	5.0
	14.0	102.1	106	3.9	3.8	103.4	106.0	2.6	2.5
	16.6	97.7	98.6	0.9	0.9	99.4	95.5	-3.9	-3.9
8000	8.5	129.9	136.1	6.2	4.8	131.7	138.2	6.5	4.9
	10.0	125.2	131.7	6.5	5.2	127.2	133.6	6.4	5.0
	11.5	121.5	127.4	5.9	4.9	123.4	129.3	5.9	4.8
	14.0	115.6	116.4	0.8	0.7	117.8	118.6	0.8	0.7
	16.6	109.9	108.9	-1.0	-0.9	112.7	101.7	-11.0	-9.8
10,000	8.5	141.3	146.2	4.9	3.5	145.4	152.8	7.4	5.1
	10.0	136.8	139.9	3.1	2.3	140.4	147.8	7.4	5.3
	11.5	131.5	134.3	2.8	2.1	136.2	143.2	7.0	5.1
	14.0	122.7	117.4	-5.3	-4.3	129.9	127.7	-2.2	-1.7
	16.6	114.5	109.8	-4.7	-4.1	123.6	110.0	-13.6	-11.0
12,000	8.5	144.1	147.7	3.6	2.5	156.7	164.0	7.3	4.7
	10.0	140.1	141.3	1.2	0.9	151.5	157.5	6.0	4.0
	11.5	133.4	135.7	2.3	1.7	145.8	151.6	5.8	4.0
	14.0	124.0	118.5	-5.5	-4.4	137.9	131.6	-6.3	-4.6
	16.6	115.7	110.8	-4.9	-4.2	129.2	122.9	-6.3	-4.9

In the parametric study in Phase 2 (Hueste and Cuadros 2003), the tensile stress limit of $7.5\sqrt{f'_c}$ was used to evaluate designs of both U54 and Type IV girders. This limit was based on the current limit for uncracked prestressed member design in the ACI 318 Building Code (ACI Committee 318 2002). For Type IV girders, the tensile stress limit controlled the maximum spans in more cases than for the U54 girders when using the LRFD Specification. For Type IV girders with 0.6-inch diameter strands, the increase in maximum spans was 1.2 to 3.6 percent of the maximum span based on the current LRFD Specification.

6.3 STRUCTURAL RELIABILITY

6.3.1 Definition of Limit State

For the reliability study, the objective was to determine the probability that the tensile stress would exceed the MOR, which would provide a measure of safety against flexural cracking for designs based on both the current and modified tensile stress limits. The tension stress limit at service governed the maximum span length for HSC U54 prestressed girders when using all 99 strand positions. This was also true with the higher tensile stress limits evaluated in the parametric study. The relative safety against flexural cracking for designs based on both tensile stress limits was investigated for different span lengths, girder spacings, and specified concrete strengths. This investigation was made for designs of U54 girders designed based on the requirements of the AASHTO LRFD Specification.

The midspan tensile stress at service under total load at the bottom fiber of the precast section is computed using Equation 6.1.

$$\sigma_b = -\frac{P_e}{A} - \frac{P_e e c_b}{I} + \frac{\left(M_d + M_{slab} + M_{non\_c}\right)c_b}{I} + \frac{\left(M_{comp} + M_L + M_I\right)}{S_{cb}} \qquad (6.1)$$

where P_e is the effective prestressing at service (lbs.), A is the cross-sectional area of the precast member (inch^2), e is the eccentricity of the prestressing strands from the center of gravity of the precast concrete section (inch), c_b is the distance from the bottom fiber of the precast concrete section to the center of gravity of the precast section (inch), I is the moment of inertia of the precast concrete cross-section (inch^4), and S_{cb} is the section modulus of the composite cross-section (in^3). M_d, M_{slab}, M_{non_c}, M_{comp}, M_L, and M_I are the midspan moments due to the weight of the precast beam, deck slab, dead loads in place before composite action occurs, dead loads added after composite action occurs, live load, and impact load, respectively (lb-inch).

6.3.2 Methodology

In this study, failure is the prediction of a tensile crack forming for service load conditions. Before applying structural reliability and comparing the safety of the current tensile stress limit and the modified stress limit, it is necessary to design the girders according to the AASHTO LRFD Specification (2000) to define the number of strands required and determine the maximum span lengths that result in an adequate design. This was done by performing the parametric study presented earlier. The reliability index, which provides a measure of safety against failure of the structure, was then determined for different girder spacings, strand diameters and nominal concrete strengths for designs based on the AASHTO LRFD Specification with both current and modified tensile stress limits.

The Monte Carlo simulation technique summarized in Chapter 2 was used to determine the sample space for each load and resistance variable considered as random. The limit state function (Equation 6.2) and all the random variables were first defined. The probabilistic description (statistical parameters and type of distribution) of the random variables was then defined (Section 6.3.3). Random numbers (u_i) between 0 and 1 were then generated separately for each random variable. For each random variable generated, each value of the sample space was determined using Equation 2.12 for variables that are normally distributed and Equation 2.13 for variables that are lognormally distributed. A total of 50,000 simulations were then applied to determine the sample space for each load and resistance variable considered. The maximum reliability index for 50,000 simulations is 4.11, which is larger than the target reliability index of 3.5 for ultimate design used in calibrating the AASHTO LRFD Specification (2000). Therefore, 50,000 simulations were found suitable for this analysis. The probability of failure was then determined for each case by finding the ratio of the number of simulations that result in the tensile stress at service due to loading applied on the structure to exceed the resistance of the structure (MOR) to the total number of simulations (Equation 2.11). This counting method is superior to other methods because the performance function of the limit state (Equation 6.2) is not normally distributed (Haldar and Mahadevan 2000). For each simulation, prestress losses were calculated by using each of the sample space data obtained for the load and resistance variables.

$$g() = R - L \tag{6.2}$$

where R is the sample space for the tensile stress at cracking (MOR), and L is the sample space for the computed tensile stresses at service using Equation 6.1.

The reliability indices were then calculated using the following relationship presented in Chapter 2.

$$\beta = -\Phi^{-1}(P_F) \tag{2.8}$$

where Φ^{-1} is the inverse standard normal distribution function, and P_F is the probability of failure of the structure (Nowak 1995).

The reliability index can vary for each set of simulations. The larger the number of simulations performed, the smaller is the variation. Therefore, the confidence interval gives an upper and a lower bound for the variation of the reliability index. The approximate 90 percent upper confidence limit for the probability of failure $P_{F(upper)}$ was found as follows:

$$P_{F(upper)} = P_F + 1.65\sqrt{\frac{P_F(1-P_F)}{N}} \tag{6.3}$$

where P_F is the probability of failure, and N is the total number of simulations (50,000). The approximate 90 percent lower confidence limit for the reliability index $P_{F(lower)}$ was found as follows.

$$P_{F(lower)} = P_F - 1.65\sqrt{\frac{P_F(1-P_F)}{N}} \tag{6.4}$$

where P_F is the probability of failure, and N is the total number of simulations (50,000). This approximate confidence interval cannot be used when the probability of failure is too small (approximately less than 0.2 percent), which was not the case in this study. In such cases, the exact confidence interval can be calculated based on the binomial distribution.

6.3.3 Statistical Parameters for Load and Resistance

The parametric study discussed in Section 6.2 was conducted using deterministic variables to determine the maximum span lengths that can be safely designed based on certain criteria. However, both the load and resistance are composed of a number of random variables. For example, the concrete compressive strength will inevitably vary at the same mixture proportions and exposure conditions. The actual mean strength is usually higher than the specified design strength in order for the design to be safe. Therefore, the bias factor, which is the ratio of the mean value to the nominal value, is higher than one. The variation in concrete strength among different specimens cast, cured, and tested under the same conditions supports the fact the strength is not deterministic.

In order to apply Monte-Carlo simulation, it is essential to have information on the statistical parameters of the load and resistance variables. The resistance variables are the concrete compressive strength f'_c, the MOR, and the ultimate tensile strength of the prestressing strands f_{pu}. The load variables are the loads applied on the structure and the impact due to live load. Table 6.7 shows the statistical parameters considered in this study. Variation in geometry of the precast section, deck, and strands due to fabrication inconsistencies was not considered.

Table 6.7. Statistical Parameters of Load and Resistance Variables.

Variable	Bias Factor	Mean	COV	Distribution	Source
f'_c	1.59 (for 6000 psi) 1.24 (for 8000 psi) 1.10 (for 10,000 psi)	-	0.091	Lognormal	Hueste et al. (2003b)
f_{pu}		280.5 ksi	0.0142	Normal	Naaman et al. (1982)
W_d	1.03		0.08	Normal	Nowak (1995)
W_{slab}, W_{non_c}, W_{comp}	1.05		0.10	Normal	Nowak (1995)
Impact		0.15	0.80	Lognormal*	Nowak (1995)
M_L	Figure 2.1		0.11	Normal	Nowak (1995)
MOR		882 psi	0.0164	Lognormal	This Study

W_d = Weight of the precast beam
W_{slab} = Weight of deck slab
W_{non_c} = Dead loads in place before composite section occurs
W_{comp} = Dead loads added after composite action occurs
* A lognormal distribution was used for impact loading rather than the normal distribution suggested by Nowak (1995)

The concrete compressive strength parameters come from the material tests conducted for HSC supplied by the Texas precasters (Hueste et al. 2003b). The COV for the concrete compressive strength was selected to be the maximum COV for one precaster (0.091), rather than the COV based on the data for all precasters (0.069) (Hueste et al. 2003b). This was done in order for the reliability analysis to be more conservative. The concrete compressive strength is needed in the calculation of prestress losses.

The statistical parameters for the MOR were determined for this study by finding the mean and COV for the adjusted MOR results shown in Figure 5.4 at 28 days. A comparison was made with the statistical parameters for the MOR obtained in the first phase of this study for all precasters, and the more conservative results were chosen. Table 6.8 is a summary of the statistical results determined for the MOR. As shown, the mean value of the adjusted data obtained for all precasters at 28 days was smaller than that obtained from the first phase of this study. This is because field exposure conditions result in lower MOR values compared to standard curing conditions. In addition, the COV for the adjusted data was larger for this study.

A smaller mean value and a larger COV results in a more conservative estimate and therefore these values were selected (mean = 882 psi, COV = 0.0164).

Table 6.8. Summary of Statistical Values for the Modulus of Rupture.

Source	Precaster	Age (days)	Mean (psi)	COV (%)
Hueste et al. (2003b)	All	28	1060	9.5
Adjusted for Exposure (This Study)	A	7	887	16.3
		28	919	20.2
		56	973	25.1
	B	7	911	7.8
		28	926	13.8
		56	949	12.5
	C	7	756	16.7
		28	849	14.0
		56	866	12.2
	All	7	820	17.2
		28	882	16.4
		56	910	17.9

The statistical parameters for the dead load variables provided by Nowak (1995) were determined for actual bridges and used in the calibration of the AASHTO LRFD Specification (Nowak 1995). The proposed live load moments for the LRFD code with the bias factors shown in Figure 2.1, were used (Nowak 1995). The statistical parameters for impact loading for bridges derived and proposed by Nowak (1995) were used and modified to a lognormal distribution instead of a normal distribution. This decision was made because the COV is large relative to the small mean value of the impact. This would result in some negative sample space for impact loading values. In real life, the impact loading would not be negative. Therefore, a lognormal distribution seemed to be a more appropriate distribution in order for the sample space of the impact loading to always be positive. However, the lognormal distribution results in higher impact values compared to the normal distribution. Therefore, the results should be more conservative. The mean value of the impact factor (0.15) is multiplied by the live load moment to determine the moment due to impact.

6.3.4 Results of Reliability Analysis

6.3.4.1 0.5-Inch Diameter Strands

Table 6.9 shows the results obtained for designs of U54 girders using 0.5-inch diameter strands. As expected, the reliability indices determined for designs using the modified tensile stress limit of $7\sqrt{f_c'}$ (this study) give smaller reliability indices compared to the current limit of $6\sqrt{f_c'}$. Designs indicated as "Both" correspond to those cases where the tensile stress limit at service did not control the maximum span. Table 6.9 shows that when the limit state governing design is tension at service, wider girder spacings and higher concrete strengths result in lower reliability indices (higher probability of the MOR being exceeded).

Figure 6.5 shows a comparison between the current tensile stress limit and the modified tensile stress limit. Reliability indices are plotted versus the span length. Only the cases where different reliability indices were determined are shown. The reliability indices determined for designs based on the current tensile stress limit range from approximately 1.5 to 2.0, whereas most of the reliability indices obtained using the modified tensile stress limit range from approximately 1.0 to 1.5. The probability of exceeding the MOR using the modified tensile stress limit of $7\sqrt{f_c'}$ is approximately twice the probability of exceeding the MOR using the current tensile stress limit of $6\sqrt{f_c'}$.

Table 6.9. Reliability Results for U54 Girders with 0.5 inch Diameter Strands.

f'c (psi)	Girder Spacing (feet)	Stress Limit	Length (feet)	Probability of Failure	Reliability Index	Confidence Interval (β_{lower} - β_{upper})
6000	8.5	Both	119.6	0.0354	1.81	1.79 - 1.83
	10.0	Both	115.7	0.0536	1.61	1.60 - 1.63
	11.5	Both	112.0	0.0734	1.45	1.44 - 1.47
	14.0	Both	106.0	0.0780	1.42	1.40 - 1.43
	16.6	Both	98.6	0.0890	1.35	1.34 - 1.36
8000	8.5	Both	136.1	0.0760	1.43	1.42 - 1.45
	10.0	Both	131.7	0.0731	1.45	1.44 - 1.47
	11.5	Both	127.4	0.0829	1.39	1.37 - 1.40
	14.0	Current	114.9	0.0229	2.00	1.98 - 2.02
		This Study	116.4	0.0489	1.66	1.64 - 1.67
	16.6	Current	107.5	0.0394	1.76	1.74 - 1.77
		This Study	108.9	0.0763	1.43	1.42 - 1.45
10,000	8.5	Current	144.2	0.0210	2.03	2.01 - 2.06
		This Study	146.2	0.0522	1.62	1.61 - 1.64
	10.0	Current	138.0	0.0236	1.98	1.96 - 2.01
		This Study	139.9	0.0552	1.60	1.58 - 1.61
	11.5	Current	132.5	0.0297	1.89	1.87 - 1.91
		This Study	134.3	0.0637	1.52	1.51 - 1.54
	14.0	Current	115.7	0.0366	1.79	1.77 - 1.81
		This Study	117.4	0.0767	1.43	1.41 - 1.44
	16.6	Current	108.2	0.0603	1.55	1.54 - 1.57
		This Study	109.8	0.1163	1.19	1.18 - 1.21
12,000	8.5	Current	145.4	0.0354	1.81	1.79 - 1.83
		This Study	147.7	0.0901	1.34	1.33 - 1.35
	10.0	Current	139.2	0.0403	1.75	1.73 - 1.76
		This Study	141.3	0.0910	1.33	1.32 - 1.35
	11.5	Current	133.6	0.0455	1.69	1.67 - 1.71
		This Study	135.7	0.1046	1.26	1.24 - 1.27
	14.0	Current	116.7	0.0556	1.59	1.58 - 1.61
		This Study	118.5	0.1113	1.22	1.21 - 1.23
	16.6	Current	109.2	0.0880	1.35	1.34 - 1.37
		This Study	110.8	0.1597	1.00	0.98 - 1.01

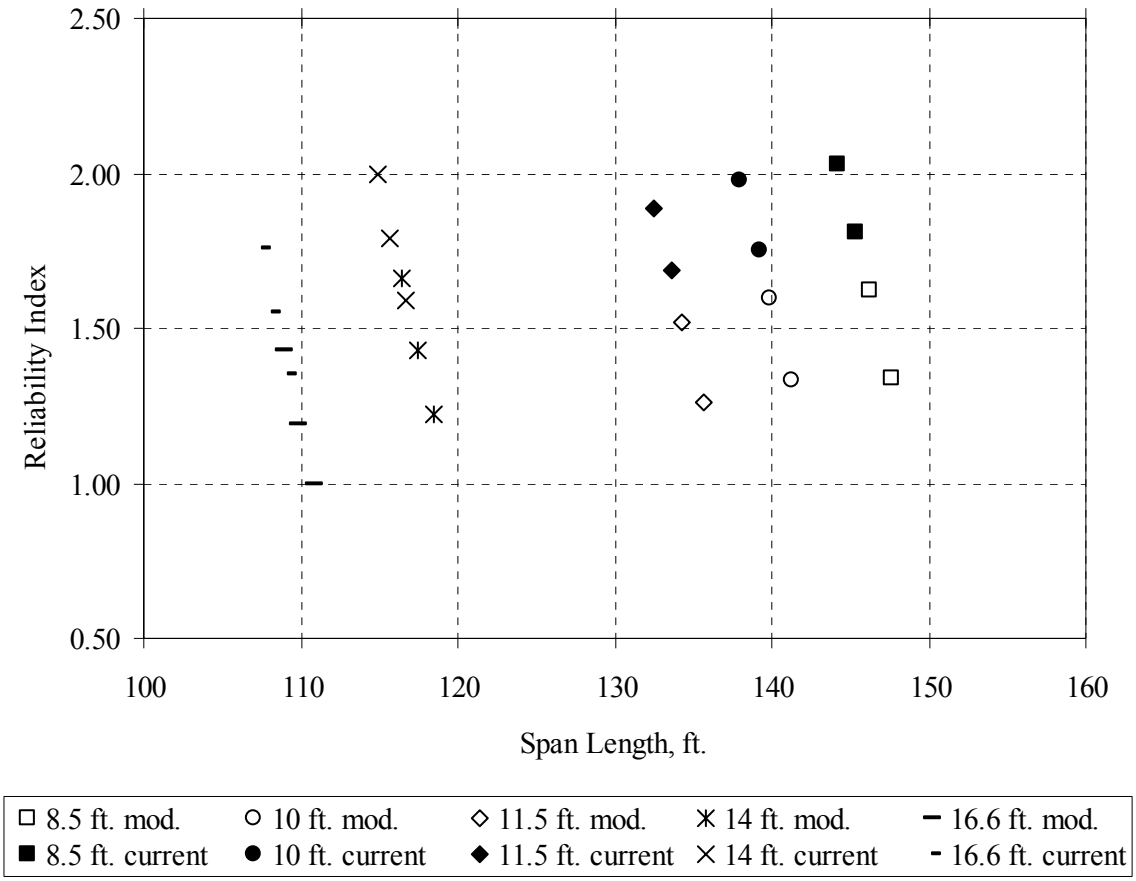

Figure 6.5. Reliability Indices for Current and Modified Tensile Stress Limits (U54 Girder with 0.5 inch Strands).

6.3.4.2 0.6-Inch Diameter Strands

Table 6.10 shows the results obtained for designs of U54 girders with 0.6-inch diameter strands. As expected, the reliability indices determined using the modified tensile stress limit of $7\sqrt{f_c'}$ (this study) are smaller compared with the current tensile stress limit of $6\sqrt{f_c'}$. Designs indicated as "Both" correspond to those cases where the tensile stress limit at service did not control the maximum span. Figure 6.6 shows a comparison of the reliability indices for designs based on the two stress limits. Reliability indices are plotted versus the span length. Only the cases where different reliability indices were determined are shown. As for the 0.5-inch strand designs, the reliability indices obtained for designs based on the modified tensile stress limit range from 1.5 to 2.0 whereas the reliability indices obtained for designs based on modified tensile stress limit range from 1.0 to 1.5.

Table 6.10. Reliability Results for U54 Girders with 0.6 inch Diameter Strands.

f'c (psi.)	Girder Spacing (feet)	Stress Limit	Length (feet)	Probability of Failure	Reliability Index	Confidence Interval (β_{lower} - β_{upper})
6000	8.5	Both	120.9	0.0435	1.71	1.71 - 1.73
	10	Both	117.0	0.0610	1.55	1.53 - 1.56
	11.5	Both	113.4	0.1111	1.22	1.21 - 1.23
	14	Both	106.0	0.1416	1.07	1.06 - 1.09
	16.6	Both	95.5	0.1537	1.02	1.01 - 1.03
8000	8.5	Both	138.2	0.1229	1.16	1.15 - 1.17
	10	Both	133.6	0.1277	1.14	1.12 - 1.15
	11.5	Both	129.3	0.1565	1.01	1.00 - 1.02
	14	Both	118.6	0.1454	1.06	1.04 - 1.07
	16.6	Both	101.7	0.2620	0.64	0.63 - 0.65
10,000	8.5	Both	152.8	0.1581	1.00	0.99 - 1.01
	10	Both	147.8	0.1553	1.01	1.00 - 1.03
	11.5	Both	143.2	0.1466	1.05	1.04 - 1.06
	14	Both	127.7	0.0720	1.46	1.45 - 1.48
	16.6	Both	110.0	0.3016	0.52	0.51 - 0.53
12,000	8.5	Current	162.8	0.0535	1.61	1.60 - 1.63
		This Study	164.0	0.1897	0.88	0.87 - 0.89
	10	Current	156.0	0.0394	1.76	1.74 - 1.77
		This Study	157.5	0.1355	1.10	1.09 - 1.11
	11.5	Current	149.7	0.0392	1.76	1.74 - 1.78
		This Study	151.6	0.0791	1.41	1.40 - 1.43
	14	Current	129.8	0.0351	1.81	1.79 - 1.83
		This Study	131.6	0.0720	1.46	1.45 - 1.48
	16.6	Current	121.3	0.0499	1.65	1.63 - 1.66
		This Study	122.9	0.0980	1.29	1.28 - 1.31

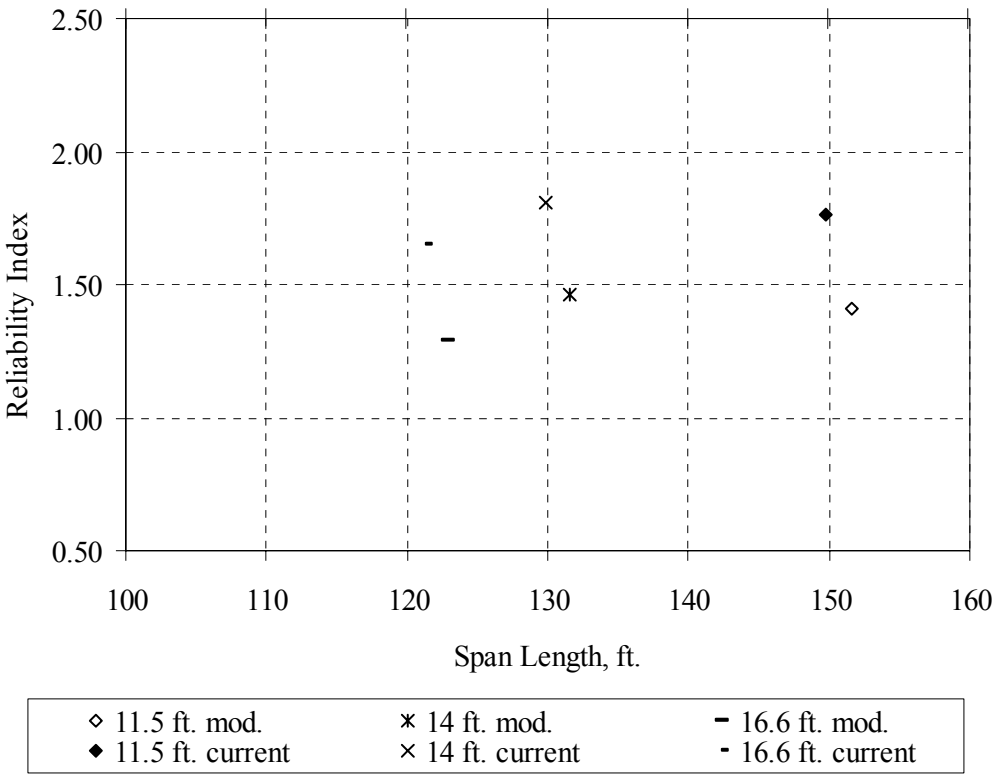

Figure 6.6. Reliability Indices for Current and Modified Tensile Stress Limits (U54 Girder with 0.6 inch Strands, *f'c* = 12,000 psi).

6.3.5 Discussion

The target reliability index β_t used in calibrating the LRFD bridge design code was 3.50 (Nowak, 1995). However, this reliability index was set for the ultimate flexural limit state. Failure at ultimate corresponds to structural collapse. Failure of a serviceability limit state involves problems in the functionality of the structure but not necessarily a collapse of the structure. For the limit state evaluated in this study, flexural cracking of the precast section may lead to eventual corrosion of the strands, which could be detrimental to the integrity of the structure. Therefore, while smaller reliability indices may be expected for serviceability limit states, engineering judgment must be used to determine the acceptability of increasing the probability that a service limit state may be exceeded. This study uses data based on a sample of current precaster practices for Texas precasters. Over time, concrete mixtures may be modified. Therefore, increased confidence in designs where the allowable stress limits are raised above

those set in the AASHTO Specification may be gained by requiring acceptance tests for mechanical properties in addition to the compressive strength, such as the MOR.

7 SUMMARY AND CONCLUSIONS

7.1 SUMMARY

HSC is regularly used for prestressed bridge girders in Texas and other states. The ACI Committee 363 (1997) defines HSC as concrete with a compressive strength exceeding 6000 psi produced without using exotic materials or techniques. The provisions for the design of prestressed concrete members according to the AASHTO Standard and LRFD Specifications are based on mechanical properties determined for normal strength concrete (NSC). Therefore, there is a need to evaluate these specifications based on the properties of HSC.

This research is part of a three-phase project sponsored by TxDOT. The first phase (Hueste et al. 2003b) focused on establishing mechanical properties for HSC mixtures typically used by Texas precasters for bridge girders. Phase 1 included testing of plant-produced concrete samples for various mechanical properties and establishing appropriate statistical parameters to describe these mechanical properties. The second phase (Hueste and Cuadros 2003) included a survey of current practice relevant to the use of HSC prestressed girders by departments of transportation in the United States. In addition, a parametric study was conducted to primarily determine the limit states that are predominant in limiting the potential span of typical HSC prestressed girders used in Texas. This included as assessment of the benefit of using higher concrete strength, 0.5 and 0.6-inch diameter strands, and an evaluation of differences in designs based on the AASHTO Standard and LRFD Specifications. The third phase (this study) focuses on evaluating the allowable stress limits for the design of HSC prestressed girders. This was accomplished through several tasks.

The first task involved an experimental study to assess the effect of several field exposure conditions on the compressive and flexural strength of HSC. The HSC mixtures tested in this study are representative of the same concrete mixtures collected from three precasters in an earlier phase of this research program (Hueste et al. 2003b). The plant-produced samples from the earlier study were laboratory-cured after the first 24 hours. Strength adjustment factors to

account for variations in field exposure conditions were determined in this study. The specified compressive strengths in this study ranged from 6000 psi to 10,000 psi, which is typical to the range considered in the first phase of this study.

Four different exposure conditions were selected for this study. Three of these exposure conditions represent actual field conditions. The fourth exposure condition represents standard laboratory curing conditions following the ASTM Standard C 192/C 192M-98 (1998a). All of the field-cured specimens were cured for 1 day (approximately 24 hours) at 107 ^{o}F and 100 percent relative humidity to represent temperature and humidity conditions measured in actual prestressed girders. After this one-day exposure period, the samples were moved to different constant temperature and humidity rooms with different exposure conditions. The four exposure conditions represent typical conditions found in the state of Texas and evaluate the effect of significant differences in the temperature and humidity.

For each of the representative concrete mixtures, 100 beams and 100 cylindrical specimens were cast from the same batch of concrete. For each of the four exposure conditions, the hydration temperature was monitored using two beams and two cylinders. Testing for compressive strength and the MOR was done at the ages of 1, 3, 7, 14, 28, and 56 days for each precaster and exposure condition.

The experimental analysis involved an investigation of concrete strength development among different exposure conditions, determination of exposure factors, statistical analysis of the effects of the variables and their interactions on the measured response, investigating the goodness of fit prediction formulas, and investigating the accuracy of the maturity method in predicting the concrete compressive strength and MOR. The exposure factors were used to adjust the strength data obtained from the first phase of this study. The adjusted data were used to develop a modified tensile stress limit.

The second task involved conducting a parametric study to evaluate the impact of the modified tensile stress limit derived from the material testing in this study when applied to the design of HSC prestressed girders. The parametric study was performed for both the AASHTO

Standard (1999) and LRFD (2000) Specifications. The specified concrete compressive strength and the girder spacing were varied. The girder type considered was the Texas U54 beam. This girder type was selected because it is widely used in the design of longer span bridges in the state of Texas. The diameter of the strands considered were 0.5 and 0.6-inch. The parameters were selected to be consistent with the larger parametric study conducted for Phase 2 of this project by Hueste and Cuadros (2003). For each combination of design specifications, concrete strength, girder spacing, and strand diameter, the maximum span length that can be achieved based on the flexural design considerations only, were determined. This was done by varying the number of strands in order to maximize the span lengths.

The third task involved conducting a reliability study to determine the probability that the tensile stress would exceed the MOR, which would provide a measure of the safety against flexural cracking for designs based on both the current and modified tensile stress limits. The tensile stress limit at service governed the maximum span length for HSC U54 prestressed girders when using all 99 strand positions. This was also true with the higher tensile stress limits evaluated in the parametric study. The relative safety of both tensile stress limits was investigated for different span lengths, girder spacings, and specified concrete strengths. This investigation was made for designs of U54 girders based on the requirements of the AASHTO LRFD Specification.

Design was done in Task 2 according to the AASHTO LRFD Specification to define the number of strands and determine the maximum span lengths that result in an adequate design for both tensile stress limits. The Monte Carlo simulation technique determined the sample space for each load and resistance variable considered as random. The probability of failure was then determined by finding the ratio of the number of simulations that result in the tensile stress at service due to loading applied on the structure to exceed the resistance of the structure (MOR) to the total number of simulations. The reliability indices were then calculated for each case considered. Confidence intervals that give an upper bound and a lower bound for the variation of the reliability index were also determined.

7.2 CONCLUSIONS

7.2.1 Effect of Exposure

7.2.1.1 Compressive Strength

1. The average 1-day compressive strength under standard exposure conditions for all precasters on average was 67 percent of the 28-day strength. The average 7-day compressive strength was 89 percent of the 28-day strength. Elevated early exposure temperatures for 1 day followed by exposure at the standard temperature (73 ^{o}F) resulted in earlier strength gain compared to standard curing conditions. However, lower strength ratios were observed when compared with specimens continuously cured at a high temperature. For this study, the longer the concrete was cured under high temperatures, the faster concrete gained compressive strength with time. However, the longer-term strength was lower.

2. The rate of strength gain for all exposure conditions was higher than that predicted using the expression suggested by ACI Committee 209 (1992). The prediction equation provided a conservative prediction of strength gain when compared to the data from this study. This may be due to the use of high range water reducers in the concrete mixtures, which disperse the cement particles and result in a faster rate of hydration.

3. It was observed that the concrete compressive strength for each precaster was not highly influenced by the variations in field exposure conditions. The results indicate that curing concrete under standard conditions results in a higher long-term strength compared to other exposure conditions used in this study. Most of the 28-day exposure factors (ratio of field-cured strength to standard laboratory cured strength) for all field exposure conditions were lower than 1.00 (0.86-0.99). The overall short-term strength for all precasters combined is higher for concrete cured at high temperatures. The 1-day exposure factor for the average of all precasters is 1.10. This increase in the short-term

strength occurs because elevated heat exposure accelerates the chemical reactions during the early hydration process.

4. The maturity method gave a reasonable prediction of the concrete short-term compressive strength. The maximum prediction error for all exposure conditions for Precasters A and B was determined to be approximately 9 percent for the first seven days. However, for Precaster C, the maximum prediction error was approximately 17 percent for the first 7 days. The maturity method was not accurate in predicting the long-term strength beyond 7 days.

7.2.1.2 Modulus of Rupture

1. The average 1-day MOR for all precasters under standard curing conditions was 68 percent of the corresponding 28-day average MOR. The 7-day average MOR was 90 percent of the 28-day average MOR for standard curing conditions. Exposure to high temperatures for one day followed by exposure at the standard temperature (73 ^{o}F) resulted in earlier strength gain compared to standard curing conditions. However, lower strength ratios were observed when compared with specimens continuously cured at a high temperature.

2. The concrete MOR was highly influenced by the variations in field exposure conditions. The results indicate that exposing concrete under standard conditions results in a higher long-term strength compared to other exposure conditions used in this study. The 28-day exposure factors for all other exposure conditions are lower than 1.00 (0.66-0.91). In general, exposing concrete to high temperatures (107 ^{o}F) with 100 percent humidity resulted in a reduction in the average MOR for all precasters and all ages compared to standard curing conditions. Exposing concrete to very low relative humidity (30 percent) and 73 ^{o}F after 1 day resulted in an overall reduction in the MOR compared to curing under standard conditions. Thus, both increased temperature and decreased humidity significantly reduced the concrete MOR.

3. Results from the statistical analysis showed that the batch averages for the MOR were significantly different among ages, precasters, and exposure conditions and among most of their interactions. The three-way interaction existed and was more significant for the MOR as compared to the compressive strength. This supported the observation that the different field exposure conditions influence the MOR more than the compressive strength.

4. All the MOR prediction formulas recommended by researchers overestimated the results obtained from this study based on the exposure condition that resulted in the lowest MOR versus compressive strength relationship. However, the AASHTO LRFD Specification (2000) expression $\left(7.5\sqrt{f_c'}\right)$ gave a lower bound to nearly all the data points. Thus, only the AASHTO LRFD Specification expression, which is the same as that of ACI 318 (2002), provides a conservative estimate of the MOR.

5. The maturity method was not intended for use in predicting the MOR. Elevated heat exposure significantly lowers the MOR beyond one day, which contradicts the basis of the maturity method. The accuracy of the maturity method for predicting the MOR was evaluated for all precaster mixtures by comparing the actual strengths for different exposure conditions with the predicted strengths obtained using the maturity method and determining the percentage error. The percentage error ranged from 2.16 to 72.3 percent, which shows a significant problem with applying the maturity method to predict the MOR.

7.2.2 Development of Modified Tensile Stress Limit

1. In modifying Phase 1 data to account for field exposure conditions, different exposure factors were considered for different precasters, ages, and exposure conditions for both the compressive strength and the MOR. This was done because the statistical analysis results showed that there was a significant difference among the interactions of precasters, ages, and exposure conditions for both the compressive strength and the MOR.

2. The exposure factors used for developing a new tensile stress limit were determined using the standard curing condition as the baseline. This was done because the specimens cured under standard conditions had the smallest difference when compared with the corresponding strength data obtained in the first phase of this study. Therefore, the standard curing condition best reflected the exposure condition considered in the first phase of this study. The modified and proposed allowable stress limit based on a lower bound to 95 percent of the adjusted data is as follows.

$$f_t = 7\sqrt{f_c'} \qquad (7.1)$$

where f_t is the allowable tensile stress (psi), and f_c' is the concrete compressive strength (psi). The lower bound to the data was found to be $f_t = 6.1\sqrt{f_c'}$.

3. When the batches collected in Phase 1 with ambient temperatures lower than 90 ^{o}F were considered separately, the standard exposure condition was also found to be the exposure factor baseline. This was because the standard exposure condition resulted in the lowest prediction errors (percent) when comparing data for both compression and MOR. The Phase 1 strength data were then adjusted based on these exposure factors. The tensile stress limit based on a lower bound of 95 percent of the adjusted data was $f_t = 6.9\sqrt{f_c'}$. The lower bound to the data was found to be $f_t = 6.4\sqrt{f_c'}$.

4. When the batches collected in Phase 1 with ambient temperatures greater than 90 ^{o}F were considered separately, the RH exposure condition was found to be the appropriate baseline exposure condition. This was because the RH exposure condition resulted in the lowest prediction errors (percent) for both compression and flexure when comparing strength data from Phase 1 and this study. The strengths obtained in the previous phase of this study were then adjusted based on these exposure factors. The tensile stress limit based on a lower bound to 95 percent of the adjusted data was $f_t = 7.6\sqrt{f_c'}$. The lower bound to the data was found to be $f_t = 6.7\sqrt{f_c'}$.

5. The possibility of using one exposure factor to modify all the data, considering the standard exposure condition as a baseline for batches collected at all temperatures, was also studied. The lowest exposure factors among exposure conditions, ages, and precasters for compression and the MOR were 0.82 and 0.60, respectively. The tensile stress limit based on a lower bound to 95 percent of the adjusted data was $f_t = 6.1\sqrt{f'_c}$. The lower bound to the data was found to be $f_t = 5.6\sqrt{f'_c}$.

6. The average exposure factors among exposure conditions, ages, and precasters for compression and the MOR were 0.93 and 0.79, respectively. The tensile stress limit based on a lower bound to 95 percent of the adjusted data was $f_t = 7.5\sqrt{f'_c}$. The lower bound to the data was found to be $f_t = 6.9\sqrt{f'_c}$.

7.2.3 Impact of Modified Tensile Stress Limit

1. The results of the parametric study show that the modified tensile stress limit ($7\sqrt{f'_c}$) determined from this study based on a lower bound to 95 percent of the adjusted data, resulted in longer maximum spans when the tensile stress limit was the controlling limit state. This was true when 99 strands, which are the maximum number of strands that the U54 beam can accommodate, are needed. For the AASHTO Standard Specification (1999) for 0.5-inch strands, the increase in span lengths ranged from 0.9 to 2.2 feet, corresponding to an increase of 0.7 to 1.6 percent. For 0.6-inch strands, the increase in span lengths ranged from 1.3 to 1.9 feet, corresponding to an increase of 1.0 to 1.5 percent. For the AASHTO LRFD Specification (2000) for 0.5-inch strands, the increase in span lengths ranged from 1.4 to 2.3 feet, corresponding to an increase of 1.3 to 1.6 percent. For 0.6-inch strands, the increase in span lengths ranged from 1.2 to 1.9 feet, corresponding to an increase of 0.7 to 1.4 percent.

2. The advantage of using the new allowable stress equation was greater when 0.5-inch diameter strands are used than when using 0.6-inch diameter strands. This was because

the maximum numbers of strands (99) was required for more combinations of concrete strengths and girder spacings and therefore, the tensile stress limit at service for more cases.

3. In general, design using the AASHTO Standard Specification was more conservative than the LRFD Specification. However, designs using the LRFD Specification tended to be more conservative for higher concrete strengths and larger girder spacings.

7.2.4 Reliability Analysis

1. The modified tensile stress limit resulted in smaller reliability indices compared to those obtained using the current allowable stress limit. For both the 0.5-inch and 0.6-inch diameter strands, most of the reliability indices obtained using the current stress limit ranged from 1.5 to 2.0, whereas most of the reliability indices obtained using the modified stress limit ranged from 1.0 to 1.5.

2. The target reliability index used in calibrating the LRFD bridge design code was 3.50 (Nowak 1995). However, this reliability index was set for the ultimate flexural limit state, which corresponds to structural collapse. Smaller reliability indices were expected for the service limit state evaluated in this study. Failure in serviceability can lead to premature durability (i.e., corrosion of the strands) problems of the structure, but not necessarily a collapse of the structure. Engineering judgement is necessary to establish an acceptable level of risk for the service limit states.

7.3 FUTURE RESEARCH RECOMMENDATIONS

1. The HSC tested in this research program had a compressive strength ranging from 6000 to 10,000 psi. Further research should be conducted to obtain mechanical properties for HSC with compressive strengths exceeding 10,000 psi.

2. An investigation of the effect of exposure conditions on the modulus of elasticity and splitting tensile strength of HSC would be beneficial in developing more representative relationships to describe these properties for actual bridge members.

3. In this study, cold weather exposure conditions were not considered due to limited facilities. Even though low temperatures do not significantly reduce the long-term strength of concrete as much as high temperatures, the short-term strength is typically lower. Therefore, it is important to investigate the effect of cold weather conditions on concrete strength.

4. In addition to the impact of curing, size effects should be considered in defining appropriate stress limits for HSC prestressed concrete bridge girders. Bazant and Li (1995) reported that as the sample size increases, the apparent cracking stress is decreased. The scope of this project did not include a study on the impact of size effects. Therefore, further research to quantify the impact of size effects for HSC prestressed bridge girders would be beneficial in establishing appropriate allowable stress limits for design.

REFERENCES

AASHTO (1999). *1999 Interim Revisions to the Standard Specifications for Highway Bridges*, Sixteenth Edition, Washington, D.C.

AASHTO (2000). *2000 Interim AASHTO LRFD Bridge Design Specification*, Second Edition, Washington, D.C.

AASHTO (2002). *Slump of Hydraulic-Cement Concrete*, T119, Standard Specifications for Transportation Materials and Methods of Sampling and Testing, 22nd Edition, Part 2a: Tests, Washington, D.C.

AASHTO (2002). *Mass per Cubic Meter (Cubic Foot), Yield, and Air Content (Gravimetric) of Concrete*, T121, Standard Specifications for Transportation Materials and Methods of Sampling and Testing, 22nd Edition, Part 2a: Tests, Washington, D.C.

AASHTO (2002). *Air Content of Freshly Mixed Concrete by the Pressure Method*, T152, Standard Specifications for Transportation Materials and Methods of Sampling and Testing, 22nd Edition, Part 2a: Tests, Washington, D.C.

AASHTO (2002). *Time of Setting of Concrete Mixtures by Penetration Resistance*, T197, Standard Specifications for Transportation Materials and Methods of Sampling and Testing, 22nd Edition, Part 2a: Tests, Washington, D.C.

ACI Committee 209 (1992). "Prediction of creep, shrinkage, and temperature effects in concrete structures," *ACI 209R-92*, American Concrete Institute, Farmington Hills, MI.

ACI Committee 211 (1993). "Guide for selecting proportions for high-strength concrete with Portland cement and fly ash." *ACI 211.4R-93*, ACI, Farmington Hills, MI.

ACI Committee 318 (2002). "Building code requirements for structural concrete (318-02) and commentary (318R-02)," *ACI 318-02/318R-02*, American Concrete Institute, Farmington Hills, MI.

ACI Committee 363 (1997). "State-of-art report on high-strength concrete," *ACI 363R-92 (reapproved 1997)*, American Concrete Institute, Farmington Hills, MI.

Ahmad, S. H. and Shah, S. P. (1985). "Structural properties of high-strength concrete and its implication for precast prestressed concrete," *PCI J.*, 30(6), 92-119.

ASTM (1997b). "Standard test method for total evaporable moisture content of aggregate by drying," *C566-97*, American Society of Testing and Materials, West Conshohocken, PA.

ASTM (1998a). "Standard practice for making and curing concrete test specimens in the laboratory," *C 192/C 192M-98*, American Society of Testing and Materials, West Conshohocken, PA.

ASTM (1998b). "Standard practice for making and curing concrete test specimens in the field," *C 31/C 31M-98*, American Society of Testing and Materials, West Conshohocken, PA.

ASTM (1998c). "Standard test method for flexural strength of concrete (using simple beam with third-point loading)," *C78-94*, American Society of Testing and Materials, West Conshohocken, PA.

ASTM (2000). "Standard test method for rubber property – durometer hardness," *D 2240-00*, American Society of Testing and Materials, West Conshohocken, PA.

ASTM (2000). "Standard test method for effect of organic impurities in fine aggregate on strength of mortar," *C87-03,* American Society of Testing and Materials, West Conshohocken, PA.

ASTM (2001). "Standard test method for compressive strength of cylindrical concrete specimens," *C39/C 39M-01*, American Society of Testing and Materials, West Conshohocken, PA.

Bazant, Z. P., and Li, Z. (1995). "Modulus of Rupture: size effect due to fracture initiation in boundary layer," *Journal of Structural Engineering.* ASCE, 121(4), 739-746.

Bentz, D., Snyder, K., and Stutzman, P. (1997). "Hydration of portland cement: the effects of curing conditions," *Proceedings of the 10th International Congress on the Chemistry of Cement*, Gothenburg, Sweden, 15-30.

Burg, R. G., and Ost, B. W. (1992). "Engineering properties of commercially available high-strength concretes," *Research and Development Bulletin RD104T*, PCA, Skokie, Ill.

Byfors, J. (1980). "Plain concrete at early ages," Swedish Cement and Concrete Research Institute Report 3:80, 464 p.

Carino, N. J., (1984). "The maturity method: theory and application," *ASTM Journal of Cement, Concretes, and Aggregates*, 6(2), 61-73.

Carino, N. J. and Tank, R. C. (1992). "Maturity functions for concretes made with various cements and admixtures," *ACI Materials Journal*, 89(2), 188-196.

Carino, N. J. and Lew, H. S. (2001). "The maturity method: from theory to application," *National Institute of Standards and Technology*, Gaithersburg, 1-19.

Carrasquillo, R. L., Slate, F.O., and Nilson A.H. (1981). "Properties of high-strength concrete subjected to short-term loads." *ACI Journal*, 78(3), 171-178.

Carrasquillo, P.M., and Carrasquillo, R.L. (1988). "Evaluation of the use of current concrete practice in the production of high-strength concrete," *ACI Materials Journal*, 85(2), 49-54.

Cetin, A. and Carrasquillo, R. L. (1995). "Effect of accelerated heat curing and mix characteristics on the heat development and mechanical properties of high performance concrete," *Research Report 580-4*, Center for Transportation Research, The University of Texas at Austin, Austin, TX.

Comite Euro-International du Beton – Federation Internationale de Precontrainte (CEB-FIP) (1993). *CEB-FIP Model Code 1990*, Thomas Telford, London.

Gross, S. P., and Burns, N. H. (2000). "Field performance of prestressed high performance concrete highway bridges in Texas." *Research Report 580/589-2 Revised Preliminary Copy*, Center for Transportation research, University of Texas at Austin, Austin, TX.

Haldar, A., and Mahadevan, S. (2000). Probability, Reliability, and Statistical Methods in Engineering Design, *John Wiley and Sons*, New York, NY.

Haugaard, M., and Riis, K. (1997). "Curing of high quality concrete," *DTI Building Technology*, P.O. Box 141, DK-2630 Taastrup, Denmark.

Hueste, M. D., and Cuadros, G. (2003), "Flexural design of high strength concrete prestressed bridge girders – review of current practice and parametric study," *Research Report 2101-3*, Texas Transportation Institute, College Station, TX.

Hueste, M. D., Trejo, D., Cline, D. and Keating, P. (2003a). "Investigation of flexural design parameters for high strength concrete prestressed bridge girders – project overview," *Research Report 2101-1*, Texas Transportation Institute, College Station, TX.

Hueste, M. D., Chompreda, P., Trejo, D., Cline, D., and Keating, P. (2003b). "Mechanical properties of high strength concrete produced for prestressed bridge girders." *Research Report 2101-2*, Texas Transportation Institute, College Station, TX.

Kern, R., Cervinka, S., and Weber, R. (1995). "Efficiency of curing methods," *Darmstadt Concrete*, 10(1), 117-122.

Khayat, K. H., Bickley, J. A., and Hooton, R. D. (1995). "High-strength concrete properties derived from compressive strength values." *Cement, Concrete, and Aggregates*, 17(2), 126-133.

Kjellsen, K. O., and Detwiler, R. J. (1993). "Later-age strength prediction by a modified maturity model." *ACI Materials Journal*, 90(3), 220-227.

Kovler, K., Schamban, I., Igarashi, S., and Bentur, A. (2000). "Influence of mixture proportions and curing conditions on compressive strength of high-performance concrete," *ACI Materials Journal*, 97(1), 21-26.

Maage, M., Smeplass, S., and Johansen, R. (1990). "Long term strength of high strength silica fume concrete," *Second International Symposium on Utilization of High Strength Concrete*, Berkeley, Calif.

Meeks, K. W., and Carino, N. J. (1999). "Curing of high-performance concrete: report of the state-of-the-art," *NISTIR 6295*, Gaithersburg, MD, 1-180.

Milton, J. S., and Arnold, J. C. (1995). Introduction to Probability and Statistics: Principals and Applications for Engineering and Computer Sciences, McGraw Hill, New York, NY.

Murdock, L. J., and Brook, K. M. (1979). *Concrete materials and practice.* Fifth Edition, E. Arnold, London, 25-88.

Myers, J. J. (2000). "The use of maturity method as a quality control tool for high performance concrete bridge decks," *PCI/FHWA/FIB International Symposium on High Performance Concrete*, 1-14.

Naaman, A.E., and Siriaksorn, A. (1982). "Reliability of partially prestressed beams at serviceability limit states." *PCI Journal*, 27(6), 66-85.

Nawy, E. G. (2000). *Prestressed concrete*, Third Edition, Prentice Hall, Upper Saddle River, NJ.

Nowak, A.S. (1995). "Calibration of LRFD Bridge Code," Journal of Structural Engineering, 121(8), 1245-1251.

Nowak, A. S. (1999). "Calibration of LRFD bridge design code." *NCHRP Report 368*, National Research Council, Washington, D.C.

PCI Industry Handbook Committee (1992). *PCI design handbook*, fourth edition, Precast/Prestressed Concrete Institute, Chicago, IL..

Pinto, R., and Hover, K. (1999). "Application of maturity approach to setting times," *ACI Materials Journal*, 686-691.

Popovics, S. (1979). *Concrete-making materials.* Hemisphere Publishing Corporation, Washington, D.C., 3-156.

Raphael. J. M. (1984). "Tensile strength of concrete," *J. American Concrete Institute*, 81 (2), 158-165.

SAS Institute Inc. (1999). *SAS user's manual-version 8.01.* Cary, N.C.

Tabsh, S. W. (1992). "Reliability based parametric study of pretensioned AASHTO bridge girders." *PCI Journal,* 3(5), 56-67.

APPENDIX A

MIXTURE INFORMATION

A summary of the mixtures used in Phase 1 of this study are presented in this appendix. Such information was used in making the appropriate adjustments for the strength data obtained for these mixture proportions, as described in Chapter 5. Tables A.1, A.2, and A.3 present information for precasters A, B, and C, respectively. These tables were adapted from Hueste et al. (2003b).

Table A.1. Mixture Information for Precaster A (Hueste et al. 2003b).

	Set 1				Set 2		
Compressive Strength Category	6000 psi	8000 psi	8000 psi (2)	10,000 psi	6000 psi	8000 psi	10,000 psi
Designation	A15-A16	A5-A6	A13-A14	A17-A18	A7-A8	A9-A10	A11-A12
Design Requirements							
Specified f'_c (psi)	6250	8573	8484	8963	5909	7540	9196
Design f'_{ci} (psi)	6250	5416	6324	6252	5284	5890	6919
Mixture Proportions							
Coarse Aggregate Type Quantity (pcy)	CRG 1989	¾"CRG 2016	CRG 1989	CRG 1989	CRG 2035	CRG 2034	CRG 1989
Fine Aggregate Type Quantity (pcy)	NRS 1214	NRS 1243	NRS 1214	NRS 1214	NRS 1232	NRS 1151	NRS 1214
Cement ASTM C 150 Type Quantity (pcy)	III 705	III 611	III 705	III 705	III 611	III 705	III 705
W/C	0.28	0.34	0.28	0.28	0.34	0.29	0.28
Retarder ASTM C 494 Type Quantity (oz/100 lbs cement)	D 3.5	D 3.5	D 3.5	D 3.5	D 3.5	D 3.5	D 3.5
HRWR ASTM C 494 Type Quantity (oz/100 lbs cement)	F 29	F 26	F 29	F 29	F 26	F 29	F 29
Fly Ash Type Quantity (pcy)	N/A	N/A	N/A	N/A	N/A	N/A	N/A
Silica Fume	N/A	N/A	N/A	N/A	N/A	N/A	N/A
Fresh Concrete							
Slump (inch)	8	7.75	8	8	6.5-7	7.5	8
Ambient Temperature (°F)	90	75	88	91	61	77	92
Ambient Relative Humidity (%)	47	98	50	51	37	97	24

Conversion Factors:

1000 psi = 6.895 MPa
1 lb/yd^3 = 0.5933 kg/m^3
1 oz = 2.957 × 10^{-5} m^3
1 inch = 25.4 mm
°F = (9/5) °C + 32

Abbreviations:

CRG = Coarse River Gravel
NRS = Natural River Sand

Table A.2. Mixture Information for Precaster B (Hueste et al. 2003b).

	Set 1				Set 2		
Compressive Strength Category	6000 psi	6000 psi (2)	8000 psi	10,000 psi	6000 psi	8000 psi	10,000 psi
Designation	B3/B4	B11/B12	B15/B16	B7/B8	B9/B10	B13/B14	B5/B6
Design Requirements							
Specified f'_c (psi)	6525	6598	8000	8983	6525	8000	8983
Design f'_{ci} (psi)	6525	6517	Not specified	6555	6525	Not specified	6555
Mixture Proportions							
Coarse Aggregate Type Quantity (pcy)	CL 1872	CL 1853	CRG 1998	CL 1850	CL 1850	CRG 2010	CL 1859
Fine Aggregate Type Quantity (pcy)	NRS 1421	NRS 1490	NRS 1369	NRS 1490	NRS 1490	NRS 1356	NRS 1493
Cement ASTM C 150 Type Quantity (pcy)	III 658	III 658	III 658	III 658	III 658	III 658	III 658
W/C	0.34		0.34	0.34	0.34	0.34	0.34
Retarder ASTM C 494 Type Quantity (oz/100 lbs cement)	B, D 3.0	B, D 3.0	B, D 3.0	B, D 3.0	B, D 3.0	B, D 3.0	B, D 3.0
HRWR ASTM C 494 Type Quantity (oz/100 lbs cement)	A, F 15	A, F 15	A, F 15	A, F 15	A, F 15	A, F 15	A, F 15
Fly Ash Type Quantity (pcy)	N/A	N/A	N/A	N/A	N/A	N/A	N/A
Silica Fume	N/A	N/A	N/A	N/A	N/A	N/A	N/A
Fresh Concrete							
Slump (inch)	5.5	5.5	5.5	5.5	5.5	5.5	5.5
Ambient Temperature (°F)	102	90	79	93	91	91	95
Ambient Relative Humidity (%)	No data	53	78	53	57	57	56

Conversion Factors:

1000 psi = 6.895 MPa
1 lb/yd^3 = 0.5933 kg/m^3
1 oz = 2.957 × 10^{-5} m^3
1 inch = 25.4 mm
°F = (9/5) °C + 32

Abbreviations:

CL = Crushed Limestone
CRG = Coarse River Gravel
NRS = Natural River Sand

Table A.3. Mixture Information for Precaster C (Hueste et al. 2003b).

	Set 1				Set 2		
Compressive Strength Category	6000 psi	8000 psi	8000 psi (2)	10,000 psi	6000 psi	8000 psi	10,000 psi
Designation	C15/C16	C3/C4	C13/C14	C17/C18	C7/C8	C11/C12	C9/C10
Design Requirements							
Specified f'_c (psi)	6500	7099	7469	9000	6178	8102	9152
Design f'_{ci} (psi)		5716	6048	Not specified	5204	6590	7034
Mixture Proportions							
Coarse Aggregate Type Quantity (pcy)	CL 1775	CL	CL 1781	CL 1759	CL 1847	CL 1760	CL 1837
Fine Aggregate Type Quantity (pcy)	NRS 1475	NRS	NRS 1477	NRS 1474	NRS 1427	NRS 1483	NRS 1448
Cement ASTM C 150 Type Quantity (pcy)	III 658	III 658	III 658	III 658	III 658	III 658	III 658
W/C	0.34	0.34	0.34	0.34	0.34	0.34	0.34
Retarder ASTM C 494 Type Quantity (oz/100 lbs cement)	B, D 3.0	B, D 3.0	B, D 3.0	B, D 3.0	B, D 3.0	B, D 3.0	B, D 3.0
HRWR ASTM C 494 Type Quantity (oz/100 lbs cement)	A, F 20	A, F 20	A, F 20	A, F 20	A, F 20	A, F 20	A, F 20
Fly Ash Type Quantity (pcy)	N/A	N/A	N/A	N/A	N/A	N/A	N/A
Silica Fume	N/A	N/A	N/A	N/A	N/A	N/A	N/A
Fresh Concrete							
Slump (inch)	4.5	4.5	4.5	4.5	4.5	4.5	4.5
Ambient Temperature (°F)	No Data	61	88	77	72	68	63
Ambient Relative Humidity (%)	No Data	60	45	84	98	45	No Data

Conversion Factors:

1000 psi = 6.895 MPa
1 lb/yd^3 = 0.5933 kg/m^3
1 oz = 2.957 × 10^{-5} m^3
1 inch = 25.4 mm
°F = (9/5) °C + 32

Abbreviations:

CL = Crushed Limestone
NRS = Natural River Sand

APPENDIX B

EXPERIMENTAL DATA

The experimental data obtained from testing for the compressive strength and the modulus of rupture are summarized in this section. The summary of compressive strength tests is shown in Table B.1 to Table B.3. The summary of MOR tests are shown in Table B.4 to Table B.6. In each table, the four different curing conditions, testing ages, specimen strength, batch averages, and coefficients of variation are presented. Note that NT indicates that the specimen was not tested. Table B.7 is a summary of Phase 1 unadjusted data and adjusted data for the compressive strength based on the curing factors obtained from this study with the standard curing condition as the baseline. Table B.8 is a summary of Phase 1 unadjusted data and adjusted data for the modulus of rupture based on the curing factors for different curing conditions obtained from this study with the standard curing condition as the baseline.

Table B.1. Summary of Compressive Strength for Precaster A.

Curing Condition	Age Tested	Specimen			Batch Avg. (psi)	Batch CV (%)
		A (psi)	B (psi)	C (psi)		
L	1	6812	6661	6891	6788	1.7
L	3	9239	9008	9159	9135	1.3
L	7	10,584	10,138	10,393	10,372	2.2
L	14	10,767	11,014	10,608	10,796	1.9
L	28	12,159	11,523	11,531	11,738	3.1
L	56	13,059	12,836	11,881	12,592	5.0
HH	1	8491	8539	8674	8568	1.1
HH	3	9517	9557	9772	9615	1.4
HH	7	10,640	9716	10353	10,236	4.6
HH	14	10,067	10,647	10,067	10,260	3.3
HH	28	10,369	10,751	10,815	10,645	2.3
HH	56	10,671	10,226	10,393	10,430	2.2
RH	1	8491	8539	8674	8568	1.1
RH	3	8754	9406	8841	9000	3.9
RH	7	10,273	9756	9812	9947	2.9
RH	14	10,441	10,297	10,409	10,382	0.7
RH	28	10,830	10,886	10,711	10,809	0.8
RH	56	11,324	11,610	11,531	11,488	1.3
RL	1	8491	8539	8674	8568	1.1
RL	3	9494	9358	9494	9449	0.8
RL	7	10,170	9931	9891	9997	1.5
RL	14	10,218	9693	10,647	10,186	4.7
RL	28	11,523	11,300	10,671	11,165	4.0
RL	56	10,258	10,098	10,552	10,303	2.2

Table B.2. Summary of Compressive Strength for Precaster B.

Curing Condition	Age Tested	Specimen			Batch Avg. (psi)	Batch CV (%)
		A (psi)	B (psi)	C (psi)		
L	1	6263	6159	6462	6295	2.4
L	3	6891	7273	7305	7156	3.2
L	7	8069	8228	7982	8093	1.5
L	14	8769	9000	9120	8963	2.0
L	28	8976	9191	9430	9199	2.5
L	56	9955	10,075	10,178	10,069	1.1
HH	1	6772	7019	7305	7032	3.8
HH	3	8276	7671	8220	8056	4.1
HH	7	9064	9533	9056	9218	3.0
HH	14	9000	8857	9080	8979	1.3
HH	28	NT	9112	9151	9132	0.3
HH	56	9621	9064	9732	9472	3.8
RH	1	6772	7019	7305	7032	3.8
RH	3	7281	7775	7807	7621	3.9
RH	7	7631	7703	7870	7735	1.6
RH	14	8395	8610	8730	8578	2.0
RH	28	8340	9430	8889	8886	6.1
RH	56	10,106	10,106	9398	9870	4.1
RL	1	6772	7019	7305	7032	3.8
RL	3	7846	8204	7974	8008	2.3
RL	7	8260	8196	7950	8135	2.0
RL	14	8658	8873	8515	8682	2.1
RL	28	7894	8666	8960	8507	6.5
RL	56	8467	9024	8626	8706	3.3

Table B.3. Summary of Compressive Strength for Precaster C.

Curing Condition	Age Tested	Specimen			Batch Avg. (psi)	Batch CV (%)
		A (psi)	B (psi)	C (psi)		
L	1	7074	6939	7106	7040	1.3
L	3	7926	7926	8005	7952	0.6
L	7	8690	8507	8650	8616	1.1
L	14	9350	8698	9000	9016	3.6
L	28	9605	9478	9581	9555	0.7
L	56	10,090	9939	9947	9992	0.9
HH	1	6525	6446	6470	6480	0.6
HH	3	8228	7297	7313	7613	7.0
HH	7	7433	7751	8547	7910	7.3
HH	14	8300	7679	8594	8191	5.7
HH	28	8841	8578	7695	8371	7.2
HH	56	8769	8889	7870	8509	6.5
RH	1	6525	6446	6470	6480	0.6
RH	3	7536	6653	6732	6974	7.0
RH	7	7536	7242	7273	7350	2.2
RH	14	7759	8507	8117	8128	4.6
RH	28	7894	7950	8793	8212	6.1
RH	56	9159	8594	8085	8613	6.2
RL	1	6525	6446	6470	6480	0.6
RL	3	7496	7417	7250	7388	1.7
RL	7	8340	8515	7695	8183	5.3
RL	14	8467	8125	8865	8486	4.4
RL	28	8929	8308	8602	8613	3.6
RL	56	8483	8976	7496	8318	9.1

Table B.4. Summary of Modulus of Rupture for Precaster A.

Curing Condition	Age Tested	Specimen			Batch Avg. (psi)	Batch CV (%)
		A (psi)	B (psi)	C (psi)		
L	1	795	668	708	724	9.0
L	3	917	1086	946	983	9.2
L	7	1005	1149	1094	1083	6.7
L	14	1120	1210	1243	1191	5.3
L	28	1284	1358	1207	1283	5.9
L	56	1254	1478	1310	1347	8.7
HH	1	770	776	806	784	2.5
HH	3	760	734	739	744	1.9
HH	7	729	727	891	782	12.0
HH	14	784	1026	954	921	13.5
HH	28	1104	923	966	998	9.5
HH	56	904	854	906	888	3.3
RH	1	770	776	806	784	2.5
RH	3	1041	951	973	988	4.7
RH	7	1043	970	1061	1025	4.7
RH	14	1012	1056	1074	1047	3.0
RH	28	1003	1092	978	1024	5.8
RH	56	1183	1205	1154	1181	2.2
RL	1	770	776	806	784	2.5
RL	3	820	795	765	793	3.5
RL	7	810	737	763	770	4.8
RL	14	683	763	725	724	5.5
RL	28	823	722	872	806	9.5
RL	56	811	804	825	813	1.3

Table B.5. Summary of Modulus of Rupture for Precaster B.

Curing Condition	Age Tested	Specimen			Batch Avg. (psi)	Batch CV (%)
		A (psi)	B (psi)	C (psi)		
L	1	798	856	780	811	4.9
L	3	1054	995	1058	1036	3.4
L	7	992	951	946	963	2.6
L	14	1043	924	956	974	6.3
L	28	1130	1024	1125	1093	5.5
L	56	1131	1148	1191	1157	2.7
HH	1	726	752	824	767	6.6
HH	3	801	916	1002	906	11.1
HH	7	763	944	856	854	10.6
HH	14	853	882	883	873	2.0
HH	28	788	NT	786	787	0.2
HH	56	915	821	859	865	5.5
RH	1	726	752	824	767	6.6
RH	3	958	986	902	949	4.5
RH	7	915	933	974	941	3.2
RH	14	898	917	973	929	4.2
RH	28	1042	884	944	957	8.3
RH	56	1002	936	1073	1004	6.8
RL	1	726	752	824	767	6.6
RL	3	836	929	784	850	8.6
RL	7	742	894	876	837	9.9
RL	14	822	740	861	808	7.6
RL	28	786	867	808	820	5.1
RL	56	912	945	875	911	3.8

Table B.6. Summary of Modulus of Rupture for Precaster C.

Curing Condition	Age Tested	Specimen			Batch Avg. (psi)	Batch CV (%)
		A (psi)	B (psi)	C (psi)		
L	1	747	741	687	725	4.6
L	3	767	865	876	836	7.2
L	7	907	977	1018	967	5.8
L	14	1067	1081	990	1046	4.7
L	28	865	1004	1005	958	8.4
L	56	969	1039	990	999	3.6
HH	1	683	638	699	673	4.7
HH	3	697	689	754	713	5.0
HH	7	708	706	NT	707	0.2
HH	14	826	624	757	736	14.0
HH	28	746	887	789	807	9.0
HH	56	846	899	883	876	3.1
RH	1	683	638	699	673	4.7
RH	3	686	729	787	734	6.9
RH	7	802	916	818	845	7.3
RH	14	833	854	814	834	2.4
RH	28	844	855	760	820	6.3
RH	56	852	931	877	887	4.6
RL	1	683	638	699	673	4.7
RL	3	670	578	638	629	7.4
RL	7	667	783	665	705	9.6
RL	14	717	730	781	743	4.6
RL	28	841	806	743	797	6.2
RL	56	805	831	815	817	1.6

Table B.7. Summary of Study Phase 1 Unadjusted Data and Study Phase 3 Adjusted Data – Compressive Strength.

Batch ID	Age Tested (days)	f'_c (Unadjusted) (psi)	f'_c (RL) (psi)	f'_c (HH) (psi)	f'_c (RH) (psi)
A15	7	10,000	9600	9900	9600
A16	7	10,433	10,016	10,329	10,016
A5	7	9755	9365	9657	9365
A6	7	9568	9185	9472	9185
A17	7	9938	9540	9839	9540
A18	7	10,459	10,041	10,354	10,041
A7	7	8757	8407	8669	8407
A8	7	8495	8155	8410	8155
A9	7	9696	9308	9599	9308
A10	7	10,027	9626	9927	9626
A11	7	8629	8284	8543	8284
A12	7	8664	8317	8577	8317
A15	28	11,813	11,222	10,713	10,879
A16	28	11,770	11,182	10,674	10,839
A5	28	11,519	10,943	10,446	10,608
A6	28	10,965	10,417	9944	10,098
A17	28	11,240	10,678	10,193	10,351
A18	28	11,976	11,377	10,861	11,029
A7	28	9920	9424	8996	9135
A8	28	9393	8923	8518	8650
A9	28	11,454	10,881	10,388	10,548
A10	28	11,561	10,983	10,485	10,647
A11	28	10,057	9554	9121	9262
A12	28	9614	9133	8719	8854
A15	56	12,277	10,067	10,169	11,201
A16	56	12,515	10,262	10,366	11,418
A5	56	12,172	9981	10,082	11,105
A6	56	11,841	9710	9808	10,803
A17	56	11,801	9677	9775	10,767
A18	56	12,189	9995	10,096	11,121
A7	56	10,360	8495	8581	9452
A8	56	10,155	8327	8412	9265
A9	56	11,717	9608	9705	10,690
A10	56	11,910	9766	9865	10,866
A11	56	10,744	8810	8899	9802
A12	56	10,601	8693	8781	9672

Table B.7. (Continued).

Batch ID	Age Tested (days)	f'_c (Unadjusted) (psi)	f'_c (RL) (psi)	f'_c (HH) (psi)	f'_c (RH) (psi)
B3	7	8546	8591	9567	8168
B4	7	8297	8341	9288	7930
B13	7	9222	9270	10324	8814
B14	7	8187	8230	9165	7825
B7	7	8491	8536	9505	8115
B8	7	9010	9057	10086	8611
B9	7	8458	8502	9468	8084
B10	7	8294	8337	9285	7927
B15	7	8059	8101	9022	7702
B16	7	8175	8218	9152	7813
B5	7	7946	7988	8895	7594
B6	7	9713	9764	10873	9283
B3	28	9865	9451	9793	9865
B4	28	9438	9042	9369	9438
B13	28	10037	9616	9964	10037
B14	28	9949	9532	9877	9949
B7	28	9635	9231	9565	9635
B8	28	10145	9719	10071	10145
B9	28	10177	9750	10103	10177
B10	28	9615	9212	9545	9615
B15	28	8896	8523	8831	8896
B16	28	9294	8904	9226	9294
B5	28	9239	8851	9172	9239
B6	28	9278	8889	9210	9278
B3	56	10037	8632	9435	9836
B4	56	9783	8413	9196	9587
B13	56	10822	9307	10173	10606
B14	56	10378	8925	9755	10170
B7	56	10366	8915	9744	10159
B8	56	10888	9364	10235	10670
B9	56	10414	8956	9789	10206
B10	56	9735	8372	9151	9540
B15	56	9594	8251	9018	9402
B16	56	10050	8643	9447	9849
B5	56	9782	8413	9195	9586
B6	56	10012	8610	9411	9812

Table B.7. (Continued).

Batch ID	Age Tested (days)	f'_c (Unadjusted) (psi)	f'_c (RL) (psi)	f'_c (HH) (psi)	f'_c (RH) (psi)
C15	7	8442	8018	7829	7202
C16	7	8723	8285	8089	7442
C3	7	7714	7327	7154	6581
C4	7	8423	8000	7811	7186
C17	7	7961	7561	7383	6792
C18	7	8073	7668	7486	6887
C7	7	8789	8348	8150	7498
C8	7	8709	8272	8076	7430
C11	7	7656	7272	7100	6532
C12	7	8201	7789	7605	6997
C9	7	8478	8053	7862	7233
C10	7	8731	8293	8097	7449
C15	28	9204	8284	8100	7915
C16	28	9300	8370	8184	7998
C3	28	8673	7806	7632	7459
C4	28	9156	8240	8057	7874
C17	28	8951	8056	7877	7698
C18	28	9244	8320	8135	7950
C7	28	9498	8548	8358	8168
C8	28	9513	8562	8371	8181
C11	28	8261	7435	7270	7104
C12	28	8911	8020	7842	7663
C9	28	9354	8419	8232	8044
C10	28	10,115	9104	8901	8699
C15	56	9239	8072	7868	7964
C16	56	8861	7741	7546	7638
C3	56	8826	7711	7516	7608
C4	56	9613	8398	8186	8286
C17	56	9466	8270	8061	8159
C18	56	9478	8280	8072	8170
C7	56	9961	8702	8483	8586
C8	56	10,015	8749	8529	8633
C11	56	9025	7885	7686	7779
C12	56	9065	7920	7720	7814
C9	56	9718	8490	8276	8377
C10	56	10206	8916	8691	8797

Table B.8. Summary of Phase 1 Unadjusted Data and Phase 3 Adjusted Data – MOR.

Batch ID	Age tested (days)	MOR (Unadjusted) (psi)	MOR (RL) (psi)	MOR (HH) (psi)	MOR (RH) (psi)
A15	7	1024	727	767	969
A16	7	1092	775	817	1033
A5	7	883	627	661	836
A6	7	889	631	666	841
A17	7	1110	788	831	1050
A18	7	1112	790	832	1052
A7	7	954	677	714	903
A8	7	910	646	681	861
A9	7	937	665	701	887
A10	7	974	692	729	922
A11	7	947	672	709	896
A12	7	970	689	726	918
A15	28	1250	825	920	998
A16	28	1293	853	952	1032
A5	28	1001	661	737	799
A6	28	1063	702	782	849
A17	28	1232	813	907	984
A18	28	1199	791	882	957
A7	28	971	641	715	775
A8	28	956	631	704	763
A9	28	1050	693	773	838
A10	28	1129	745	831	901
A11	28	934	616	687	746
A12	28	998	659	735	797
A15	56	1397	838	938	1224
A16	56	1420	852	954	1244
A5	56	1070	642	719	938
A6	56	1099	659	738	963
A17	56	1277	766	858	1119
A18	56	1291	775	867	1131
A7	56	1217	730	817	1067
A8	56	1147	688	770	1005
A9	56	1261	757	847	1105
A10	56	1454	872	977	1274
A11	56	1072	643	720	939
A12	56	958	575	643	840

Table B.8. (Continued).

Batch ID	Age tested (days)	MOR (Unadjusted) (psi)	MOR (RL) (psi)	MOR (HH) (psi)	MOR (RH) (psi)
B3	7	922	775	818	772
B4	7	937	787	831	784
B13	7	1047	880	929	877
B14	7	1025	861	909	858
B7	7	1076	904	954	901
B8	7	1069	898	948	895
B9	7	1039	873	922	870
B10	7	1011	850	897	846
B15	7	1005	845	891	841
B16	7	1014	852	899	849
B5	7	1088	914	965	911
B6	7	1041	875	923	872
B3	28	930	699	670	763
B4	28	948	712	683	777
B13	28	1112	835	801	912
B14	28	1170	879	842	959
B7	28	1077	809	775	883
B8	28	1107	832	797	908
B9	28	1134	852	817	930
B10	28	1117	839	804	916
B15	28	1113	836	801	913
B16	28	1108	832	798	909
B5	28	1146	861	825	940
B6	28	1139	856	820	934
B3	56	1093	863	820	955
B4	56	1126	890	845	984
B13	56	1177	930	883	1028
B14	56	1131	893	848	988
B7	56	1093	863	820	955
B8	56	1079	852	809	943
B9	56	1035	818	776	904
B10	56	1136	897	852	993
B15	56	1105	873	829	965
B16	56	1035	818	776	904
B5	56	1139	900	854	995
B6	56	1118	883	839	977

Table B.8. (Continued)

Batch ID	Age tested (days)	MOR (Unadjusted) (psi)	MOR (RL) (psi)	MOR (HH) (psi)	MOR (RH) (psi)
C15	7	914	666	668	841
C16	7	1031	751	753	949
C3	7	769	560	562	708
C4	7	792	577	579	729
C17	7	985	718	720	906
C18	7	883	643	645	813
C7	7	858	625	627	790
C8	7	844	615	617	777
C11	7	908	661	663	836
C12	7	928	676	678	854
C9	7	842	613	615	775
C10	7	988	720	722	909
C15	28	1010	798	768	851
C16	28	1025	810	779	863
C3	28	847	669	644	713
C4	28	908	717	690	765
C17	28	1107	875	841	932
C18	28	1103	871	838	929
C7	28	1009	797	767	850
C8	28	1016	803	772	856
C11	28	953	753	724	803
C12	28	880	695	669	741
C9	28	1048	828	796	883
C10	28	1111	878	844	936
C15	56	1089	877	928	951
C16	56	1055	850	899	921
C3	56	802	646	683	700
C4	56	902	727	768	788
C17	56	1084	873	924	947
C18	56	1022	823	871	893
C7	56	983	792	837	859
C8	56	1025	826	873	895
C11	56	861	694	734	752
C12	56	918	739	782	802
C9	56	1012	815	862	884
C10	56	1025	826	873	895

APPENDIX C

INPUT FILES

The input file created for the statistical data analysis presented in Chapter 4 is shown below. This program was used for the compressive strength and MOR. The input file shown below is for the concrete compressive strength. In order to use this input file for the MOR, the table of compressive strength data shown below should be substituted with the MOR data. Note that only part of the compressive strength data is presented here.

(a) Full Model

```
data Batches; *summaries for each batch;
input Precaster $ Curing $ Age Cyl1-Cyl3;
NoCyl=n(of Cyl1-Cyl3); BAvg=mean(of Cyl1-Cyl3);
CVBatch=std(of Cyl1-Cyl3)/BAvg; LogBAvg=log10(BAvg);
LogDsgn = log10(Design);
Cards;

A        L        01       6812     6661     6891
A        L        03       9239     9008     9159
A        L        07       10584    10138    10393
A        L        14       10767    11014    10608
A        L        28       12159    11523    11531
A        L        56       13059    12836    11881
A        HH       01       8491     8539     8674
A        HH       03       9517     9557     9772
A        HH       07       10640    9716     10353

;;;
run;
proc print data=Batches;
run;
data Distr;
set Batches;
LCyl1=Log10(Cyl1);
LCyl2=Log10(Cyl2);
LCyl3=Log10(Cyl3);
AveofLog=mean(of LCyl1-LCyl3);
E=Cyl1-BAvg;
```

```
EL=LCyl1-AveofLog; output;
E=Cyl2-BAvg;
EL=LCyl2-AveofLog; output;
E=Cyl3-BAvg;
EL=LCyl3-AveofLog; output;
drop Cyl1-Cyl3;
run;
proc glm data=Batches; * basic check of relationship;
class Precaster Curing Age;
model LogBAvg = Curing Precaster|Age Curing*Precaster Curing*Age/ss3;
run;
```

(b) Reduced Model

```
data Batches; *summaries for each batch;
input Precaster $ Curing $ Age Cyl1-Cyl3;
NoCyl=n(of Cyl1-Cyl3); BAvg=mean(of Cyl1-Cyl3);
CVBatch=std(of Cyl1-Cyl3)/BAvg; LogBAvg=log10(BAvg);
LogDsgn = log10(Design);
if (Curing="L") then CC="L";
if (Curing="HH") then CC="F";
if (Curing="RH") then CC="F";
if (Curing="RL") then CC="F";
Cards;

A          L          01         6812       6661       6891
A          L          03         9239       9008       9159
A          L          07         10584      10138      10393
A          L          14         10767      11014      10608
A          L          28         12159      11523      11531
A          L          56         13059      12836      11881

;;;
run;
proc print data=Batches;
run;
data Distr;
set Batches;
LCyl1=Log10(Cyl1);
LCyl2=Log10(Cyl2);
LCyl3=Log10(Cyl3);
AveofLog=mean(of LCyl1-LCyl3);
drop Cyl1-Cyl3;
run;
proc glm data=Batches; * basic check of relationship;
```

```
class Precaster CC Age;
model LogBAvg = CC Precaster|Age CC*Precaster CC*Age/ss3;
```

(c) Three-Way Interaction

```
data Batches; *summaries for each batch;
input Precaster $ Curing $ Age Cyl1-Cyl3;
NoCyl=n(of Cyl1-Cyl3);
LCyl=Log10(Cyl1);output;
LCyl=Log10(Cyl2);output;
LCyl=Log10(Cyl3);output;
Cards;

A          L          01         6812       6661       6891
A          L          03         9239       9008       9159
A          L          07         10584      10138      10393
A          L          14         10767      11014      10608
A          L          28         12159      11523      11531
A          L          56         13059      12836      11881

;;;
run;
proc print data=Batches;
run;
data Distr;
set Batches;
LCyl=Log10(Cyl1);output;
LCyl=Log10(Cyl2);output;
LCyl=Log10(Cyl3);output;
drop Cyl1-Cyl3;
run;
proc glm data=Batches; * basic check of relationship;
class Precaster Curing Age;
model LCyl = Curing Precaster|Age Curing*Precaster Curing*Age Precaster*Curing*Age/ss3;
run;
```

APPENDIX D

CASE STUDIES

Several case study designs for U54 beams were checked with the results obtained from Phase 2 (Hueste and Cuadros 2003). The Phase 2 design approach was checked by Hueste and Cuadros (2003) to verify consistency of the results with TxDOT design practices. Table D.1 is a summary of the design parameters for this case study. Table D.2 is a comparison between the two designs. Results show that the designs are consistent. Note that minor differences occur between the design in this study and the equivalent case for Phase 2 design (Hueste and Cuadros 2003). The maximum difference between the two designs for calculating the maximum span lengths that can be safely designed was found to be 0.8 feet, which is equivalent to 0.6 percent of the span. This small difference was probably due to a difference in the number of iterations considered in refining the calculation of prestress losses.

Table D.3 is a summary of the design parameters and variables used in the reliability analysis. The procedure followed to obtain the limit state function $g(\ )$ is shown for one simulation. Note that μ_x is the mean of variable x for a normal distribution; σ_x is the standard deviation of the variable x for normal distribution; z_i is the inverse standard normal distribution function applied to random number u_i; μ_{lnx} is the mean of the variable x for a lognormal distribution, and μ_{lnx} is the standard deviation of variable x for a lognormal distribution.

Table D.1. Summary of Design Parameters – Case Study Comparison.

Parameters	Phase 2	Phase 3 (This Study)
SPAN LENGTH	90 feet	90 feet
TYPE OF BEAM	U54 beam	U54 beam
GIRDER SPACING	11.5 feet	11.5 feet
CODE	Standard Specification	Standard Specification
LOADS		
Live Load	HS25	HS25
Impact Factor	1.23	1.23
Distribution Factor	1.045	1.045
Non-Composite Loads:		
Haunch	0.027 klf	0.027 klf
Diaphragms	3 kips	3 kips
Composite Loads	0.197 klf	0.197 klf
MATERIALS		
Concrete Strength - CIP Slab	4000 psi	4000 psi
Concrete Strength - Precast Beam	8000 psi	8000 psi
Unit Weight of Beam and Slab	0.150 klf	0.150 klf
Strand Diameter	0.5 inch	0.5 inch
Strand Ultimate Strength	270 ksi - low relaxation	270 ksi - low relaxation
PRESTRESS LOSSES	AASHTO-refined method	AASHTO-refined method
OTHER		
Relative Humidity	75%	75%
Modular Ratio: $n=E_{CIP}/E_{Precast}$	0.707	0.707

Table D.2. Comparison of Results – Parametric Study.

Design Results	Phase 2	Phase 3 (This Study)	% Difference
Concrete Strength Requirement (psi)			
Initial (f'_{ci}):	6000	6000	-
Final (f'_c):	8000	8000	-
Stresses (psi)			
Release (at ends) TOP	92	88	-4.9
Release (at ends) BOTTOM	-1729	-1716	-0.8
Interm. Stage (at midspan) TOP	-1687	-1697	0.6
Final Stage (at midspan) TOP	-2043	-2053	0.5
Final Stage (at midspan) BOTTOM	490	520	5.8
Number of Strands	37	37	0.0
Losses (ksi)			
Initial:	4.76	4.71	-1.0
Final:	13.59	13.49	-0.8
Ultimate Moment Req. (kip-feet)	7079	7079	0.0
Nominal Moment (kip-feet)	7198	7198	0.0

Table D.3. Design Parameters and Variables - Reliability Analysis (One Iteration).

Description	Parameters	Values
Design Information	*# of strands*	99
	Girder Spacing (feet)	10
	span L (feet)	145
f_{pu} (Normal)	f_{pu} *(specified)* (psi)	270,000
	COV	0.0142
	μ_x	280,449
	σ_x	3982
	u_i	0.845
	z_i	1.01
	f_{pu} (psi)	284,486
f'_c (Lognormal)	f'_c *(Specified)* (psi)	10,000
	Bias	1.1
	COV	0.091
	σ_{lnx}	0.0908
	$\mu_{\ln x}$	9.302
	u_i	0.458
	z_i	-0.105
	f'_c (psi)	10,851
MOR (Lognormal)	μ_x	882
	COV	0.164
	σ_{lnx}	0.1630
	$\mu_{\ln x}$	6.769
	u_i	0.365
	z_i	-0.345
	MOR (psi)	823

Table D.3. (Continued).

Distribution	Parameters	Values
M_d (Normal)	W_d *(specified)* (kips/inch)	0.0972
	Bias	1.03
	COV	0.08
	μ_x	0.1
	σ_x	0.008
	u_i	0.583
	z_i	0.209
	W_d	0.102
	M_d (kip-inch)	38,533
W_{slab} Normal	W_{slab} *(specified)* (kips/inches)	0.0833
	Bias	1.05
	COV	0.1
	μ_x	0.0875
	σ_x	0.00875
	u_i	0.338
	z_i	-0.418
	W_{slab}	0.0838
	M_{slab} (kip-inches)	31,729
W_{non_c} Normal	W_{non_c} *(specified)* (kips)	3.00
	Bias	1.05
	COV	0.1
	μ_x	3.15
	σ_x	0.315
	u_i	0.427
	z_i	-0.184
	W_{non_c}	3.09
	M_{non_c} (kip-inch)	2330

Table D.3. (Continued).

Distribution	Parameters	Values
M_{comp} Normal	*Wcomp (specified)* (kips/inch)	0.0092
	Bias	1.05
	COV	0.1
	μ_x	0.00963
	σ_x	0.000963
	u_i	0.391
	z_i	-0.275
	Wcomp	0.0094
	Mcomp (kip-inch)	3542
Impact (Lognormal)	*Impact (specified)* (kips)	0.33
	Bias	0.15
	COV	0.80
	σ_{lnx}	0.7030
	$\mu_{\ln x}$	-3.253
	u_i	0.339
	z_i	-0.415
	Impact (kips)	0.0289
M_L (Normal)	$M_{L\text{-}conc.}$ *(specified)* (kip-feet)	2330
	Bias	1.25
	COV	0.11
	μ_x	2912.5
	σ_x	320.4
	u_i	0.0632
	z_i	-1.53
	$M_{L\text{-}conc.}$ (kip-feet)	2423
	$M_{L\text{-}distr.}$ *(specified)* (kip-feet)	1682
	Bias	1.25
	COV	0.11
	μ_x	2103
	σ_x	231
	u_i	0.2750
	z_i	-0.60
	$M_{L\text{-}distr.}$ (kip-feet)	1964
	M_L+M_I (kip-feet)	2728

Table D.3. (Continued).

Distribution	Parameters	Values
	f_{pe} (psi)	136661
	P_e (lbs.)	2,935,888
	L (psi)	132.8
	R (psi)	822.9
	$g( )=R - L$	690.1